Experimental investigation of H_2/D_2 isotope separation by cryo-adsorption in metal-organic frameworks

Von der Fakultät Chemie der Universität Stuttgart
zur Erlangung der Würde eines Doktors der
Naturwissenschaften (Dr. rer. nat.) genehmigte Abhandlung

Vorgelegt von Julia Sonja Teufel
aus Stuttgart

Hauptberichter: **Prof. Dr. Emil Roduner**
Mitberichter: **Prof. Dr. Gisela Schütz**

Tag der mündlichen Prüfung: **18.12.2012**

Max-Planck-Institut für Intelligente Systeme
Stuttgart
2012

Contents

Abbreviations/ Abkürzungsverzeichnis

BET	Brunauer-Emmett-Teller model to describe adsorption
Br	bromine
χ	delocalization
Cl	chlorine
CMS	carbon molecular sieve
Co	cobalt
COF	covalent organic framework
CrNi	chromium/nickel thermocouple
Cu	copper
DFT	density functional theory
DMF	dimethylformamide
ε	well depth
FeAu	iron/gold thermocouple
GCMC	grand canonical Monte Carlo technique in theoretical physics
IAST	ideal adsorption solution theory
k_B	Boltzmann's constant
λ	de Broglie wavelength
LHe	liquid helium
LN_2	liquid nitrogen
MD	molecular dynamics computer simulation, technique in theoretical physics
MFU	Metal-organic Framework University of Ulm
MFU-4(Zn, Br)	MFU-4 framework with zinc metal centers and a pore aperture formed by chlorine atoms
MFU-4(Co, Cl)	MFU-4 framework with cobalt metal centers and a pore aperture formed by chlorine atoms
MFU-4(Zn, Cl)	MFU-4 framework with zinc metal centers and a pore aperture formed by chlorine atoms
molec/uc	molecules per unit cell
MOF	metal-organic framework
Pt	platinum temperature sensor
QLDFT	quantized liquid density functional theory
QENS	quasi-elastic neutron scattering
RT	room temperature
S/S_{molar}	(molar) selectivity
SAM	self-assembling monolayer
SEM	scanning electron microscopy
ssa	specific surface area
T [K]	absolute temperature
TDS	thermal desorption spectroscopy
TST	transition state theory
U_{LJ}	Lennard-Jones potential
U_{FH}	Feynman-Hibbs potentials
wt%	weight percent
XRD	X-ray diffraction
ZIF	zeolitic imidazolate framework
Zn	zinc
ZPE, E_0	zero-point energy

1. Introduction

When a new class of highly porous hybrid substances called metal-organic frameworks, abbreviated MOF, came up in the 1990[s], they were instantly discovered as potential materials for a great variety of applications due to their accurately tunable framework structure. Twenty years later some out of an innumerable number of advanced MOFs are close to application. A couple of Fe-based frameworks are non-toxic, biocompatible and biodegradable and therefore suitable for controlled drug delivery and as carriers for contrast agents in magnetic resonance imaging.[1] Others are applicable for the sensing of molecules.[2] Also the use in electronic devices is possible due to the tunable band gap, the great variety in dielectric constants, magnetic properties and in some special cases semiconducting behavior.[3]

One of the main research topics concerning MOFs is gas adsorption. Gases can be stored in porous materials by physisorption[4] whereat the amount of adsorbed hydrogen at 77 K is proportional to the specific surface area (ssa) of the material independent of its chemical nature.[5] Continuous development within the last years led to the synthesis of MOFs with specific surface areas of more than 6000 m^2/g; thereby offering a much larger specific surface area than the high ssa activated carbons.[6] These MOFs of ultra-high porosity are possibly used for the low pressure on-board hydrogen storage in automobiles like the F-125, a hybrid fuel cell car presented by Mercedes at the IAA 2011.[7] MOFs could also be used for industrial gas separation either by size exclusion of molecules with a diameter larger than the pore, or by difference in adsorption enthalpy as done in pressure swing adsorption.[8,9] The pore sizes of MOFs range from nanopores to mesopores whereat the pore size can be tuned by applying adequate framework precursors. In materials with sufficiently small pores, also light gas isotope mixtures can be separated by the so-called quantum sieving effect.[10] Owing to this phenomenon isotopes exhibit different adsorption and diffusion behavior under cryogenic conditions in nanoporous materials. But the conventional experimental techniques utilized to study quantum sieving, e.g. quasi-elastic neutron scattering (QENS) for kinetic information and adsorption isotherms for the gas uptake, are restricted to the use of pure gases. As the separation performance is not directly accessible by applying isotope mixtures, it can only be estimated by the molar D_2/H_2 ratio obtained by isothermal pure gas adsorption experiments.

Deuterium is indispensable for many applications like nuclear power production, neutron scattering experiments and isotope tracing. But deuterium only makes up 0.0156% of the naturally occurring hydrogen isotopes.[11] Its direct extraction from natural hydrogen gas by conventional isotope separation methods like cryogenic distillation is rather inefficient, energy intensive and therefore expensive. Thus, the separation of natural hydrogen gas by quantum sieving in MOFs with accurately tuned pore size may be considered as a potential alternative to the conventional deuterium production procedures.

The current work will reveal the potential of MOFs to separate H_2/D_2 isotope mixtures. Small-pore MOFs are tested for the quantum sieving effect by applying H_2/D_2 mixtures in low temperature thermal desorption spectroscopy (TDS). The results obtained for the small-pore MOFs are related to their framework features as well as the exposure conditions to the isotope mixture, e.g. sample temperature and exposure time. Additionally, MOFs with larger pores that do now allow quantum sieving are investigated and their separation performance is compared to the values obtained for small-pore MOFs. Based on the experimental results, technical implementations of the MOF based H_2/D_2 isotope separation are suggested.

2. Fundamentals

2.1. Modern porous materials

2.1.1. MOFs and SURMOFs

MOF is an abbreviation for metal-organic framework, a new class of ultra-porous crystalline hybrid materials consisting of inorganic connectors and organic linkers (see Figure 2.1)

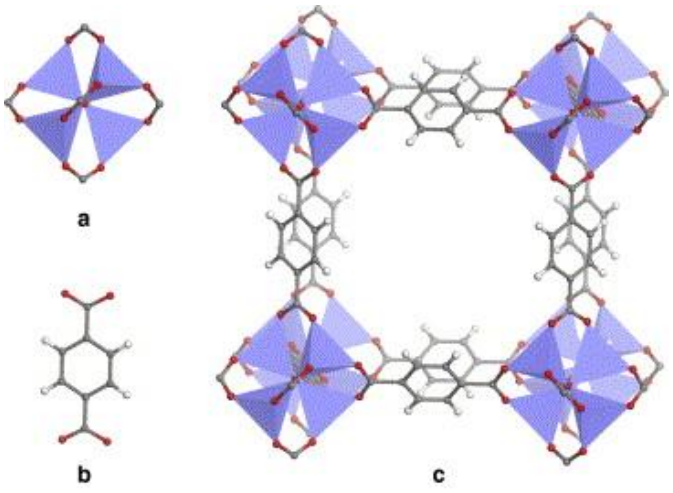

Figure 2.1: Principle constructing of a MOF framework (c) by a metal-cluster (a) as a connector and an hydrocarbon chain as a linker (b).[12]

The inorganic connector is a metal cluster with mainly Zn, Fe, Al, Mg, Co or Cu centers. Some MOFs possess open metal sites that act as strong adsorption sites for small molecules like hydrogen.[13] The organic linkers are mostly hydrocarbon based chains that are tunable in length. Thus, the choice of an appropriate linker allows an adjustment of the pore size,[14] which is termed isoreticular design (see Figure 2.2).

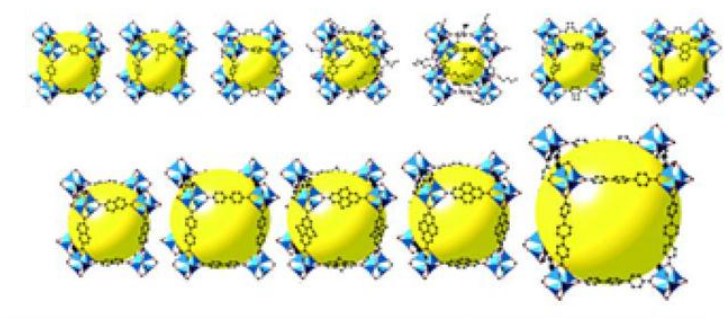

Figure 2.2 : Scheme of the isoreticular framework design on the basis of MOF-5 (IRMOF-1). The pores size can be changed by introducing linkers of different length.[14]

Owing to their ultra-high porosity, MOFs offer a huge specific surface area which can reach values up to more than 6000 m^2/g.[6] Owing to their replaceable metal centers, tunable pore size and functional groups reaching into the pores, MOFs are discussed as potential materials for a wide range of applications like sensors, adsorbents, drug delivery and many others.[15,16] MOFs are conventionally produced by solvothermal synthesis where the building

units are mixed in solution. The developing frameworks in the solution can grow into each other, i.e. they can be interpenetrating, and finally precipitate as powder. But MOFs can also be grown as a thin film on modified or unmodified substrate surfaces.[17] A special way of film deposition is the layer-by-layer method[18] where a substrate, covered with a self-assembling monolayer (SAM), is immersed alternately in a solution containing either the organic or the inorganic framework component with thoroughly rinsing after each immersion step (see Figure 2.3). The process results in a non-penetrating framework and a highly epitaxial layer whereat the layer orientation is directed by the SAM.

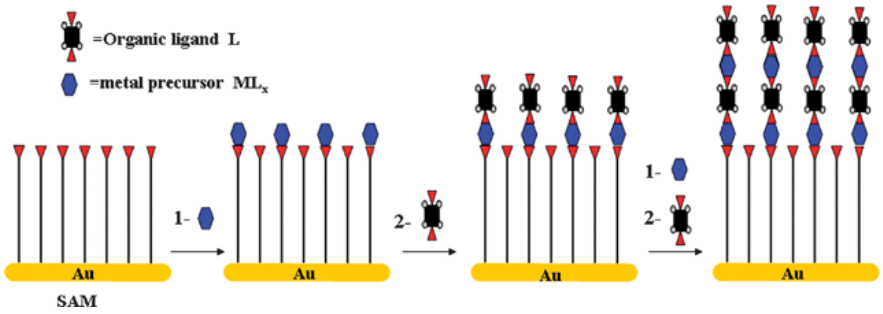

Figure 2.3: Illustration of the layer-by-layer method. First a SAM is deposited on the substrate. Afterwards alternately the inorganic and the organic framework components are attached. The resulting thin film is highly epitaxial and nearly single-crystalline.[17] Reproduced by permission of the Royal Society of Chemistry.

2.1.2. Other porous materials

There is a great variety of anterior and novel porous structures. Some important examples are given below.

Zeolites are amorphous or crystalline aluminosilicate based materials that occur naturally and that are produced synthetically. The structure possesses cages after water removal. Zeolites are conventionally used as catalysts, ion exchangers and adsorbents.[19] They are characterized by their uniform pore size directed by the zeolite geometry. Especially artificial crystalline zeolite molecular sieves are widely used in industry.[20] Rather novel crystalline highly porous materials residing between zeolite and MOF are the zeolitic imidazolate frameworks (ZIFs) where silicon and oxygen atoms of the zeolite topology are replaced by transition metal ions and organic units like imidazolate (see Figure 2.4). ZIFs combine desired properties of zeolites, like the thermal and chemical stability, with those of MOFs, like flexibility.[21-23]

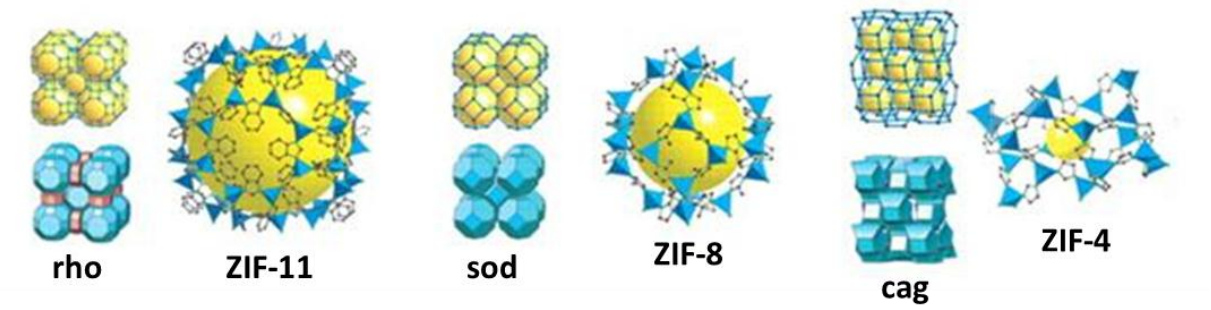

Figure 2.4: Three exemplary ZIF structures with their corresponding zeolite topology shown on the left of each ZIF.[24]

Covalent organic frameworks (COFs) are synthesized by condensing organic monomers that only contain elements with strong covalent binding character like hydrogen, carbon, boron, oxygen and nitrogen. Owing to their construction, most COFs have larger pores than MOFs or ZIFs.[25] COFs are not just interesting for gas storage. They can have very interesting optical and electrical properties like high luminescence and conductivity due to the π-electron system.[26]

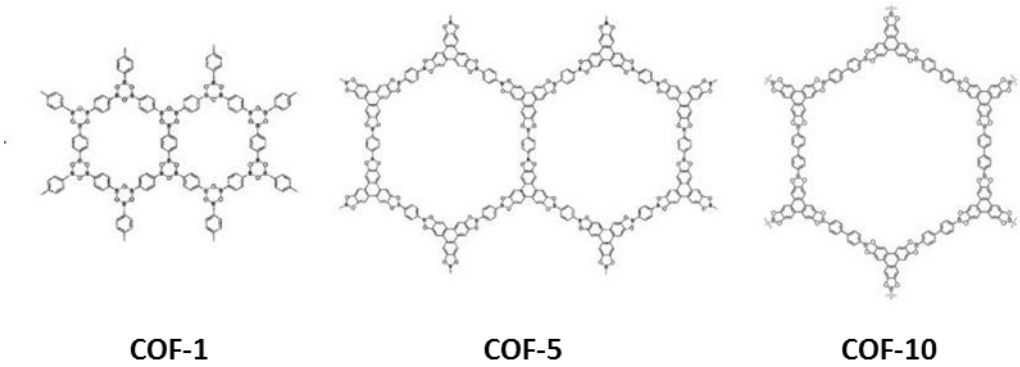

Figure 2.5: Structure of COF-1, COF-5 and COF-10 with pore sizes of 15 Å, 27 Å and 34 Å.[129, 130]

Activated carbon[27] is produced by burning organic substances like wood, coconut shell, coal and others. The high specific surface area of more than 1000 m^2/g can be achieved in two ways. Either additives are used to avoid sintering of the carbon particles during the burning process and are removed after burning. Or the carbon is activated after the burning process by water vapor, air or carbon dioxide containing gas at 700°C-900°C in order to etch pores into the carbon material.[27] Thus, activated carbon possesses an open and rather irregular porosity compared to MOFs. A special variant of a carbon material is the carbon molecular sieve (CMS). It is also maintained by burning organic raw materials but as the process is more controlled, CMSs show a more defined porosity and structure. The first CMSs were fabricated in the 1960s and possessed pore sizes between 4 Å-6 Å.[28] Since that

great efforts have been done in order to control the pore size accurately either by selecting suitable precursors or post-synthetic pore size modification.[29] A novel way of pore size control is templating, which is especially used for mesoporous CMSs.[30] For this process a porous structure, like a silica molecular sieve, is used as a template. The pores of the template are filled with a solution, containing the carbon precursor and a catalyst if necessary. Heating the filled template to more than 1000 K burns the precursor to carbon. Afterwards the remaining and still intact template is etched off.[30]

Summing up the discussion about porous materials, one can state that MOFs are remarkably superior to the anterior porous structures. MOFs possess a defined uniform pore size in contrast to activated carbons. Further the pore size and pore structure in MOFs is tunable for different applications whereas in zeolites the pore size cannot be controlled by choice of the precursor and the pore structure is restricted by the zeolite geometry. Additionally, zeolites are brittle and have to be synthesized at fairly extreme conditions, i.e. high temperature and pressure. In contrast MOFs can be synthesized under rather mild conditions, i.e. ambient pressure and moderate temperatures of the solution. The novel porous structures like the COFs also allow precise control of the structure and the synthesis conditions are similar to those of MOFs but small pores are hardly achievable. ZIFs are the materials most similar to MOFs. They are synthesized under mild conditions and small pores can be realized. Their mechanical properties are also rather similar to those of MOFs; in particular both can exhibit flexibility. [23,31]

2.2. Quantum sieving

Quantum sieving is a phenomenon separating gaseous isotope mixtures by cryogenic adsorption in nanoporous structures. It is characterized by preferred adsorption and faster diffusion of the heavier isotope with respect to the lighter one. This separation mechanism was first proposed by Beenakker[10] who also introduced the term "quantum sieving". This term combines the cause of this separation, i.e. quantum effects, and the separation mechanism, which is a sieving process.

For the discussion below it is important to note that for data obtained with pure gases the separation performance of a material is estimated as the molar ratio of the deuterium uptake to the hydrogen uptake, i.e. $n(D_2)/n(H_2)$. The term "selectivity" corresponds to the adsorbed $n(D_2)/n(H_2)$ ratio in the presence of a 1:1 isotope mixture and has only been attempted in theoretical predictions up to now.

2.2.1. Phenomenological aspects

Quantum sieving only occurs if the pore is small enough to quantize the motion of the adsorbed molecule at least in one dimension. The latter is the case if the following equation is fulfilled for a molecule adsorbed in a cylindrical pore[10]

$$d - \sigma \approx \lambda. \qquad (2.1)$$

In the equation above d is the pore diameter, σ is the size of the molecule assumed to be a hard sphere and λ is the de Broglie wavelength of the molecule. The zero-point energy (ZPE) of the adsorbing molecule strongly increases with decreasing pore size (see Figure 2.6).

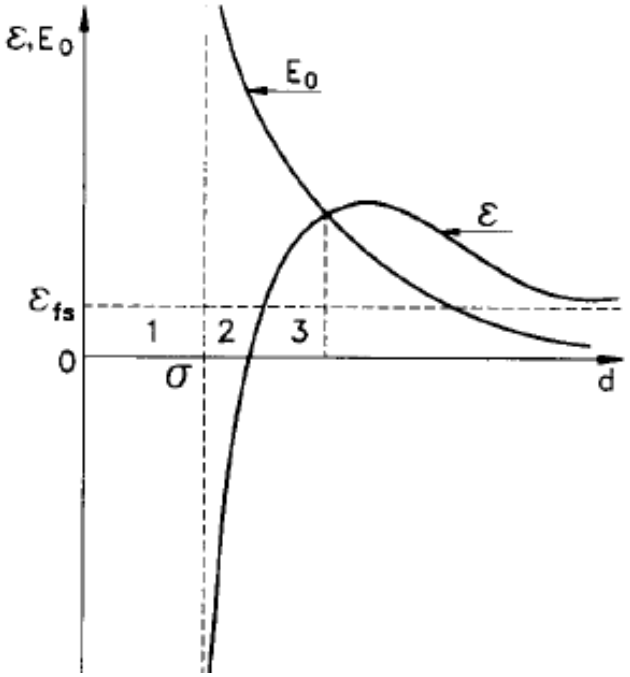

Figure 2.6: Zero-point energy E_0 and the well-depth ε as a function of pore size. The ZPE increases with decreasing pore size and converges to zero for larger pores. Three regions are marked in the plot. In region 1 no adsorption occurs as the radius of the molecule is larger than the pore radius. In region 2 the zero-point energy overcompensates the well-depth. Therefore the free gas molecules encounter an energy barrier and the gas density will be determined by a Boltzmann factor (see equation (2.3)). Sector 3 corresponds to the region where quantum sieving occurs.[10]

In Figure 2.6 the well depth, representing the interaction energy of the adsorbing molecule with the pore walls, and the ZPE of the adsorbing molecule are plotted versus the pore size. The adsorption is exponentially dependent on the difference between these two quantities according to equation (2.3). The well depth is negative for pores that are just slightly larger than the gas molecules which therefore feel electrostatic repulsion of the electron shells when approaching the pore channel. For large pores the well depth converges to a constant value equal to the flat surface ε_{fs} as the curvature of the pore walls becomes marginal. The ZPE converges to zero for large pores and increases drastically with decreasing pore size. According to the courses of the two quantities $\varepsilon(r)$ and $E_0(r)$, one can distinguish between three regions concerning the adsorption processes. In region 1 the size of the molecule exceeds the pore size and therefore adsorption is impossible. In region 2 the free gas molecules encounter a penetration barrier as the ZPE overcompensates the well depth. The activation barrier can only be overcome by thermal excitation. Therefore the gas density in the channel is determined by a Boltzmann factor as given in equation (2.3). Quantum sieving

only occurs in region 3. The increasing ZPE with decreasing pore size is directly related to the quantized motion of a molecule adsorbed in a nanopore. For the model system of a cylindrical pore, the molecular motion along the axial direction is free but quantized in radial direction due to the restricted radial dimension.[10] Consequently the energy levels of the molecule are quantized and they are inversely proportional to their mass as well as the difference between pore size and molecular size, i.e.[10]

$$E_i = \frac{2\gamma_i^2 \hbar^2}{m(d-\sigma)^2} \qquad (2.2)$$

where m is the particle's mass and γ_i are zeros of the Bessel function. The density of the particle in the pores or channels is dependent on E_i as denoted in the equation below[10]

$$n = n_v \frac{\pi}{4}(d-\sigma)^2 \sum_i \exp\left(\frac{\varepsilon - E_i}{k_B T}\right) \qquad (2.3)$$

where n_v is the density of the particle in the gas phase outside the framework, k_B is Boltzmann's constant and T is the absolute temperature. From this equation one can see that the densities of the isotopes in the channel are dependent on their energy values in the pore and therefore on their mass (see equation (2.2)). Owing to the higher mass, the energy of the heavier isotope is lower and therefore its density in the channel will be increased. If both isotopes only occupy the ground state and the well depth is the same for both isotopes, their density ratio in the channel pores can be calculated by[10]

$$\alpha = \frac{n_1}{n_2} = \exp\left(\frac{E_{01} - E_{02}}{k_B T}\right) \qquad (2.4)$$

where n_1 and n_2 as well as E_{01} and E_{02} are the density and energy of isotope 1 and 2 in the channel pore, respectively. The equations (2.3) and (2.4) show that the densities of two isotopes in a channel pore vary if the zero-point energy cannot be neglected with respect to the well depth which is only the case in small pores. Additionally, the ZPE only determines the molecular energy at cryogenic temperatures, strictly speaking at 0 K. At higher temperatures higher degrees of freedom, i.e. the rotation, are activated. The molecule's energy is then given by $3/2 \cdot k_B T$. Therefore, quantum sieving only occurs at sufficiently low temperatures.

It is important to note that equation (2.3) is only valid for moderately low temperatures (~77 K) because the Maxwell-Boltzmann statistics were applied. At low temperatures the bosonic nature of the para-hydrogen is not well accommodated by the Maxwell-Boltzmann statistics and therefore requires the Bose-Einstein statistics.

The calculations performed by Beenakker based on the pore size dependent zero-point energy model can be visualized and the mathematical procedure can be understood if one returns to basic quantum mechanics. There the adsorbed molecule can be considered as a particle in a box, i.e. it is treated wavelike. Its energy can be calculated for a one-dimensional box by

$$E_n = \frac{n^2 h^2}{8mL^2} \qquad (2.5)$$

where E_n is the energy of the particle, n is an integer characterizing the particle's energy level, h is Planck's constant, m is the mass of the particle and L is the length of the box. If the pore size is close to the molecular size of the adsorbed gas, only one molecule is adsorbed per pore. Thus, only one particle resides in the box and therefore occupies the ground state at low temperatures. The wavelength of such a particle in the ground state is $\lambda / 2$ and its corresponding energy term can be written as

$$E_0 = \frac{h^2}{2m\lambda^2}. \qquad (2.6)$$

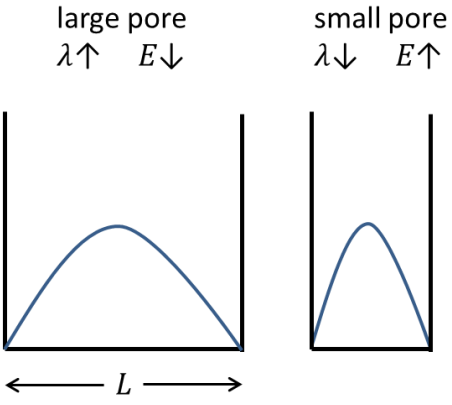

Figure 2.7: Illustration of the pore size dependence of the zero-point energy applying the model of a wavelike particle in a one dimensional box. Obviously, with increasing pore size the wavelength increases, leading to a lower zero-point energy value.

It is important to note that hydrogen and deuterium must possess the same wavelength as this quantity is determined by the length of the box, i.e. the pore size. The formalism described above for a wave-like particle in a one-dimensional box has been performed by Beenakker for a cylinder.

For most isotopes like the uranium isotopes the mass difference and therefore the difference in ZPE is only a few percent. But for the hydrogen isotopes the difference is significant as deuterium possesses twice the mass of hydrogen and therefore the ratio between the zero-point energies is $\sqrt{2}$.[32]

What remains to be discussed in details are the inverse kinetics of the quantum sieving phenomenon, i.e. the reason why the heavier isotope is not only adsorbed in larger amounts but also diffuses faster through the porous framework with respect to the lighter one. In order to deeply understand the kinetic sieving, one has to analyze the quantum sieving phenomenon on a more complex theoretical basis as done by Kumar.[33] Kumar and Bhatia performed molecular dynamic simulations in order to study H_2/D_2 quantum sieving in zeolite rho. Quantum effects were incorporated in the calculations by Feynman-Hibbs corrections (see chapter 2.2.2 for details on this method). The most important results and conclusions are shown in Figure 2.8.

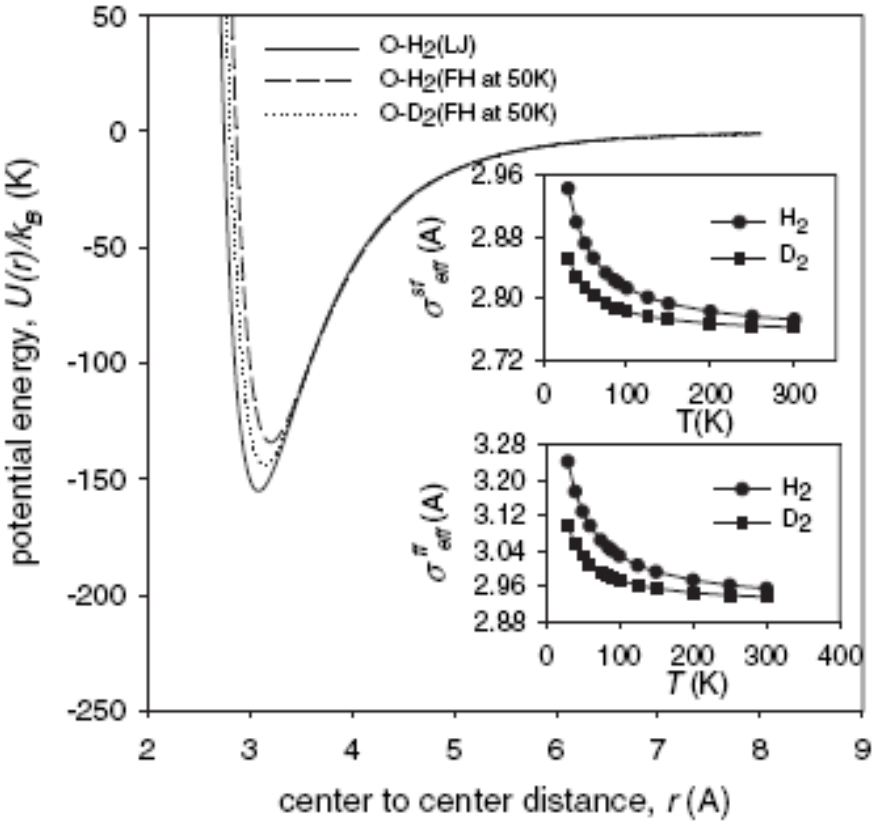

Figure 2.8: Potential energy curves calculated for hydrogen without quantum effects (LJ potential) and for hydrogen and deuterium with quantum effects (FH potential) at 50 K. The insets represent the size parameters for the solid-fluid and fluid-fluid-interaction, respectively.[33]

The classical adsorption potential (see also chapter 2.2.2), i.e. the Lennard-Jones potential, exhibits a deeper minimum compared to the Feynman-Hibbs potential. Kumar found that this change in the potential curve yields an increase in effective size parameters of the solid-fluid and the fluid-fluid interaction (Figure 2.8) sometimes referred to as "quantum mechanical swelling" (Figure 2.9). As hydrogen is lighter compared to deuterium, it is affected more strongly by quantum effects and its swelling is more pronounced. According to the larger effective radius, hydrogen diffuses more slowly through the framework of zeolite rho.

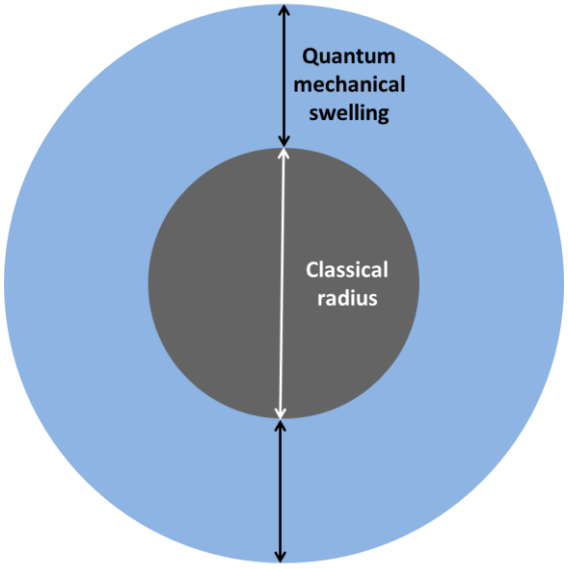

Figure 2.9: Hydrogen and deuterium suffer an increase in effective size when quantum effects occur. This is termed quantum mechanical swelling. As hydrogen is lighter than deuterium, it suffers a stronger swelling.

The publications of Kowalczyk based on path-integral Monte Carlo simulations also address the theoretical insights into the quantum sieving phenomenon, thereby simultaneously combining an explanation for an enhanced uptake and a higher diffusivity of the heavier isotope.[34-38] In principle, Kowalczyk corrects the classical thermodynamic and kinetic quantities by quantum fluctuations. In quantum mechanics, the kinetic energy is proportional to the curvature of the wave function Ψ according to the Schrödinger equation:

$$\mathrm{H}\Psi = \mathrm{E}\Psi \rightarrow -\frac{\hbar^2}{2\mathrm{m}}\nabla^2\Psi + \mathrm{V}\Psi = \mathrm{E}\Psi \qquad (2.7)$$

where H is the Hamiltonian, E is the total energy, $\hbar$ is reduced Planck constant, ∇^2 is Laplace operator and V is the potential energy.

Owing to these quantum kinetic contributions, both isotopes are accelerated to higher velocities if adsorbed in a nanoporous structure but hydrogen possesses the higher velocity due to its lower mass. The kinetic energy of both isotopes and the corresponding difference in kinetic energy are shown in Figure 2.10. The smaller the pore, the larger is the difference in kinetic energy for the isotopes; thereby increasing the selectivity (see Figure 2.10).

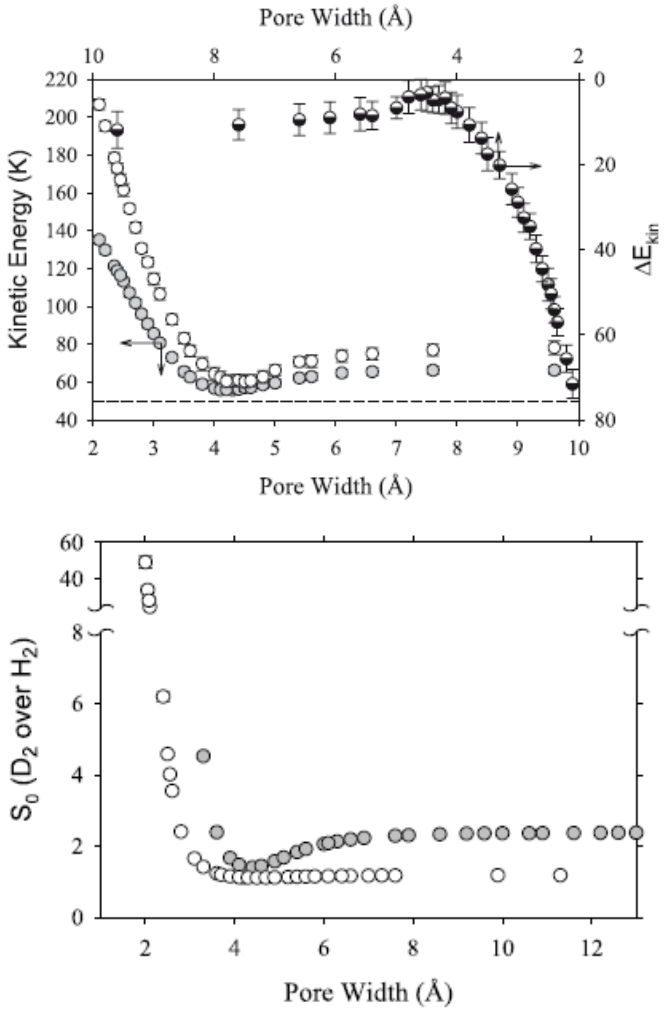

Figure 2.10: Kinetic energy values of hydrogen and deuterium as well as their difference ΔE_{kin} as a function of pore size computed for an infinitely long carbon slit pore at 33 K and zero-coverage (top) and the resulting equilibrium selectivity (bottom).[36] On the top white and gray circles represent hydrogen and deuterium, respectively. The horizontal dashed line corresponds to the classical kinetic energy at 33 K. On the bottom, white and grey circles correspond to 77 K and 33 K, respectively.

The quantum kinetic contributions affect the thermodynamics and the kinetics of adsorption. From a thermodynamic point of view, the sticking probability of hydrogen on the surface and its enthalpy of adsorption are decreased which is in good agreement with the calculations of Kumar. Concerning the diffusion, the larger kinetic energy of hydrogen leads to an enhanced delocalization. The delocalization is directly related to the probability density. A larger degree of delocalization enlarges the area where the quantum particle can be found, i.e. the probability density is broadened. An estimation of the delocalization is possible based on the momentum (p)-position (x) uncertainty principle of Heisenberg

$$\Delta x \cdot \Delta p \geq h. \qquad (2.8)$$

The lower-boundary value of the delocalization χ can be roughly estimated by[35,39]

$$\chi \equiv \langle (\Delta x)^2 \rangle^{1/2} \approx \frac{h^2}{\langle (\Delta p)^2 \rangle^{1/2}} \approx \left(\frac{\hbar^2}{m k_B T} \right)^{1/2}. \qquad (2.9)$$

Applying equation (2.9), the delocalization for hydrogen and deuterium molecules at 40 K and 77 K are calculated (see Table 2.1). As equation (2.9) is only a very rough estimation, the calculated values of delocalization should just be used for a qualitative comparison between the two isotopes at different temperatures. The delocalization of the lighter hydrogen is larger for both temperatures, suggesting that it is more strongly affected by quantum effects. But at higher temperature the delocalization difference between the isotopes is smaller. Stronger localization with rising temperatures indicates that the particles tend to behave classically.

Table 2.1: Estimated delocalization values for hydrogen and deuterium at 40 K and 77 K.

Temperature	**40 K**	**77 K**
$\chi(H_2)$ **[Å]**	**0.78**	**0.56**
$\chi(D_2)$ **[Å]**	**0.55**	**0.40**

Basically, the delocalization described by Kowalczyk and quantum mechanical swelling described by Kumar explain the same phenomenon. After consideration of the works from both authors, it is possible to understand the faster diffusion of the heavier isotope. The diffusion retardation of the lighter isotope is caused by the larger increase in effective size

due to quantum mechanical swelling/delocalization which enlarges the scattering cross section, thereby increasing the scattering probability.

2.2.2. Treatment of quantum sieving in theoretical physics

In theoretical physics the quantum sieving phenomenon is mainly addressed by path integral molecular dynamics simulations (PIMD) or grand canonical Monte Carlo simulations (PIMC) applying quantum corrected interaction potentials. The basic equations are presented in this subchapter.

The classical interaction potential for structureless spherical particles is given by the Lennard-Jones potential (LJ potential)

$$U_{LJ}(r) = 4\varepsilon\left[\left(\frac{\Theta}{r}\right)^{12} - \left(\frac{\Theta}{r}\right)^{6}\right] \qquad (2.10)$$

where ε is the depth of the potential well, Θ corresponds to the distance at which the potential becomes zero and r is the distance of the interacting particles.

Considering quantum particles instead of classical particles, one has to apply the Feynman-Hibbs approach where the quantum particle is treated as a Gaussian wave packet of width[40]

$$w = \frac{\hbar}{\sqrt{12\mu k_B T}} \qquad (2.11)$$

where μ is the reduced mass. Introducing the Gaussian wave packet and averaging over the LJ potential yields the effective Feynman-Hibbs potential. Exemplarily the quadratic Feynman-Hibbs potential is given below[41,42]

$$U_{FH} = U_{LJ}(r) + \frac{\hbar^2}{24\mu k_B T}\left[U''_{LJ}(r) + \frac{2U'_{LJ}(r)}{r}\right] \qquad (2.12)$$

where U''_{LJ} and U'_{LJ} are the derivatives of the LJ potential. Sometimes also higher order derivatives are used for calculations.[33,43]

The Feynman-Hibbs potential is needed to correct the isosteric heat of adsorption by quantum fluctuations[40,44]

$$q = \frac{2}{5}k_B T - \frac{\langle EN\rangle - \langle E\rangle\langle N\rangle}{\langle N^2\rangle - \langle N\rangle^2} \qquad (2.13)$$

where q is the isosteric heat of adsorption, N is the number of adsorbed molecules and E is the total energy, i.e. the sum of potential and kinetic energy.

The total energy can be calculated by applying the Feynman-Hibbs potential as follows[40]

$$E = \underbrace{\frac{3}{2}Nk_B T}_{\substack{\text{classical}\\ \text{kinetic}\\ \text{energy}}} + \underbrace{\sum_{i<j}^{N}\beta\frac{dU_{FH,ij}^{ff}}{d\beta} + \sum_{i}^{N}\beta\frac{dU_{FH,i}^{sf}}{d\beta}}_{\substack{\text{quantum corrections}\\ \text{of kinetic energy}}} + \underbrace{\sum_{i<j}^{N}U_{FH,ij}^{ff} + \sum_{i}^{N}U_{FH,i}^{sf}}_{\text{potential energy}} \qquad (2.14)$$

where β is equal to $1/k_B T$, U_{FH}^{ff} and U_{FH}^{sf} correspond to the fluid-fluid and the solid-fluid potentials, respectively. In equation (2.14) the first term is equal to the kinetic energy of a classical particle, the second and third term correspond to the quantum corrections of the kinetic energy whereat the forth and fifth term are potential energies. For low gas pressure the fluid-fluid interaction can be neglected (zero pressure limit).

When a particle passes a narrow entrance in order to get into a pore, it has to pass a transition state, i.e. it has to overcome a state of higher energy. The rate of passing the transition state can be calculated by applying the transition state theory (TST). The corresponding rate is calculated by[45]

$$k = \frac{k_B T}{h}\frac{Q^{\dagger}}{Q}\exp\left(-\frac{E_b}{k_B T}\right) = \frac{k_B T}{h}\frac{Q^{\dagger}}{Q_{trans}Q_{rot}}\exp\left(-\frac{E_b}{k_B T}\right) \qquad (2.15)$$

where E_b is the height of the energy barrier, $Q^{\dagger}$ is the partition function of the transition state, Q_{trans} and Q_{rot} are the translational and rotational partition functions, respectively. In equation (2.15) the term containing the partition functions can be regarded as an entropic barrier as the degrees of freedom are restricted in a very small pore or a narrow opening. The exponential term corresponds to an enthalpic barrier.

From equation (2.15) it is obvious that the restriction in the rotational degrees of freedom plays a crucial role for the transition rate and therefore for the selectivity.

The selectivity is defined as

$$S(1/2) = \frac{x_1 / x_2}{y_1 / y_2} \qquad (2.16)$$

where x and y refer to the mole fractions of species 1 and species 2 in the adsorbed phase and the gas phase, respectively.

Assuming uncoupled rotational and translational degrees of freedom, one can calculate the selectivity for the zero-pressure limit S_0 according to the following equation[46,47]

$$S_0(1/2) = \frac{Q_2^{free} Q_1}{Q_1^{free} Q_2} = \frac{m_2 Q_2^{free-rot}}{m_1 Q_1^{free-rot}} \left[\frac{\sum_i \exp\left(\frac{-E_1^i}{k_B T} \right)}{\sum_i \exp\left(\frac{-E_2^i}{k_B T} \right)} \right] \qquad (2.17)$$

where Q^{free} is the molecular partition function of an ideal gas, $Q^{free-rot}$ is the free rotor partition function, Q is the partition function in the adsorbed state and E^i corresponds to the energy levels in the adsorbed state. The notations 1 and 2 correspond to the two isotopes.

The above discussed simulations require great computational efforts and the interpretation of the resulting data is non-trivial. In addition they are classical simulations with modified potentials rather than a quantum mechanical description of the system. There is a less laborious and more straight-forward alternative approach to yield the free adsorption energy as well as the gas uptake taking into account the quantized translational motion of a molecule adsorbed in a nanoporous framework. The alternative procedure is the so-called quantized liquid density functional theory (QLDFT).[48-50] In the following the principal formalism of the QLDFT approach will be described.[48] For a featureless particle of an ideal gas, the stationary Schrödinger equation in a time-independent potential induced by the host framework can be by written as in equation (2.7). Solving the Schrödinger equation numerically and assuming periodic boundary conditions yields the spectrum of eigenstates Ψ_i and the corresponding energies ε_i according to

$$q = \sum_i \exp\left(-\frac{\varepsilon_i}{k_B T} \right). \qquad (2.18)$$

The corresponding density matrix yields the probability distribution

$$\rho(r,r') = \frac{1}{q}\sum_i \Psi_i^*(r)\Psi_i(r)\exp\left(-\frac{\varepsilon_i}{k_B T}\right) \qquad (2.19)$$

where Ψ_i^* is the conjugate complex solution. Comparing the partition function of the adsorbed molecule to the free state, yields the adsorption free energy ΔF

$$\Delta F = -RT\ln\frac{q}{q_{free}} \qquad (2.20)$$

where R is the gas constant.

The storage capacity is equal to the equilibrium constant

$$K_{eq} = \frac{q}{q_{free}}. \qquad (2.21)$$

Thus, for an ideal gas, the storage capacity is only a function of temperature but independent of gas pressure. The QLDFT approach can also be carried out for a real gas. However, as quantum sieving only occurs at low pressures, the reader is referred to the corresponding literature if interested in the QLDFT approach for high pressures. [48-50]

2.2.3. Experimental approaches and measured materials

Experimentally, quantum sieving in nanoporous frameworks is investigated mainly by volumetric isothermal pure gas adsorption studies of hydrogen and deuterium. The experiment is performed as follows. The sample is cooled in a vacuum chamber to the temperature of the adsorption study (usually 77 K). A reservoir volume is filled with hydrogen or deuterium gas up to a certain pressure. Afterwards the valve between reservoir and the evacuated sample chamber is opened enabling gas expansion into the sample chamber. When the sample adsorbs gas, the pressure will not only decrease due to the volume expansion but additionally by the adsorbed amount. Thus, the additional pressure decrease is directly proportional to the adsorbed amount of gas. Consequently, the volumetric isothermal pure gas adsorption measurements yield the equilibrium uptake of the corresponding isotope as a function of adsorption temperature and gas pressure. Based on these pure gas data the separation performance of the considered framework is given by the molar ratio between the deuterium and hydrogen uptake, i.e. $n(D_2)/n(H_2)$. Thus, the isotherm measurements mainly address the preferred uptake of the heavier isotope. Restricted information about the adsorption kinetics, i.e. the adsorption rate constants, is also available in isotherm measurements. However, the isothermal adsorption study is

restricted to the use of only one type of isotope per experiment. Sometimes the selectivity is calculated on the basis of the pure gas adsorption data by ideal adsorption solution theory (IAST).[51-53]

Diffusion data can be obtained by fitting the elastic peak obtained in a quasi-elastic neutron scattering experiment (QENS). The larger the broadening, the higher the diffusivity.[54]

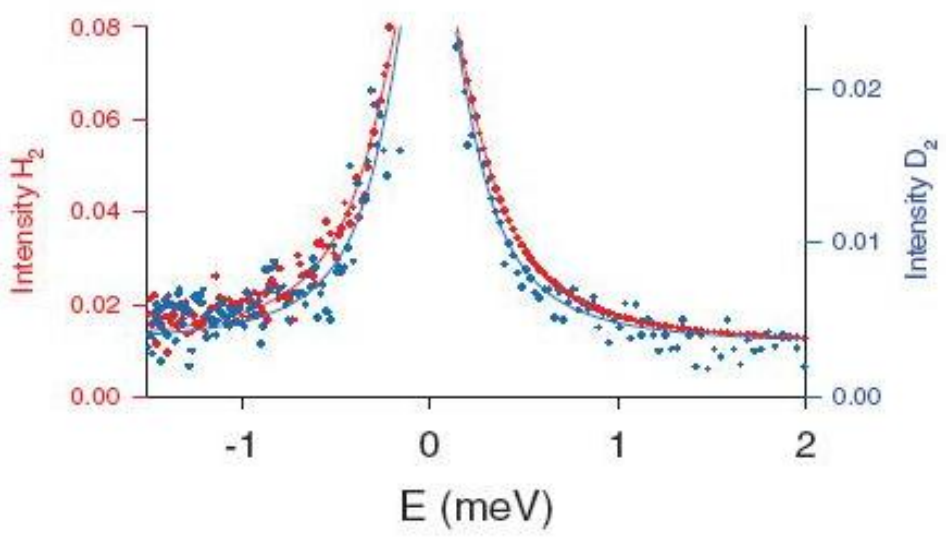

Figure 2.11: QENS spectrum of Takeda 3A obtained at 120 K after loading 0.5 mmol/g hydrogen and deuterium. Circles and lines correspond to measured values and the fitted curves, respectively.[54]

Hydrogen scatters purely inelasticly whereas deuterium scatters elastically and inelasticly. Therefore, only the self-diffusivity is measurable for hydrogen but both, self-diffusivity and transport diffusivity, can be obtained for deuterium.[54] In case of low loading pressure, transport and self-diffusivity can be considered equal.

Up to now, only a very limited number of publications present experimental data about the quantum sieving effect in porous materials. The following section will present selected literature data directly related to this work. The presented data are measured on different porous zeolites, carbon materials and MOFs.

Zhao et al. measured pure gas hydrogen and deuterium adsorption in Takeda 3A at 77 K up to 100 kPa (see Figure 2.12).[55] The deuterium uptake exceeds the hydrogen uptake in Takeda 3A over the whole measured pressure range. Only very slight deviations of the desorption curves from the adsorption curves are visible, indicating full reversibility of the adsorption process. According to the error bars, the calculated D_2/H_2 ratio seems to be

constantly below 1.07 over the measured pressure range. Also the adsorption/desorption kinetics have been presented in this work clearly revealing higher rate constants of adsorption and desorption for deuterium.

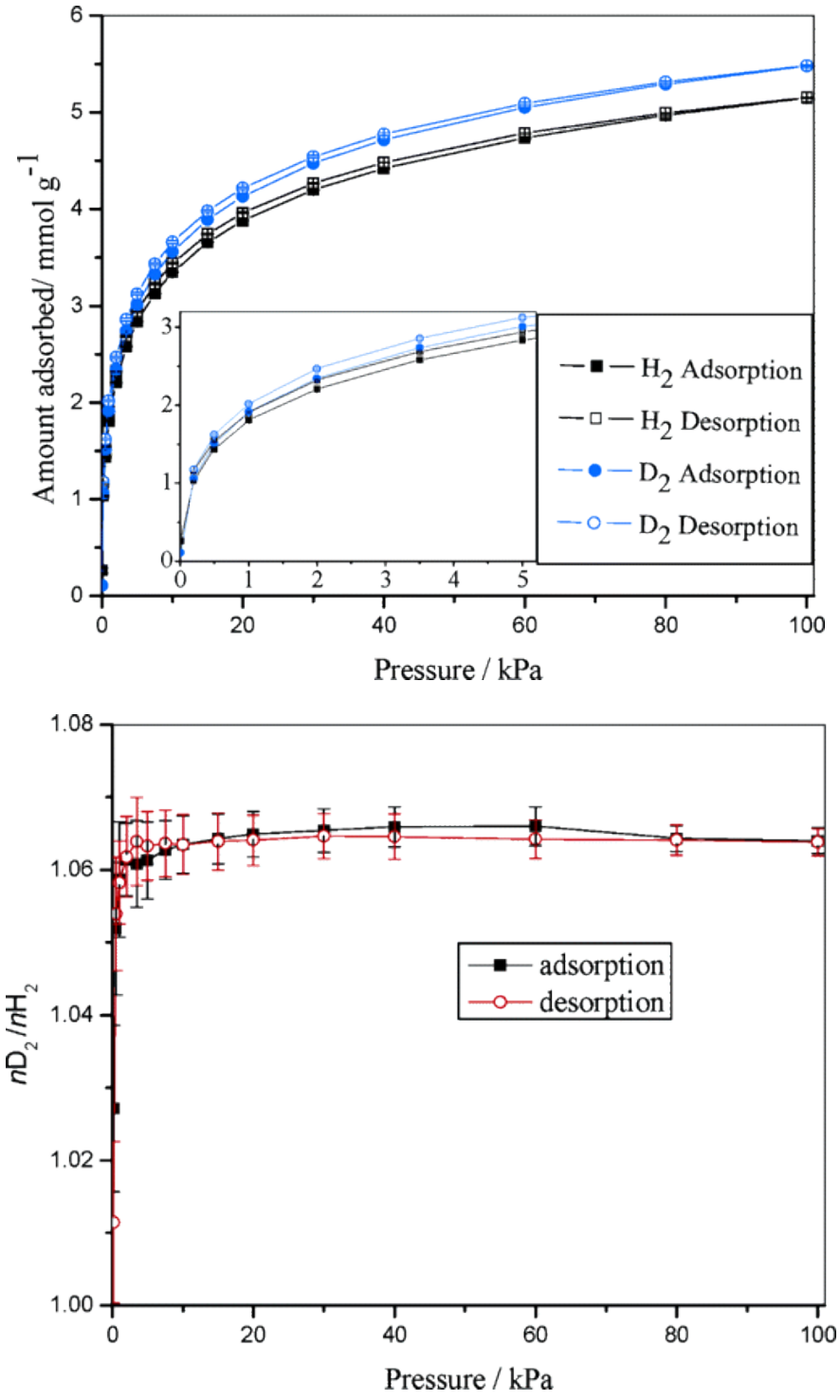

Figure 2.12: Hydrogen and deuterium adsorption and desorption curves measured for Takeda 3A at 77 K (top) and the corresponding isotope ratio calculated on the basis of the pure gas isotherms (bottom).[55]

Hydrogen and deuterium diffusion in Takeda 3A was also addressed experimentally by quasi-elastic neutron scattering.[54]

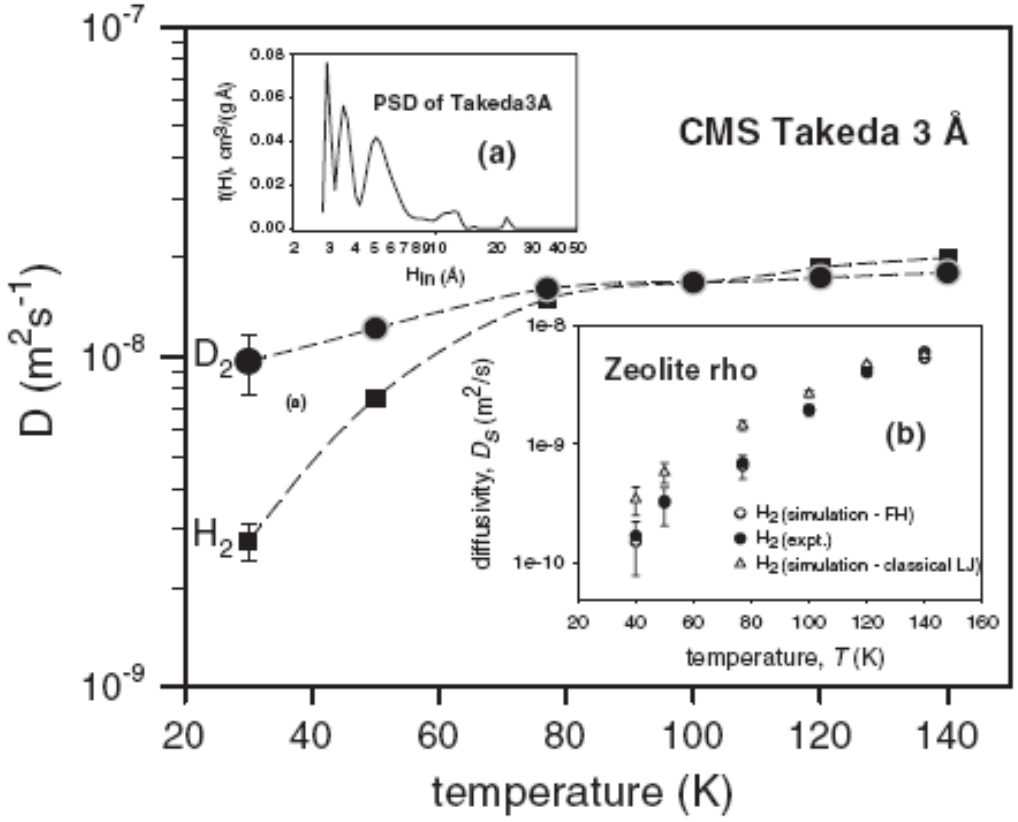

Figure 2.13: Diffusion coefficients of hydrogen and deuterium for different temperatures obtained by QENS measurements after loading 0.5 mmol/g. The inset on the top presents the results of the pore size analysis for the investigated Takeda sample based on carbon dioxide adsorption. The inset on the bottom contains experimental and MD based diffusivity of hydrogen in zeolite rho for different temperatures.[54]

The QENS measurements (see Figure 2.13) yield a crossover in the diffusivity values of hydrogen and deuterium at 100 K. Below 100 K deuterium diffuses faster and above 100 K hydrogen diffuses faster in Takeda 3A. The inset on the bottom of Figure 2.13 compares experimentally obtained hydrogen diffusion data in zeolite rho to theoretically obtained values calculated in case of purely classical interaction (Lennard-Jones potential) and in the presence of quantum effects (Feynman-Hibbs potentials). Below 120 K the classical potential yields larger hydrogen diffusivity than the experimental values whereas the Feynman-Hibbs potentials lead to diffusivity values comparable to the experimental values. With increasing temperature the diffusivity values by classical potentials converge the experimental values. At 140 K the diffusivity value calculated applying the classical potential yields the

experimental value. Thus, quantum effects in zeolite rho are measured below 140 K and the influence of quantum effects induced retardation of hydrogen diffusion increases with decreasing temperature.

Chu et al. performed volumetric pure gas adsorption measurements at 77 K on a set of microporous and mesoporous samples (mainly zeolites). The obtained equilibrium uptakes and rate constants are plotted versus the pore size (see Figure 2.14).

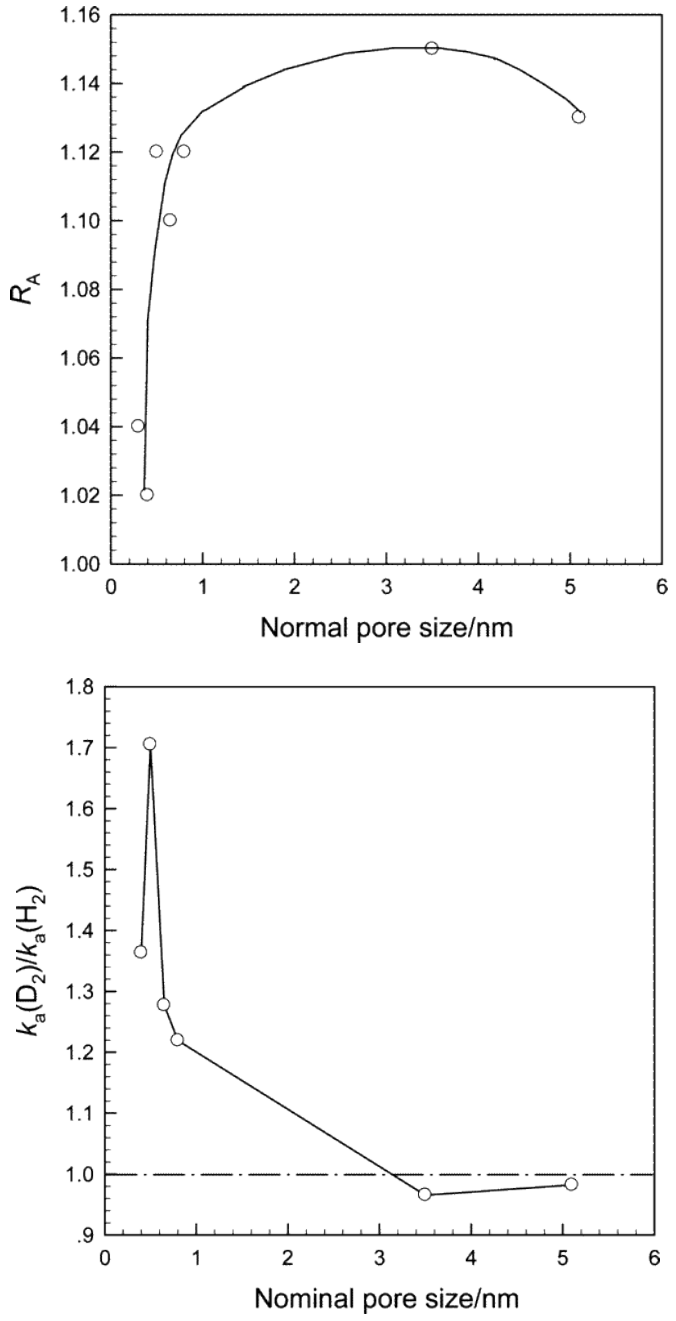

Figure 2.14: Equilibrium D_2/H_2 adsorption ratio as a function of pore size obtained at 0.1 MPa (top) and the adsorption rate ratio obtained after initial loading of 0.022 MPa (bottom).[56]

The maximum D_2/H_2 ratio is observed for pore sizes in the range of 30 Å to 40 Å. However the largest ratio of the adsorption rate constants is found for pore sizes below 10 Å. Thus, kinetic isotope separation requires pore sizes of less than 10 Å. However, isotope effects of non-kinetic origin also occur for pores larger than 10 Å.

Noguchi et al. measured H_2 and D_2 adsorption isotherms on a Cu-MOF called CuBOTf at 77 K and 40 K and compared the experimental data to quantum-corrected GCMC simulations.[53] The CuBOTf framework possesses channel pores with cross section of 2x2 Å² and 8.7x8.7 Å². Hydrogen isotope adsorption only occurs in the larger pores as the kinetic diameters of hydrogen and deuterium exceed the diameter of the smaller channels. The simulated adsorption isotherms applying the classical potentials yield larger uptake values compared to the quantum corrected simulation which fit the experimental curves acceptably. The lower uptake compared to classical adsorption clearly suggests that the adsorption is influenced by quantum effects. The adsorption isotherms at 40 K (see Figure 2.15) exhibit a hysteresis indicating that the desorption is kinetically hindered. The authors could also show pronounced kinetic limitations of the adsorption process as the establishment of the equilibrium pressure takes 6-10 h and 2-3 h for hydrogen and deuterium, respectively. Based on the measured and simulated pure gas isotherm data, the selectivity in the presence of a 1:1 isotope mixture is estimated applying IAST, i.e. assuming no interaction between the adsorbed species and the same chemical potential of an isotope in the gas phase and the adsorbed phase. These calculations yield selectivity values of 1.2 and 2.6-5.8 at 77 K and 40 K, respectively over the pressure range from 10^{-5} to 10^{-3} MPa. However, the selectivity values are semi-experimental and the calculations are based on assumptions and simplifications not necessarily fulfilled in the presence of quantum effects.

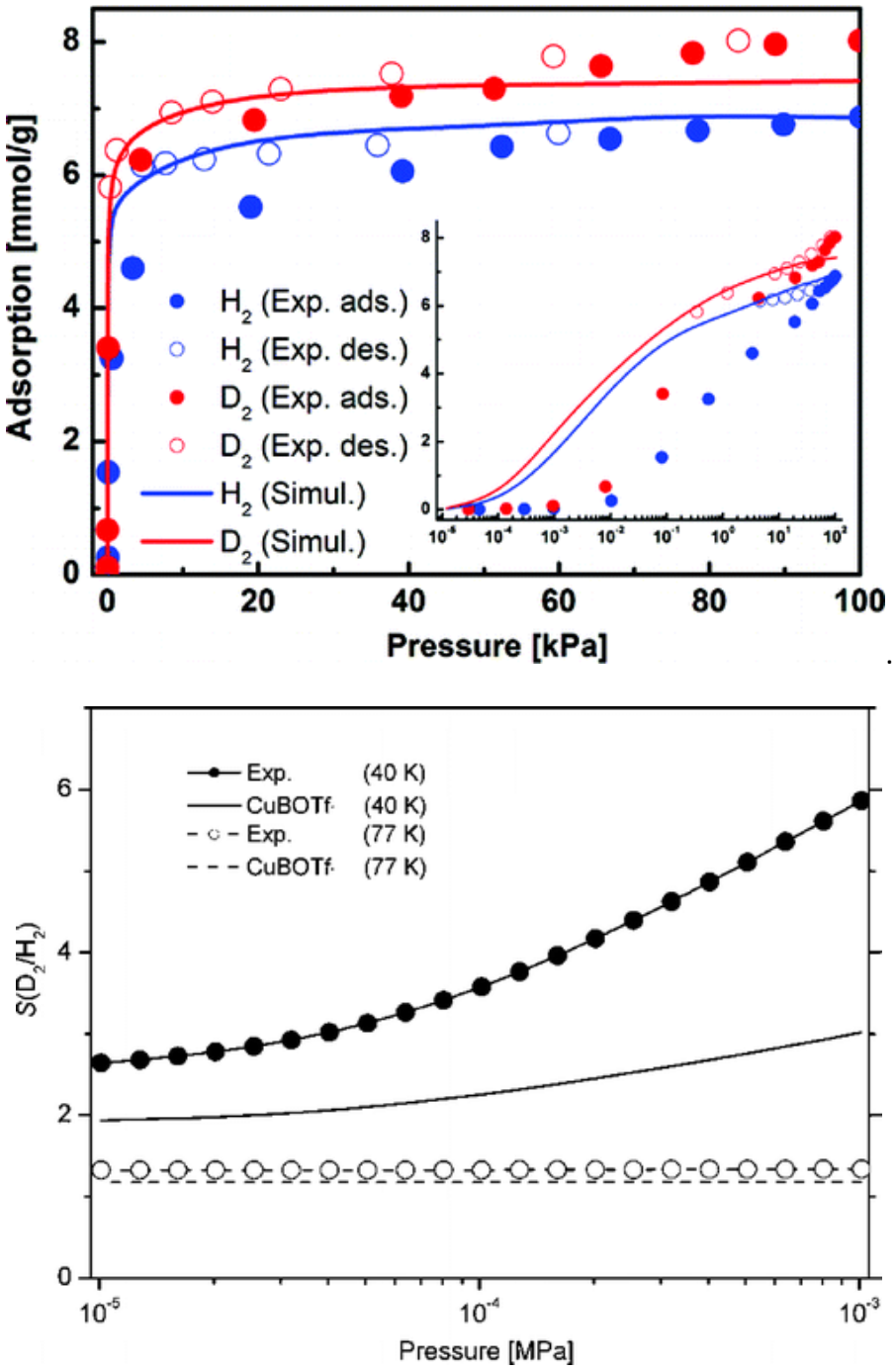

Figure 2.15: Hydrogen and deuterium adsorption isotherm measured at 40 K and simulated by GCMC (top) as well as the selectivity values at 40 K and 77 K obtained applying IAST (bottom). The circles and the lines represent experimental and simulated values, respectively.[53]

Summing up the literature, one can state that the published experimental results have been obtained after pure gas loading and therefore the separation capability is usually estimated on the basis of these pure gas adsorption data by the $n(D_2)/n(H_2)$ ratio. Isotope mixtures cannot be used in the isothermal adsorption experiments as just the total pressure but no partial pressures are registered. The only attempt to get separation data in the

presence of isotope mixtures is the semi-experimental approach of applying ideal adsorption solution theory (IAST) to the experimentally obtained low temperate adsorption isotherms. The neutron experiments yield valuable information about the isotope diffusion and therefore allow a direct observation of quantum kinetic effects. But it is not applicable as the standard method for large-scale sample investigations as the measurements are laborious and expensive.

2.2.4. Parameters influencing the selectivity

The experimentally or theoretically determined selectivity values depend on gas composition, adsorption temperature, gas pressure and pore structure. The influence of gas composition is not a matter of the quantum system rather than an effect of external operating conditions, i.e. there is no need to discuss this parameter. However, temperature, pressure and framework structure are directly related to the occurrence of quantum effects and therefore require further discussion.

The influence of temperature and pressure on the quantum effects of hydrogen adsorption is systematically studied in the three isoreticular frameworks IRMOF-1, IRMOF-10 and IRMOF-11 by Xu and coworkers applying GCMC simulations.[41] At 40 K the adsorption is dominated by quantum effects in all three frameworks, i.e. classical contributions are negligible. At 60 K the quantum effects still dominate the adsorption in the smallest pores (about 80% quantum contributions) whereas in IRMOF-1 and IRMOF-10 the adsorption can be considered 50% classical in nature. At 77 K quantum adsorption and classical adsorption contribute equally in the small-pore framework IRMOF-11. A more classical behavior of the particles is due to the decreasing significance of the quantum corrections with rising temperature according to equation (2.12) where the quantum correction terms of the effective Feynman-Hibbs potential are multiplied by the inverse temperature. Therefore, with increasing temperature the effective potential approaches the classical Lennard-Jones potential. The temperature dependent diffusivity measurement performed by Nguyen also evidences that the kinetic selectivity decreases with temperature reaching a value of 1 at approximately 100 K for the CMS Takeda 3A (see chapter 2.2.2).[54]

Xu finds a pressure dependence of constant selectivity value above atmospheric pressure and strong increase below atmospheric pressure.[41] Kowalczyk calculates the selectivity as a function of pressure for slit-shaped pores of different size at 77 K applying GCMC simulations.[36]

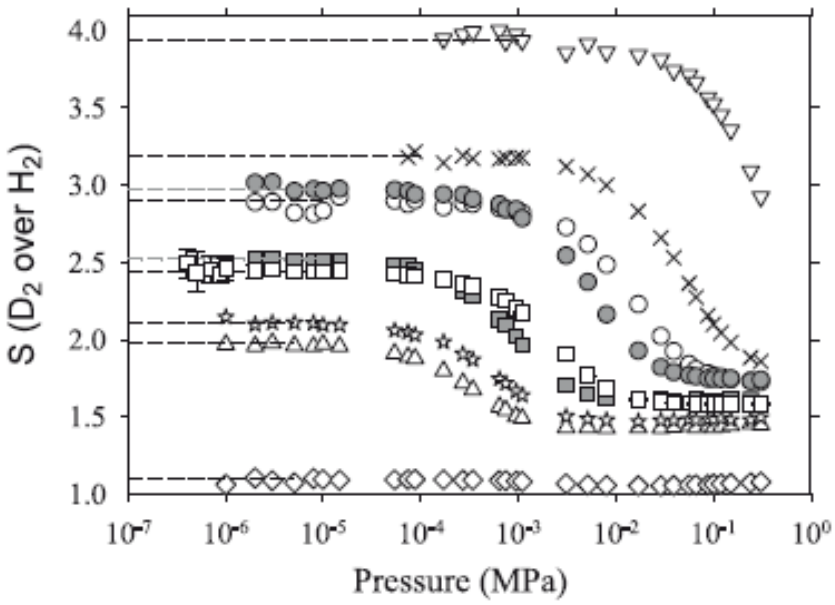

Figure 2.16: Selectivity as a function of pressure for a 1:1 isotope mixture at 77 K. The symbols imply slit pores of different size. The highest selectivity is found for a pore size of 2.6 Å (triangles up). The triangles down refer to a pore size of 2.2 Å. The curves between the two triangular ones correspond to pore sizes between 2.2 Å-2.6 Å. The diamond symbols reflect a pore size of 6.6 Å.[36]

A maximum selectivity is found at 2.6 Å which remains constant up to a maximum pressure of ~10^{-2} MPa. For the smaller pores the selectivity value is smaller and it drops at even lower pressures. For larger pores, i.e. in this case 6.6 Å, the selectivity remains at a negligible value independent of pressure. From the results obtained by Kowalczyk one can state that the selectivity is maximized for slit pores of ~3 Å in diameter. However, the selectivity value is only large in the mbar-range.

It is important to note that the selectivity is affected by the pore topology rather than the pore size because the pore topology determines the course of the potential in the pore. For example in square shaped pores, the potentials generated from four walls overlap, yielding a stronger solid-fluid potential compared to slit shaped pores of the same size where the potentials of only two pore walls overlap.[36] For H_2/D_2 separation in tubular shaped pores, a minimum value is found for a tube diameter of around 8 Å applying Monte Carlo simulations.[34] The pore size of minimum selectivity is only determined by the pore or channel geometry but not affected by the chemical composition of the tube. However, the absolute selectivity values are governed by the chemical nature of the tube because it determines the steepness of the potential well; thereby strongly influencing the selectivity.[34] The above discussed pores possess a simple geometry like tubes, slits or squares. However,

for many real structures, the channel size will vary along the channels or the pores have to be accessed via a narrow aperture, i.e. in real structures bottlenecks will occur. The publication of Hankel addresses the transport of hydrogen isotopes through cavities only accessible via a pore mouth applying TST.[45]

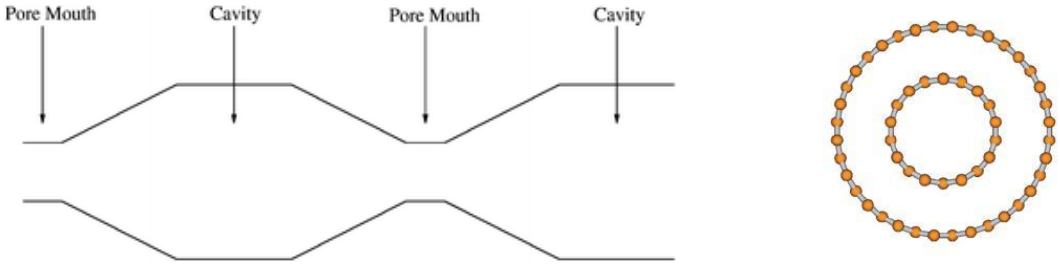

Figure 2.17: Model structure (CMS) of a cavity which is only accessible via a narrow pore mouth (left) and the corresponding test structure for the theoretical calculations (right).[45] Reproduced by permission of the Royal Society of Chemistry.

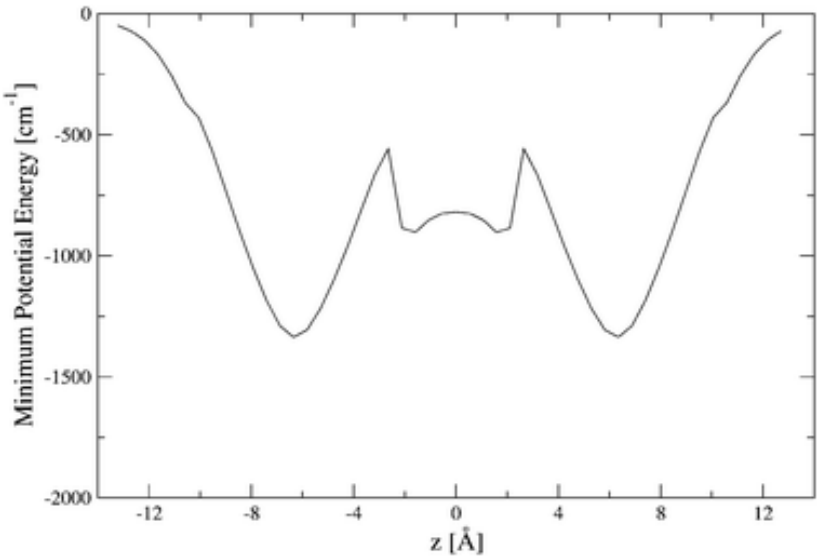

Figure 2.18: Minimum energy path of a hydrogen molecule entering the bottleneck from the gas phase and penetrating the cavity.[45] When the molecule approaches the structure it feels attractive forces. By approaching closer the molecule will also feel repulsive forces aligning the molecule parallel to the tube axis, yielding a barrierless approach. The minimum in energy path is associated with the molecule arranged in the pore mouth. When the molecule has passed the mouth, it will feel the restriction of its motion by the cavity walls, yielding a sharp peak in the energy profile. The molecule will now align along the pore walls corresponding to the mound around the zero position.[45] Reproduced by permission of the Royal Society of Chemistry.

The selectivity of this rather complex structure strongly depends on the coiling of the analyzed tube structure. The adsorbed molecules clearly tend to move along the tube walls

rather than passing along the center axis. Minimum energy is reached in the bottleneck assuming suitable orientation of the molecule in order to allow a barrierless approach.

For hydrogen and deuterium two spin isomers, namely ortho-form and para-form, exist. Both spin isomers coexist whereat their equilibrium ratio depends on temperature. Hydrogen consists of 75% and 0,2% ortho-H_2 at 300 K and 20 K, respectively. Deuterium consists of 66.7% and 97.8% ortho-D_2 at 300 K and 20 K, respectively.[57] However, the conversion is slow when the gas is cooled, leading to deviations from the equilibrium ortho/para ratios. The spin isomers differ in adsorption behavior, and they could be separated by the same quantum effects as H_2/D_2.[58-61] Ortho-H_2 and ortho-D_2 are more favorably adsorbed compared to para-H_2 and para-D_2. But according to the slow conversion, the spin isomer effects are not expected to be visible in most adsorption experiments. However, when the isomers are adsorbed, their conversion can be accelerated. This has also been observed for hydrogen adsorbed in MOFs where the metal centers act as spin catalysts; thereby promoting the spin conversion.[62,63] One can conclude that in the presence of spin catalysts which promote the conversion of both isotopes, the H_2/D_2 selectivity will be enhanced as deuterium will prevail in the more favorably adsorbed ortho-form whereas hydrogen will prevail in the less favorably adsorbed para-form.

2.2.5. Other ways of H_2/D_2 isotope separation

Hydrogen occurs in three isotopes: protium (~99.99%), deuterium (<0.02%) and tritium (10^{-15}%).[27] As isotopes behave chemically identical, they can only be separated by physical methods. In principal there are numerous techniques to separate hydrogen isotopes like cryogenic distillation[64], chromatography[65], thermal diffusion[66], electrolysis[67] and others. In cryogenic distillation the gas mixture is liquefied and afterwards the components are separated due to their different boiling temperature which is 20.39 K[68] for hydrogen and 23.65 K[68] for deuterium. In gas chromatography the gas mixture is transported by a carrier gas to a stationary phase in a separation column. As the dwell time in the stationary phase is different for the two isotopes, they can be separated at the end of the separation column. Thermal diffusion exploits the fact that in the presence of a temperature gradient the heavier component of a gas mixture diffuses to the colder place whereas the lighter molecules diffuse to the hot areas. Electrolysis is based on a faster discharge of light water compared to heavy water.

2.3. Thermal desorption spectroscopy (TDS)

2.3.1. Overview - The method and its applications

Thermal desorption spectroscopy (TDS), sometimes called temperature programmed desorption (TPD), is an analytical method to study desorption of gases from surfaces and from bulk. This offers information about catalysis,[69,70] surface defects[71], desorption kinetics[72], adsorption sites,[73,74] in some cases the nature of the adsorption process, i.e. physisorption or chemisorption,[75] and decomposition effects. For the study of adsorption in porous materials the measurement principle is illustrated in Figure 2.19. The adsorbent is exposed to a defined gas atmosphere at a chosen temperature and subsequently cooled under the gas atmosphere to the boiling temperature of the applied gas in order to fix the adsorbed molecules at the surface. In the next step the remaining, not adsorbed gas molecules are pumped off until high vacuum is reached again. Finally a temperature program with a constant heating rate is applied in order to thermally activate desorption. The desorbing molecules are continuously detected by a mass spectrometer. The result of a TDS measurement is a TDS spectrum, i.e. the partial pressure of the recorded masses versus sample temperature. The desorption temperature is related to the adsorption strength of the adsorbed molecule to its distinct adsorption site. The area under a desorption peak is proportional to the number of desorbing gas molecules. Thus, careful calibration of the mass spectrometer signal enables also quantitative information. Additionally, the TDS method is mass specific as several masses can be recorded at the same time, i.e. gas mixtures can be applied in the experiment. Also kinetic data is available if several curves are recorded applying different heating rates. The peak shift with change in heating rate is related to the kinetics of the desorption and can be analyzed by the Redhead analysis.[72,76-78]

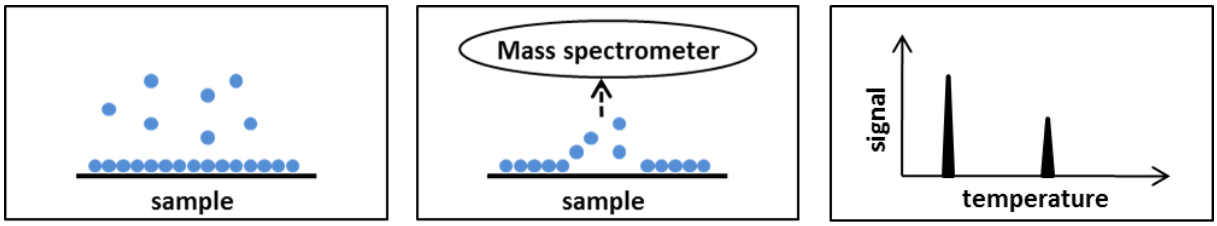

Figure 2.19: Principle of the low temperature TDS method. The sample is exposed to a defined gas atmosphere and afterwards cooled down under the gas atmosphere close to the boiling temperature of the adsorptive. The remaining gas molecules are pumped off until HV is reached again. A controlled temperature program, usually at a constant heating rate, thermally activates desorption. The desorbing molecules are detected by a mass spectrometer.

In the last years low-temperature TDS has been extensively used for investigations of suitable nanoporous materials for on-board hydrogen storage.[73,74,79,80]

2.3.2. Extraction of kinetic data

The curves obtained by TDS and FDS (flush desorption spectroscopy) can be exploited for yielding kinetic desorption data.[76,77,81] The mathematical procedures performed in order to get kinetic information from the TDS spectra is often referred to as the Redhead analysis; named after P. A. Redhead.[78] The following section will exemplarily present the data treatment for first-order kinetics, pure physisorption and one sort of adsorption site.[72]

The desorption rate r can be calculated by the Polanyi-Wigner equation:

$$r = -\frac{dn}{dt} = -\frac{d\Theta}{dt} = \upsilon n \cdot \exp\left(-\frac{E_d}{k_B T}\right) \qquad (2.22)$$

where n is the concentration of admolecules, Θ is the surface coverage, ν is a preexponential factor and E_d is the energy of desorption. As the experiment is performed in a UHV chamber which is pumped at a constant rate, the partial pressure p in the chamber is proportional to the desorption rate of the admolecules:

$$n(t) = \text{const} \cdot \int_t^\infty p\,dt\,. \qquad (2.23)$$

The $p(t)$ curves can easily be transformed to $p(T)$ curves for a constant heating rate β, according to:

$$T = T_0 + \beta t \rightarrow dT = dT_0 + td\beta + \beta dt \rightarrow dt = \frac{dT}{\beta}. \quad (2.24)$$

This leads to

$$n(T) = \frac{1}{\beta} \cdot const \cdot \int_t^{\infty} p dT = \frac{1}{\beta} \cdot const \cdot N(T). \quad (2.25)$$

With

$$p(T) = -\frac{dN(T)}{dT} \quad (2.26)$$

and

$$\gamma \equiv \frac{\upsilon}{\beta} \quad (2.27)$$

one gets the final formula

$$p(T) = \frac{\upsilon}{\beta} \cdot N(T) \cdot \exp\left(-\frac{E_d}{k_B T}\right). \quad (2.28)$$

If the TDS spectra are measured for different heating rates, the pre-exponential factor and the enthalpy of desorption can be obtained by an Arrhenius plot where the logarithm of the maximum desorption pressure is plotted versus the inverse temperature of the desorption maximum (see Figure 2.20).

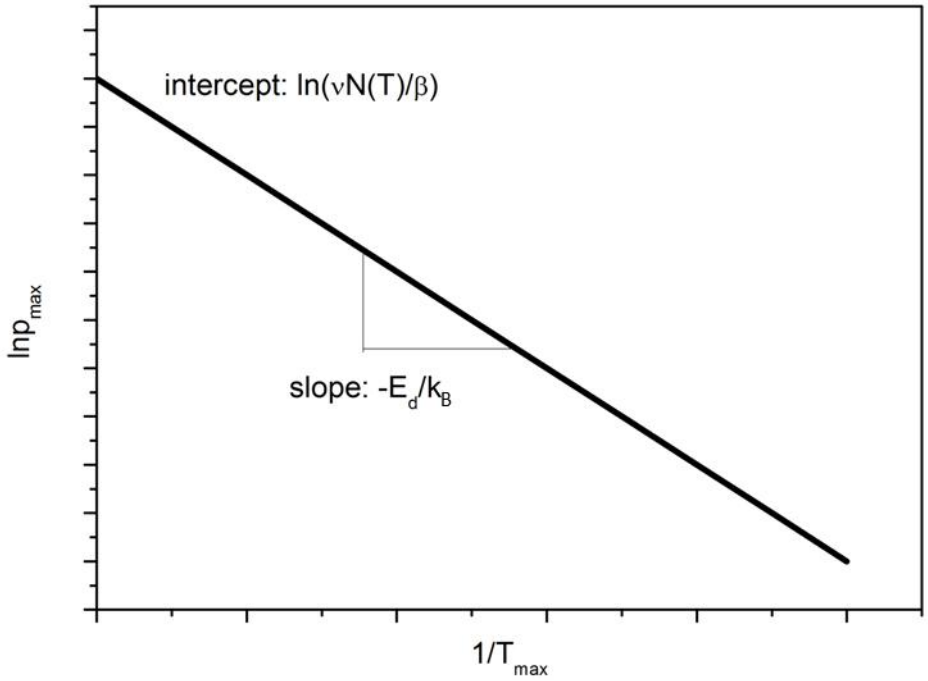

Figure 2.20: Illustration of the Arrhenius plot and the applicable kinetic data.

2.3.3. Measuring the selectivity by TDS

If the separation performance of a material for a 1:1 bimolecular gas mixture is estimated on the basis of pure gas adsorption isotherms, the ratio of the molar gas uptakes is considered as a measure for the separation capability.

But the separation performance can also be addressed directly by applying a gas mixture in a mass-specific adsorption experiment like TDS. In this case, also the ratio of the molar uptakes is considered as a measure for the separation performance. However, the uptake ratio is termed “selectivity” if a mixture has been applied to measure it. Strictly speaking, the ratio of the molar uptakes represents the selectivity only if an equimolar gas mixture is used and the gas composition does not change noticeably with exposure time. It can also be calculated for a bimolecular gas phase of arbitrary gas composition by applying equation (2.16). The adsorbed amounts of the two gases can be quantified after careful calibration of the mass spectrometer signal. The area under a desorption signal (see Figure 2.21) is proportional to the desorbing amount of gas. Therefore, the multiplication of the peak area with the calibration constant yields the quantitative gas uptake. The molar selectivity can be calculated from the following equation

$$S_{1,2} = \frac{A_2 \cdot C_2}{A_1 \cdot C_1}. \qquad (2.29)$$

A_1 and A_2 refer to the areas under the corresponding desorption peaks of component 1 and component 2, respectively. C_1 and C_2 refer to the calibration constants of the two components. It is important to note that the integration of the mass spectrometer signal is performed over time and not over temperature. If the mass spectrometer signal is plotted versus temperature, the peak area will depend on the applied heating rate as the measurement chamber is pumped at a constant rate.

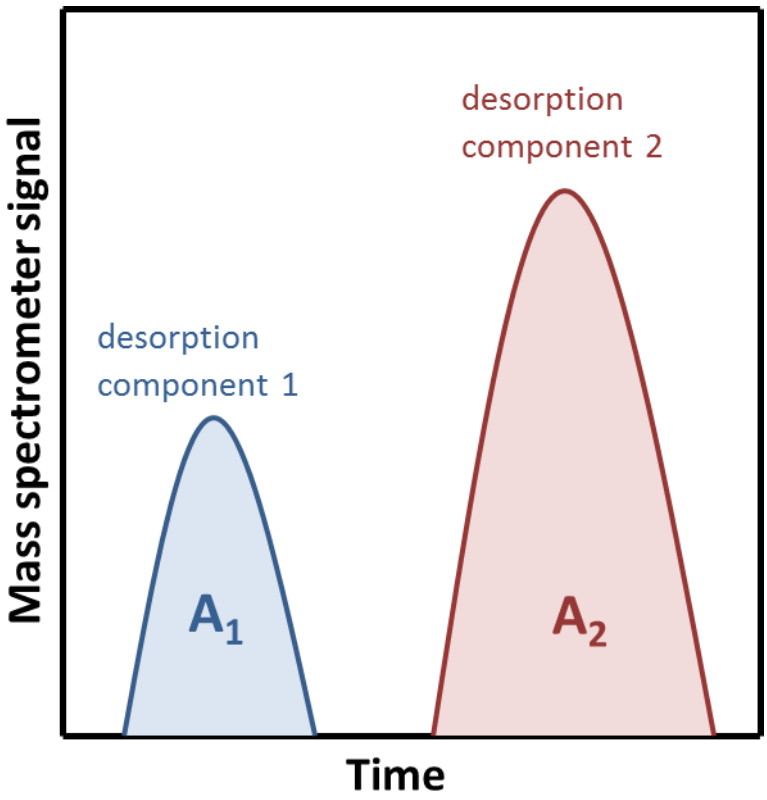

Figure 2.21: Schematic desorption spectrum obtained after exposure to a gas mixture containing component 1 (blue) and component 2 (red). The area under the corresponding desorption peak is proportional to the amount of desorbing gas. This amount can be quantified after calibration of the mass spectrometer signal.

For hydrogen desorption studies, the samples were usually loaded at RT.[73,74] The corresponding temperature and pressure development in the sample chamber during sample loading is shown in Figure 2.21. Before loading, the sample resides in a vacuum chamber at RT. Then the gas is loaded with a certain pressure and the sample remains under

the gas atmosphere at RT for a chosen time. Afterwards the sample is cooled under the gas atmosphere to 20 K in order to fix the adsorbed molecules. In Figure 2.22 the pressure is assumed not to drop with temperature. After reaching 20 K one has to wait for several minutes in order to ensure that the sample reached evenly 20 K. Finally the excess gas is pumped off until high vacuum is reached again.

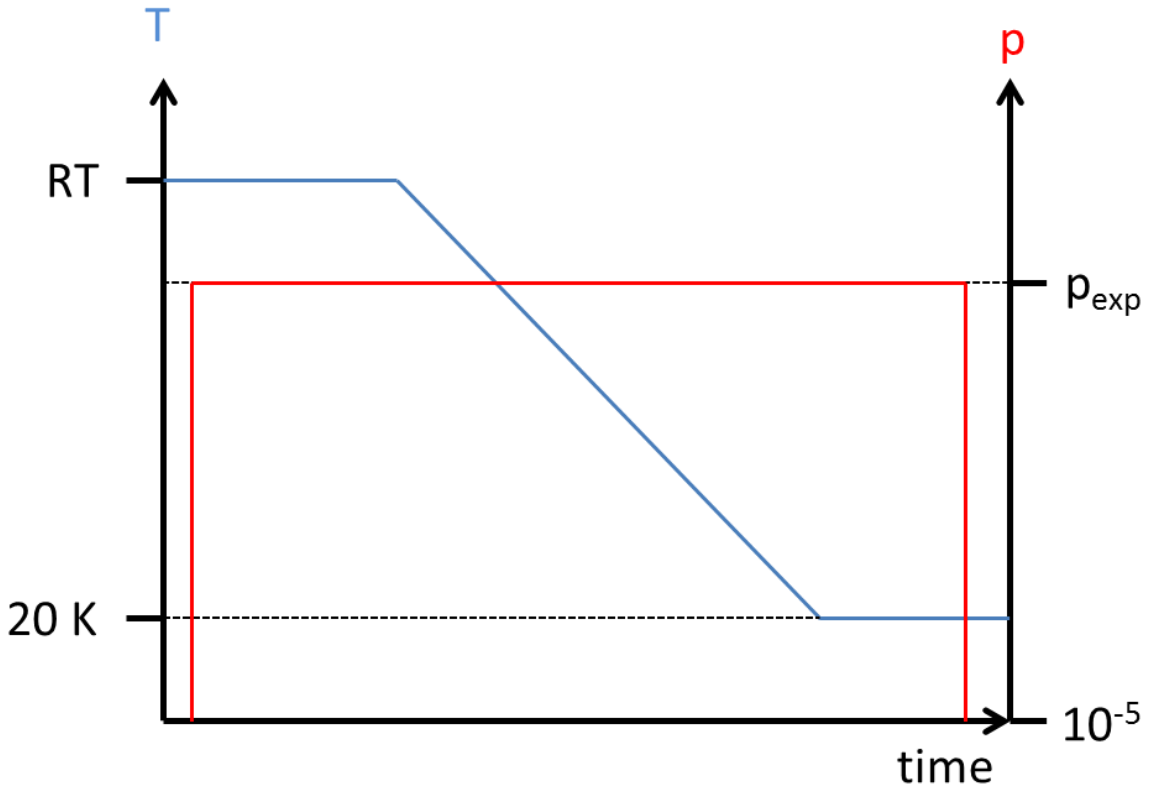

Figure 2.22: Illustration of the temperature and pressure development in the sample chamber in case of RT hydrogen isotope loading.

For the above described loading procedure, it is obvious that a large temperature window is crossed under the gas atmosphere when cooling to 20 K. Therefore, the desorption spectra do not reflect the adsorption state at RT.

For studying low temperature adsorption effects like quantum sieving, RT exposure is not reasonable as quantum effects are only significant at sufficiently low temperatures. Therefore, the sample needs to be cooled to low temperatures ($T_{exp}>T_{boil}$) before gas exposure, as shown in Figure 2.23.

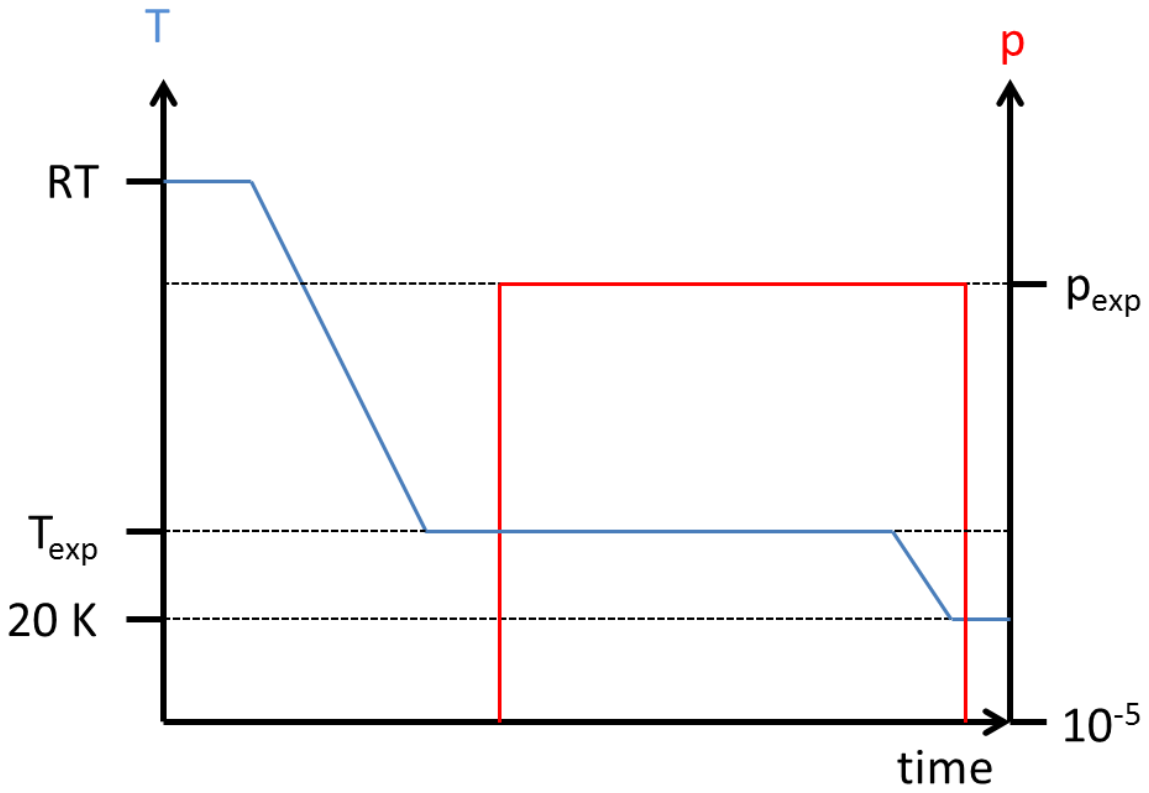

Figure 2.23: Temperature and pressure development in the sample chamber in case of low temperature loading of hydrogen isotopes.

As the sample is first cooled to low temperatures before gas exposure, a smaller temperature window has to be crossed when rapidly cooling to boiling temperature of the gas. Therefore it can be assumed that the desorption spectrum reflects the adsorption state at the exposure temperature well. However, slight influences on the adsorption layer by cooling to the boiling temperature might occur for frameworks that do not strictly limit the diffusion. The cooling to the boiling temperature cannot be omitted as the molecules have to be fixed at the adsorption site, i.e. the adsorption state at the exposure temperature has to be frozen. Otherwise the adsorption layer will become unstable and evaporate when reaching high vacuum which is particularly true for large-pore frameworks with low heats of adsorption. Small-pore frameworks are less critical to outgassing when reaching high vacuum, as they exhibit higher heats of adsorption and the diffusion of the molecules adsorbed in the interior of the framework to the powder particle surface is very slow. However, cooling to 20 K can also not be omitted for small-pore frameworks as the near-surface regions of the powder particles might deplete when reaching high vacuum which would drastically falsify the gas uptake and therefore the selectivity because adsorption in

the near-surface regions plays a major role in case of frameworks exhibiting strong diffusion limitations.

3. Experimental details

3.1. Samples

3.1.1. Takeda 3A

The Takeda company produces commercially a series of carbon molecular sieves (CMS) sold in form of pellets. The add-on "3A" gives the pore size of the considered CMS in Angstroms. Takeda 3A with its 3 Å pores is used for N_2/O_2 separation (air separation).[82] Takeda 3A exhibits a pore size distribution presented in Figure 2.13 (see chapter 2.2.3).[54] The first maximum in the pore size distribution around 3.4 Å corresponds to the pores that are responsible for the air separation. Another maximum in the pore size distribution occurs for micropores between 4 Å and 7 Å. Also a fraction of larger pores up to roughly 30 Å can be seen. These pores are probably attributed to the partially disordered structure of Takeda 3A.[82]

Hydrogen and deuterium TDS experiments after RT loading were measured for the Takeda series with pore sizes in the range of 3 Å to 5 Å (see Figure 3.1).[83] The TDS spectra of Takeda 3A reveal low temperature signals, ranging from 20 K to roughly 100 K which can be attributed to the disordered areas of the CMS that possess cavities and larger voids of different sizes. The desorption signal between 100 K and 150 K is related to the characteristic 3 Å pores. For the low loading pressure of only 50 mbar, the low temperature desorption signal dominates the TDS spectra. Only exposure to gas of several hundred millibar allows the clear detectability of the high temperature signal. Usually, the strongest adsorption sites are saturated first and therefore occur at low pressure. However, as diffusion in Takeda 3A is slow, only a small amount of gas molecules can penetrate the 3Å nanopores of the sample during the exposure time and the remaining gas molecules adsorb in larger voids during cooling.

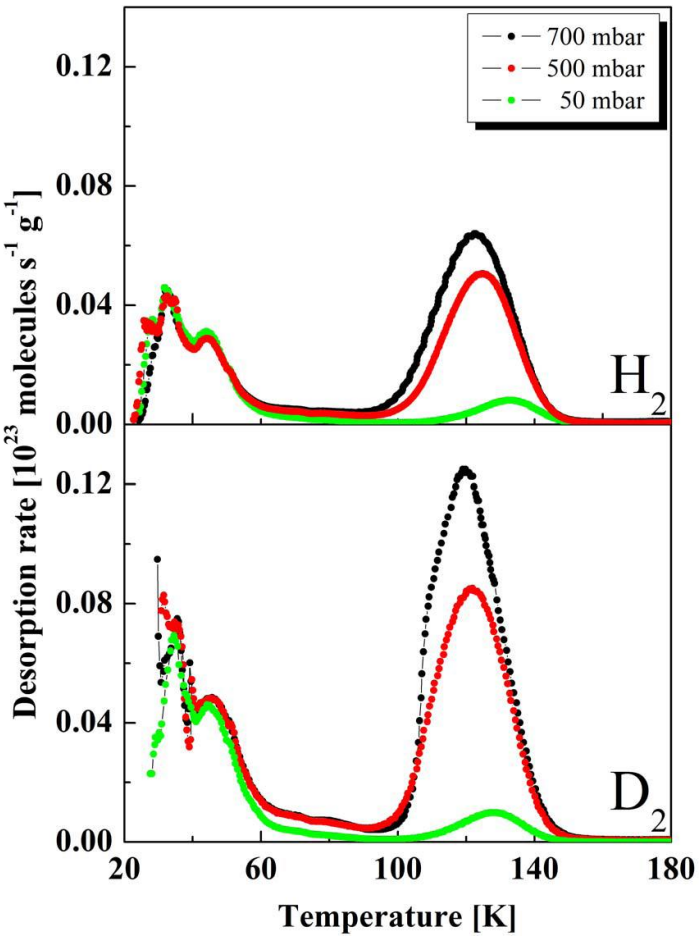

Figure 3.1: TDS spectra obtained after exposure to pure hydrogen and deuterium gas at RT for different loading pressures.[83]

3.1.2. MFU-4(Zn, Cl)

MFU is an abbreviation for **M**etal-organic **F**ramework University of **U**lm, a series of MOFs with equal topology. The derivative MFU-4(Zn, Cl)[84] is synthesized solvothermally by $ZnCl_2$ and H_2-BBTA in DMF.[85] The linkers are dianionic $BBTA^{2-}$ linkers {H_2-BBTA = 1H,5H-benzo(1,2-d:4,5-d')bistriazole} and the inorganic connector units are $[Zn_5Cl_4]^{6+}$. The elemental formula is $Zn_5C_{18}H_6Cl_4N_{18}$. The synthesis products are cubic crystals that have grown together during the synthesis (see Figure 3.3). The atomic structure of the MFU-4(Zn, Cl) framework is illustrated in Figure 3.2.

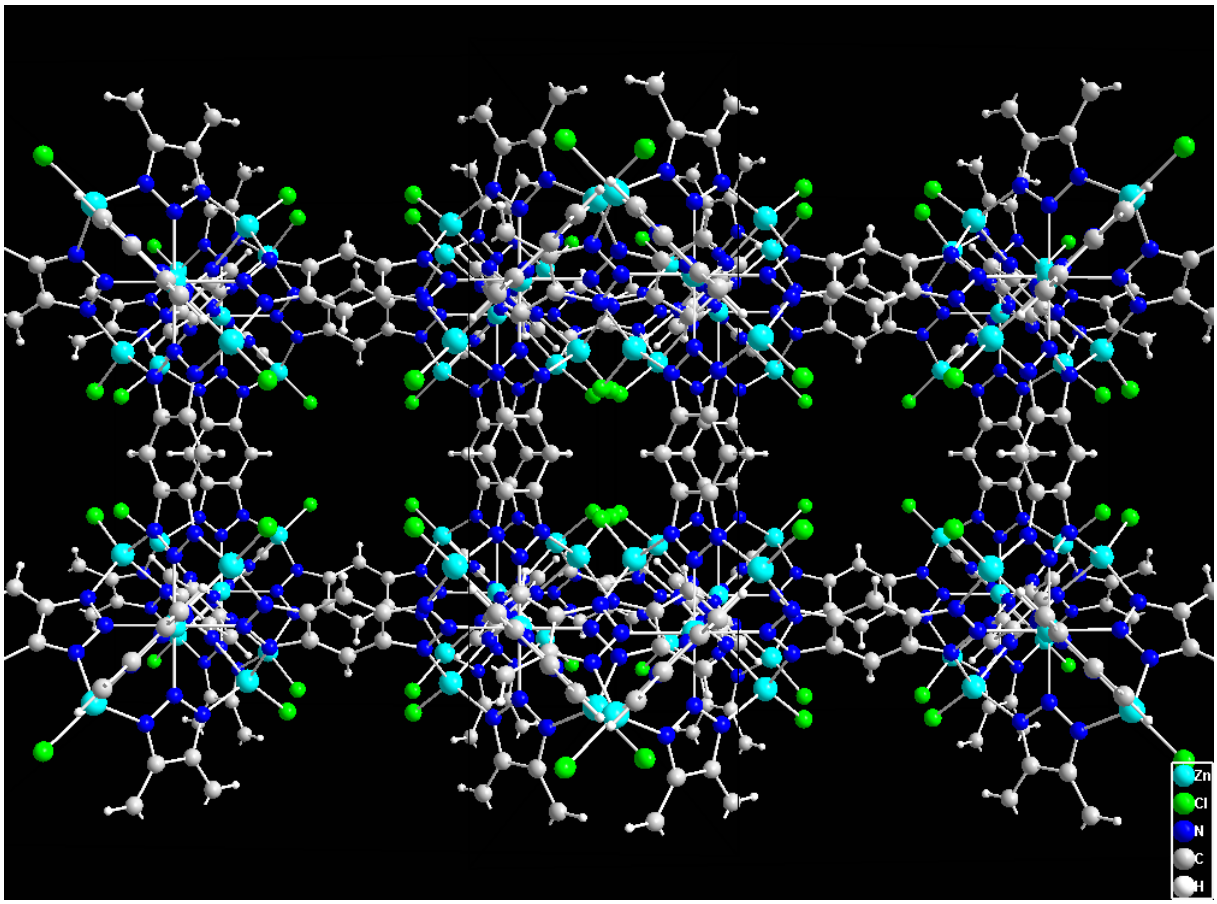

Figure 3.2: Structure of the cubic MFU-4 framework with its bimodal pore structure. The small and large pores are connected by a small window formed by four chlorine atoms. The structure was resolved on the basis of single-crystal diffraction data.[86]

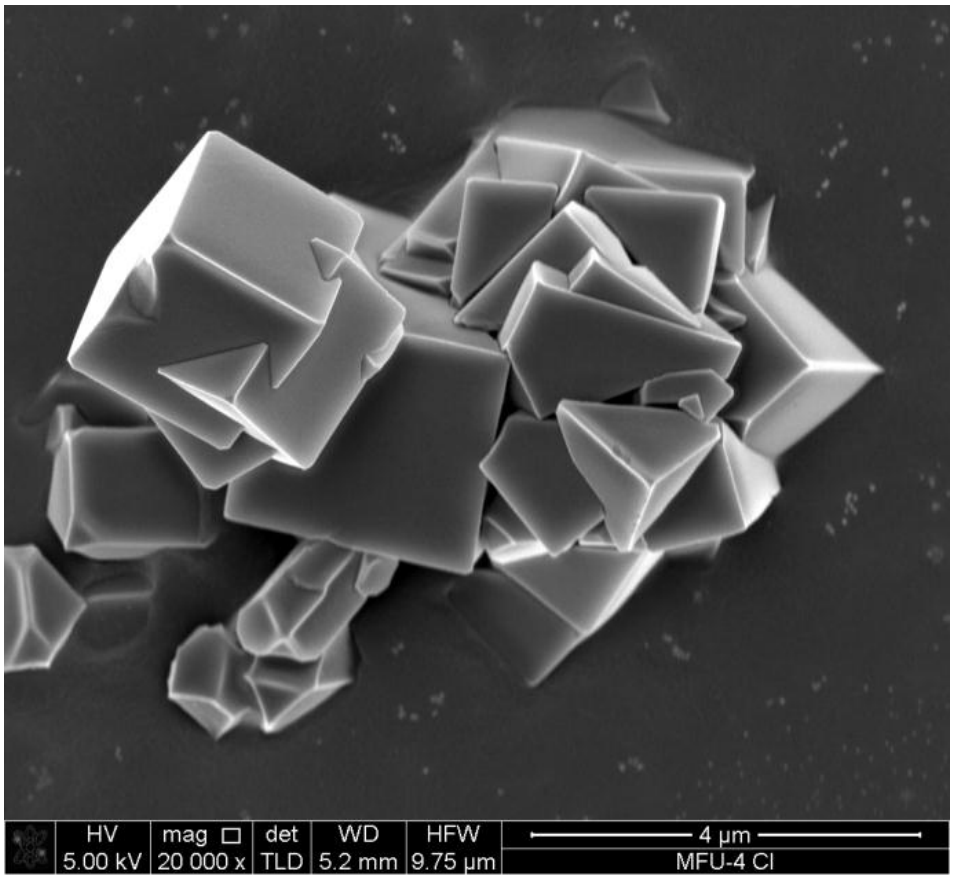

Figure 3.3: SEM images of MFU-4(Zn, Cl). The grains are cubic and have grown together during the solvothermal synthesis.[87]

The framework exhibits a bimodal pore structure with a small A-pore of 3.88 Å and a larger B-pore with 11.94 Å in diameter.[88] The unit cell is cubic (space group: Fm-3m)[85] containing four small and four large pores. The large pore can only be entered via the small pore. Thus, MFU-4(Zn, Cl) shows an experimentally observed gating effect (see Figure 3.4).[88] The gating is further amplified as the A-pore and the B-pore are connected by a small window/aperture with only 2.52 Å in diameter formed by four chlorine atoms. The size of the pore aperture is calculated by the diagonal center-to-center distance of two Cl atoms minus twice the Van der Waals radius of Cl. Thus, the calculation assumes a covalent bond between the Zn and the Cl which is reasonable as the bond length between them is only 2.1 Å[86] whereas an ionic bond would be ~2.5 Å according to the ionic radii.

Owing to the gating effect, molecules with a small kinetic diameter like water and hydrogen can penetrate the framework whereas larger molecules like nitrogen are excluded.

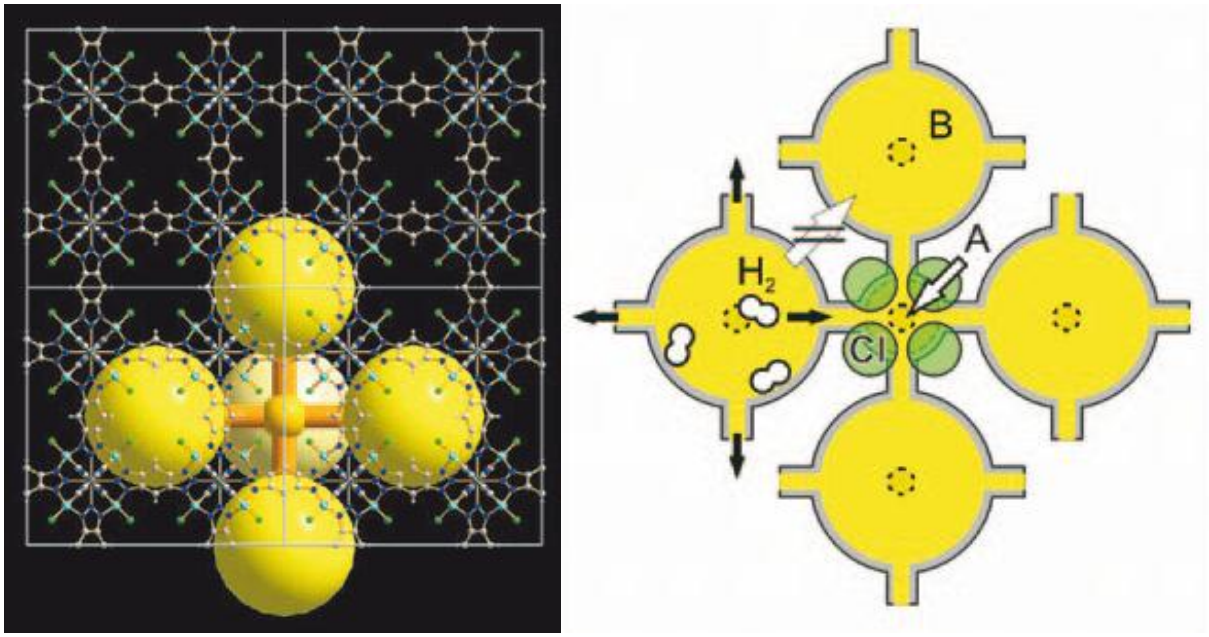

Figure 3.4: Illustration of the gating effect in MFU-4(Zn, Cl). Owing to the alternating pore structure, the large pore B is only surrounded by small pores A. The A-pore and B-pore are connected by a narrow window formed by four chlorine atoms. Any molecule diffusing in the framework has to pass both pores and the connecting window.[88]

As nitrogen cannot penetrate, the specific surface area of MFU-4(Zn, Cl) cannot be determined experimentally by the standard N_2 BET method. However, the ssa has been calculated theoretically for hydrogen and argon from the XRD deduced crystal structure. The ssa values are 1736 m²/g and 1350 m²/g for hydrogen and argon, respectively.[88,89] In

principle, the ssa can also be determined experimentally by hydrogen BET[90] but this has not been performed up to now.

Hydrogen adsorption and desorption studies were performed on MFU-4(Zn, Cl).[83,88,91] Adsorption isotherms were measured between 77 K and 298 K up to 20 bar. The excess hydrogen uptake at 20 bar and 77 K is found to be 2.5 wt% and the isosteric heat of adsorption lies between 6 kJ/mol and 8 kJ/mol.[88] The hydrogen isotherms exhibit type I behavior, i.e. they show a steep increase at low pressure followed by saturation at higher pressure. The uptake decreases with increasing adsorption temperature.

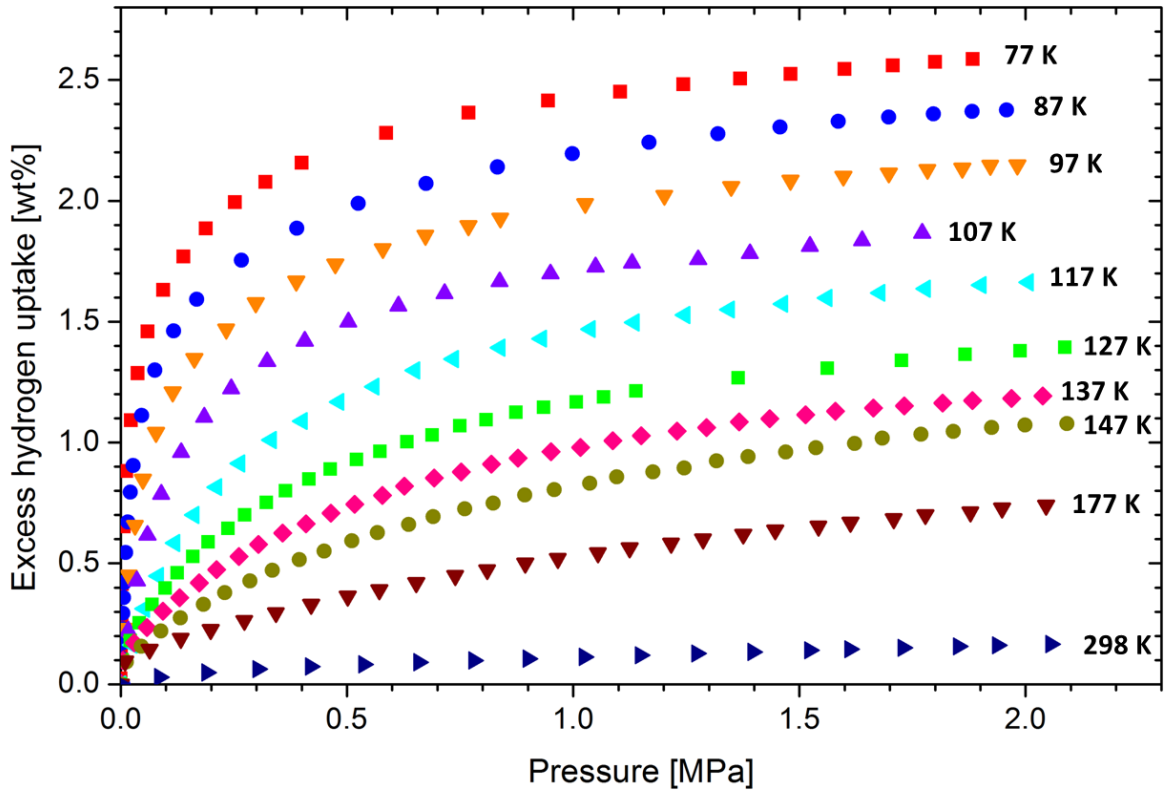

Figure 3.5: Hydrogen adsorption isotherms measured volumetrically from 77 K to RT up to 20 bar.[91]

TDS experiments after exposing MFU-4(Zn, Cl) to 700 mbar pure hydrogen gas at RT are presented in Figure 3.6.[88] Additional spectra can be found in reference 83. The hydrogen desorption maximum is centered between 70 K and 80 K if a heating rate of 0.1 K/s is applied.

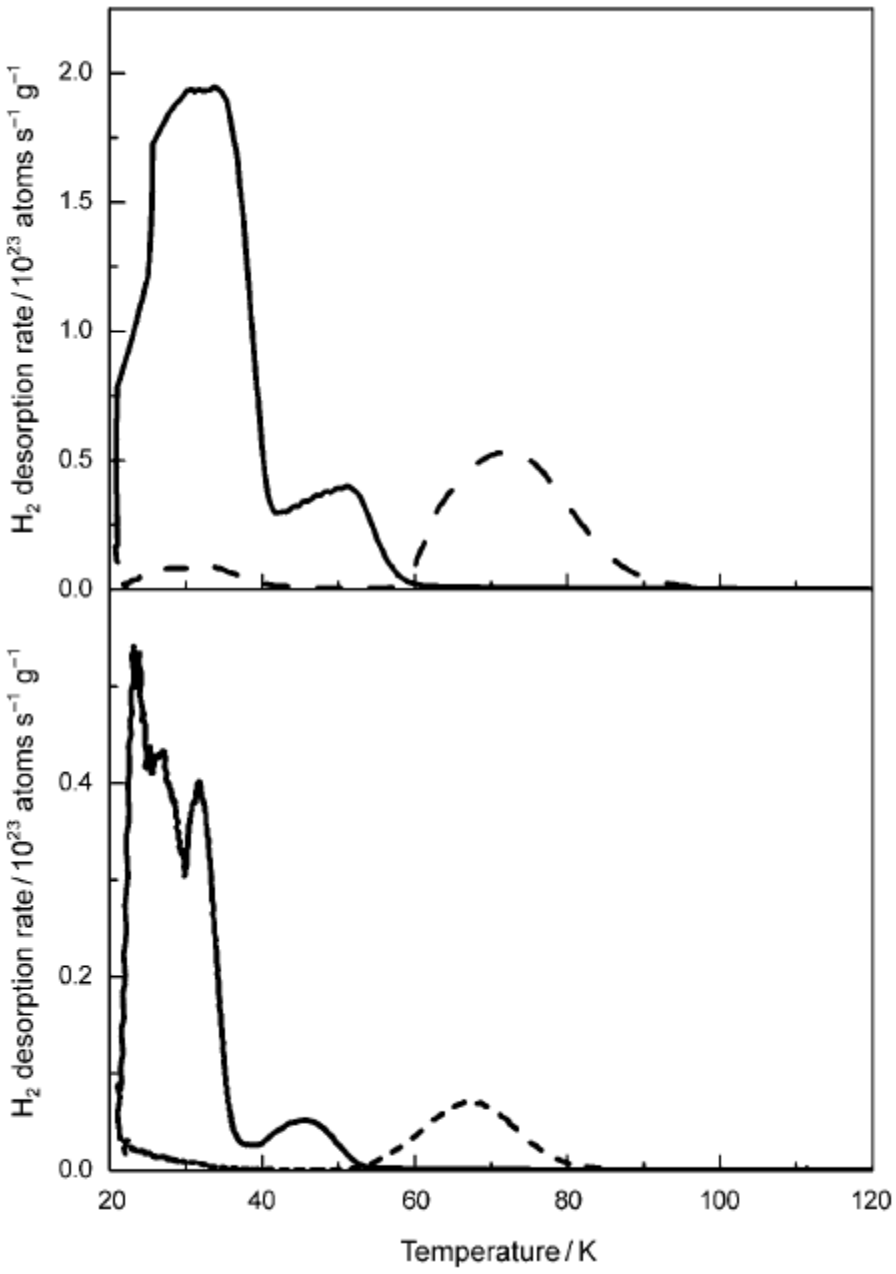

Figure 3.6: TDS spectra of MFU-4(Zn, Cl) (dashed line) and MFU-4 *large* (solid line) obtained after exposing the samples to 700 mbar hydrogen at RT. The desorption curves were measured applying heating rates of 0.1 K/s (top) and 0.01 K/s (bottom).[88]

3.1.3. MFU-4(Co, Cl)

MFU-4(Co, Cl)[84] is a MFU-4 derivative where the Zn ions are replaced by Co ions. It is synthesized by $CoCl_2$ and H_2-BBTA in DMF in presence of LiCl. It cannot be synthesized by ion exchange of MFU-4(Zn, Cl) because the large Co ions are excluded from the framework due to the gating effect. MFU-4(Co, Cl) exhibits the same framework topology but the pores and the pore aperture are slightly larger. The pore diameters are 4.43 Å and 11.97 Å. The window between the large and the small pore is 2.98 Å. The molecular construction of MFU-4(Co, Cl) is shown in Figure 3.7.

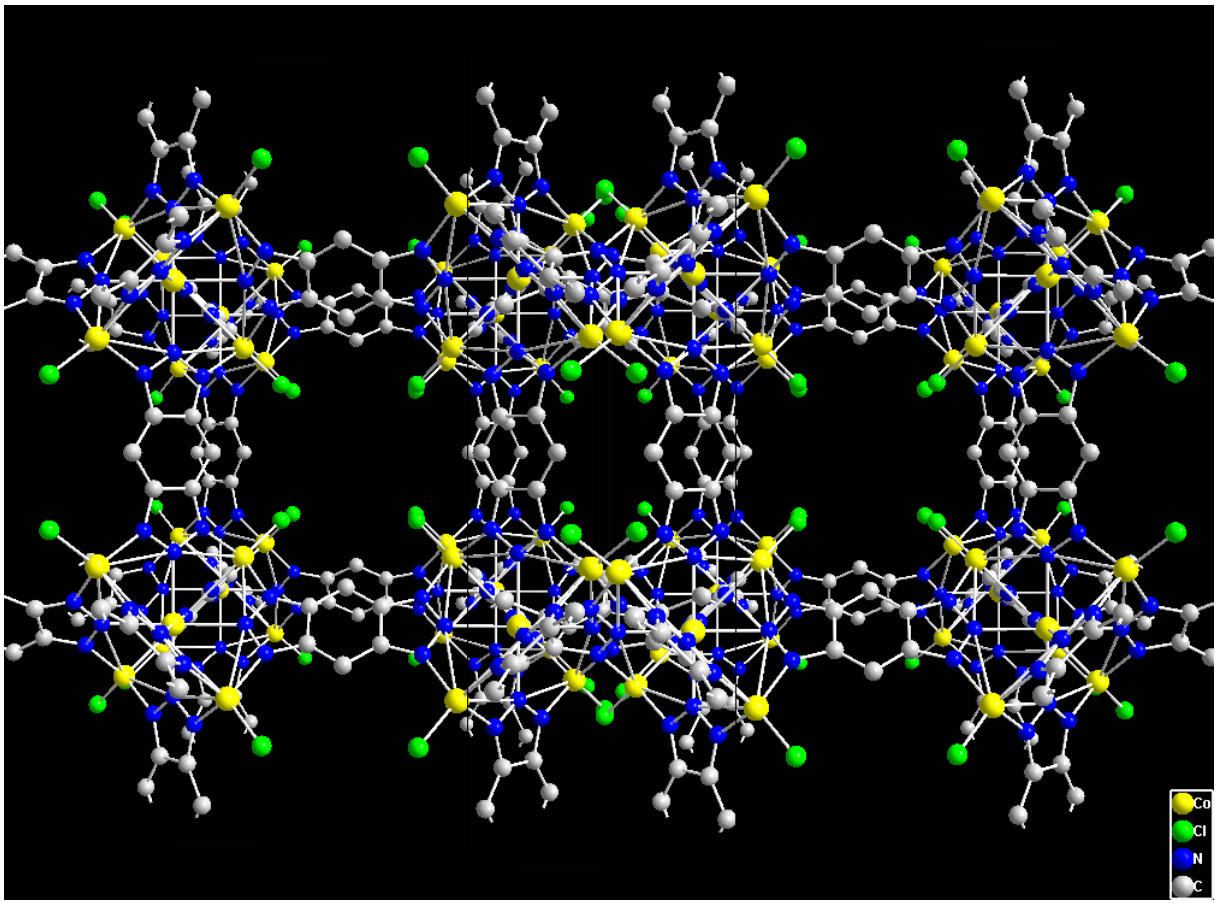

Figure 3.7: Structure of MFU-4(Co, Cl). The hydrogen atoms are omitted. The structure was resolved by XRD applying a powder sample. [92]

No TDS experiments have been performed up to now. However, hydrogen adsorption isotherms were measured from 77 K to 125 K up to 25 bar (see Figure 3.8).[93] The excess hydrogen uptake of MFU-4(Co, Cl) at 77 K and 20 bar is roughly 2.8 wt% and therefore comparable to the value obtained for MFU-4(Zn, Cl).

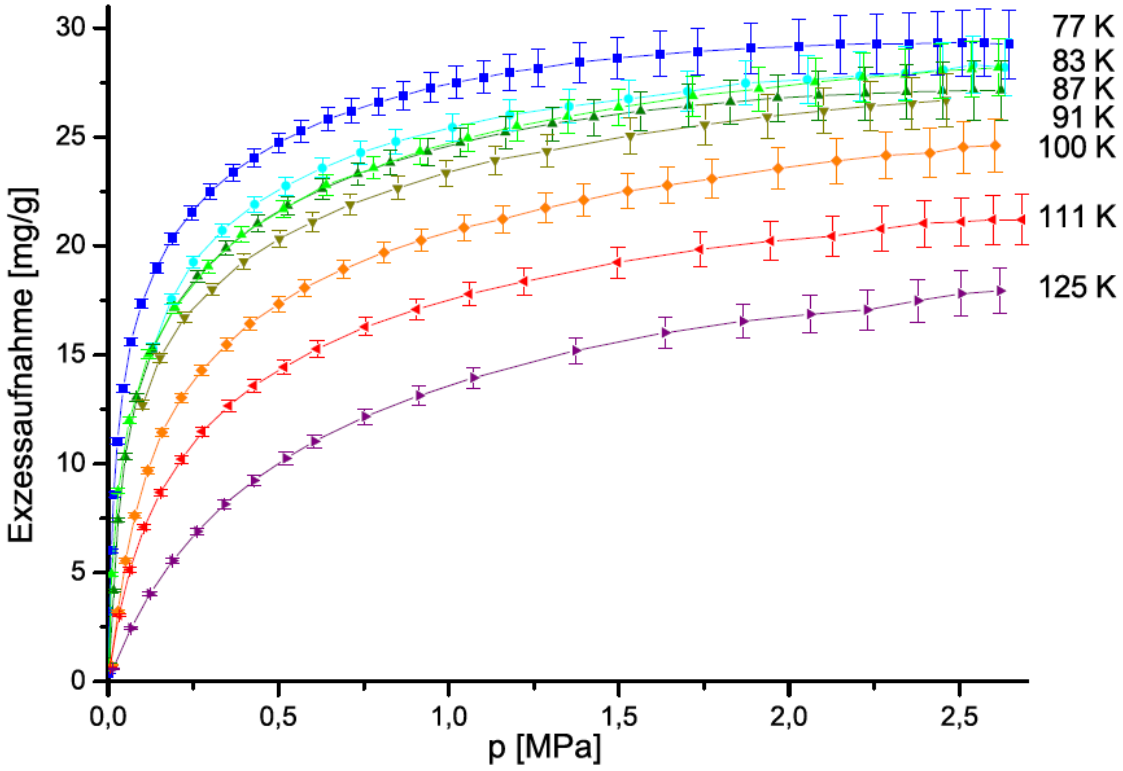

Figure 3.8: Hydrogen adsorption isotherms of MFU-4(Co, Cl) measured volumetrically from 77 K to 125 K up to 25 bar.[93]

3.1.4. MFU-4(Zn, Br)

MFU-4(Zn, Br) is a MFU-4 derivate where the chlorine atoms are exchanged by bromine. As bromine possesses a larger atomic radius than chlorine, the pore aperture is reduced. In the Br-derivative the window is only 2.33 Å. The framework of the Br-derivate is illustrated in Figure 3.9. No adsorption experiments for this sample are available up to now. The hydrogen ssa has also not been determined theoretically.

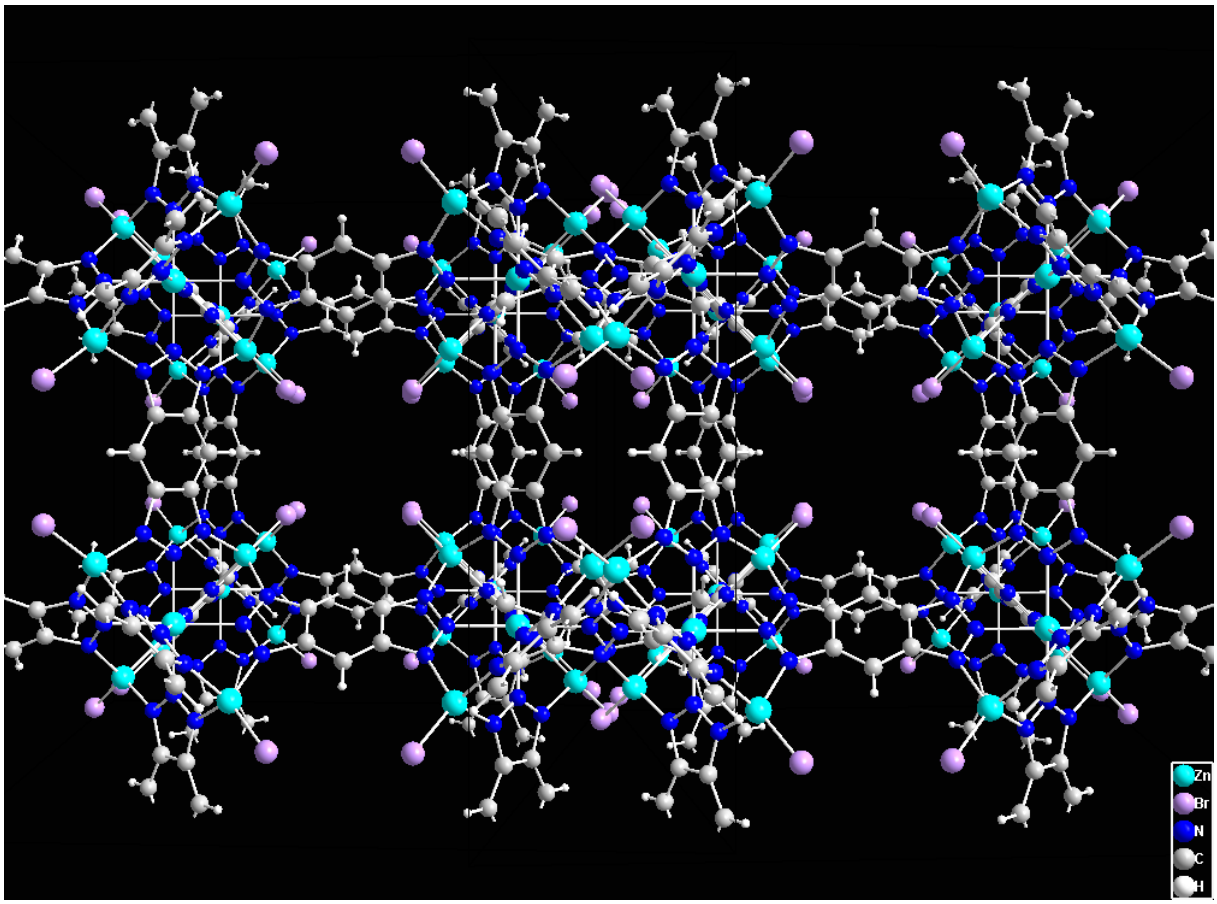

Figure 3.9: Structure of MFU-4(Zn, Br) obtained by powder XRD.[94]

In this work two MFU-4(Zn, Br) samples are investigated that are synthesized differently. According to the XRD data obtained by the group of Prof. Volkmer, both samples exhibit the same XRD pattern and therefore possess the same framework structure which is illustrated in Figure 3.9. The differences between the two MFU-4(Zn, Br) samples, i.e. MFU-4(Zn, Br)_T1 and MFU-4(Zn, Br)_T2, are discussed in the following.

MFU-4(Zn, Br)_T1

MFU-4(Zn, Br)_T1[95] is synthesized via the solvothermal route. For this purpose, anhydrous $ZnBr_2$ and H_2-BBTA are dissolved in *N,N*-Diethylformamide (DEF) and the glass tube containing the solution is sealed. The solution is heated for three days at 120 C. Afterwards the cooled suspension is filtered and the MFU-4(Zn, Br)_T1 crystals are washed with DEF and dried in air.[96]

SEM images exhibit that the synthesis product are cubic crystals with a bimodal particle size distribution (see Figure 3.10). The larger grains are approximately between 1 µm and 4 µm. The smaller particles are below 0.5 µm. However, the small grains also exhibit the same cubic shape as the large ones.

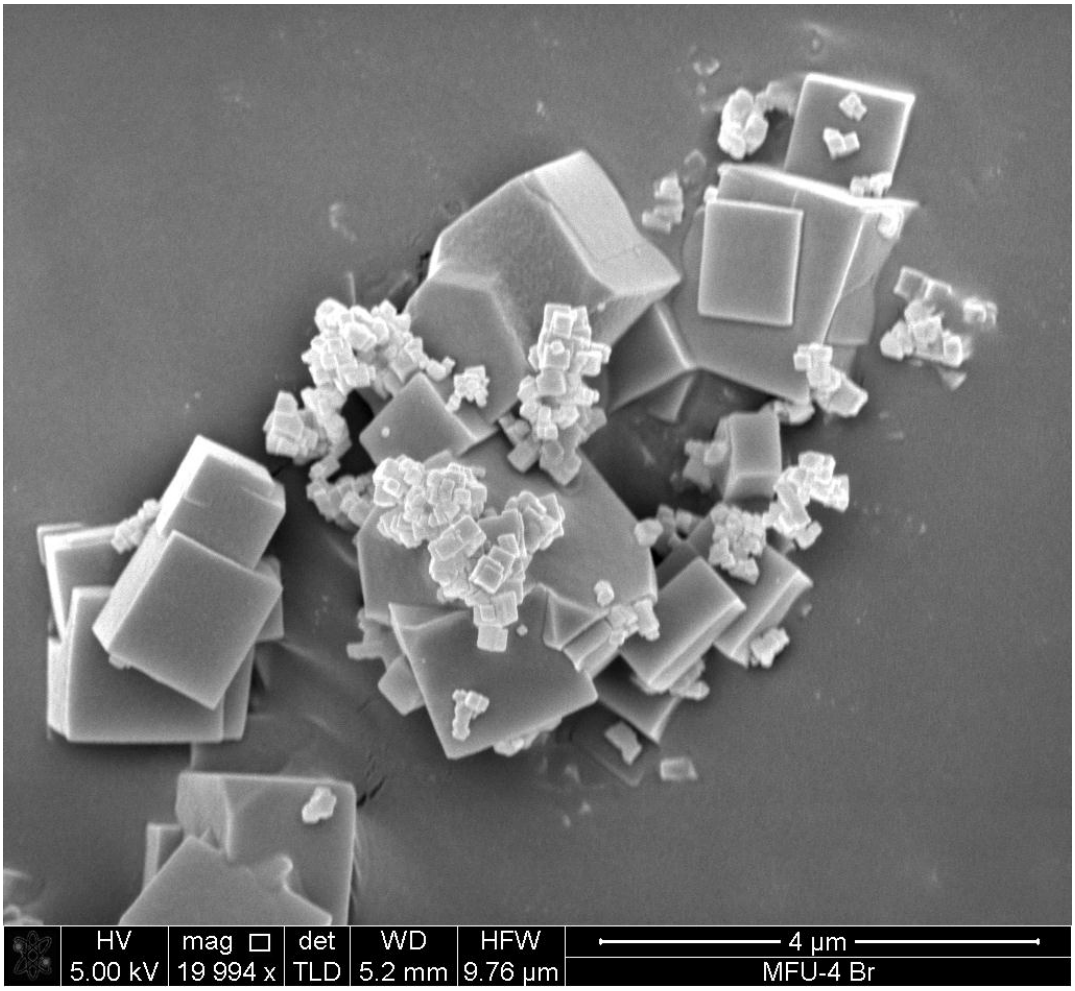

Figure 3.10: SEM image of the solvothermally synthesized sample MFU-4(Zn, Br)_T1.[87]

MFU-4(Zn, Br)_T2

MFU-4(Zn, Br)_T2[95] is synthesized applying the microwave irradiation method. A mixture of $ZnBr_2$ and H_2-BBTA in DEF is placed in a Pyrex tube which is sealed afterwards. The solution is placed in a microwave synthesizer (CEM, Discover S) where the mixture is heated to 100°C at 150 W for 10 min. After cooling to RT, the product is filtered and washed with DEF and methanol and dried under ambient conditions.[96]

SEM images reveal that the product consists of rather uniformly sized cubic crystals that are mainly much smaller than 0.5 µm (see Figure 3.11). The nanocrystals tend to form agglomerates or have grown together during synthesis (see Figure 3.12).

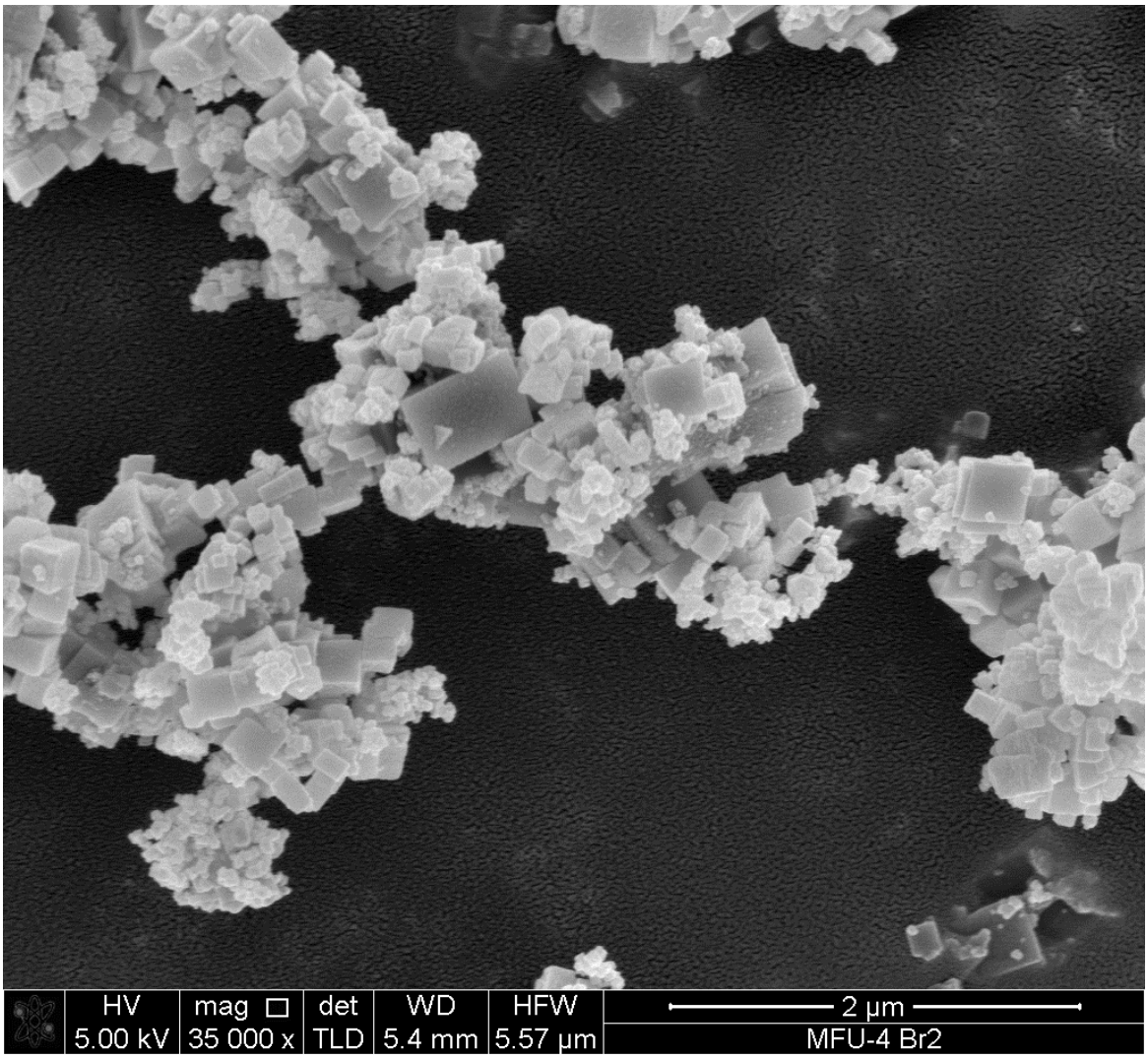

Figure 3.11: SEM images of the MFU-4(Zn, Br)_T2 sample.[87]

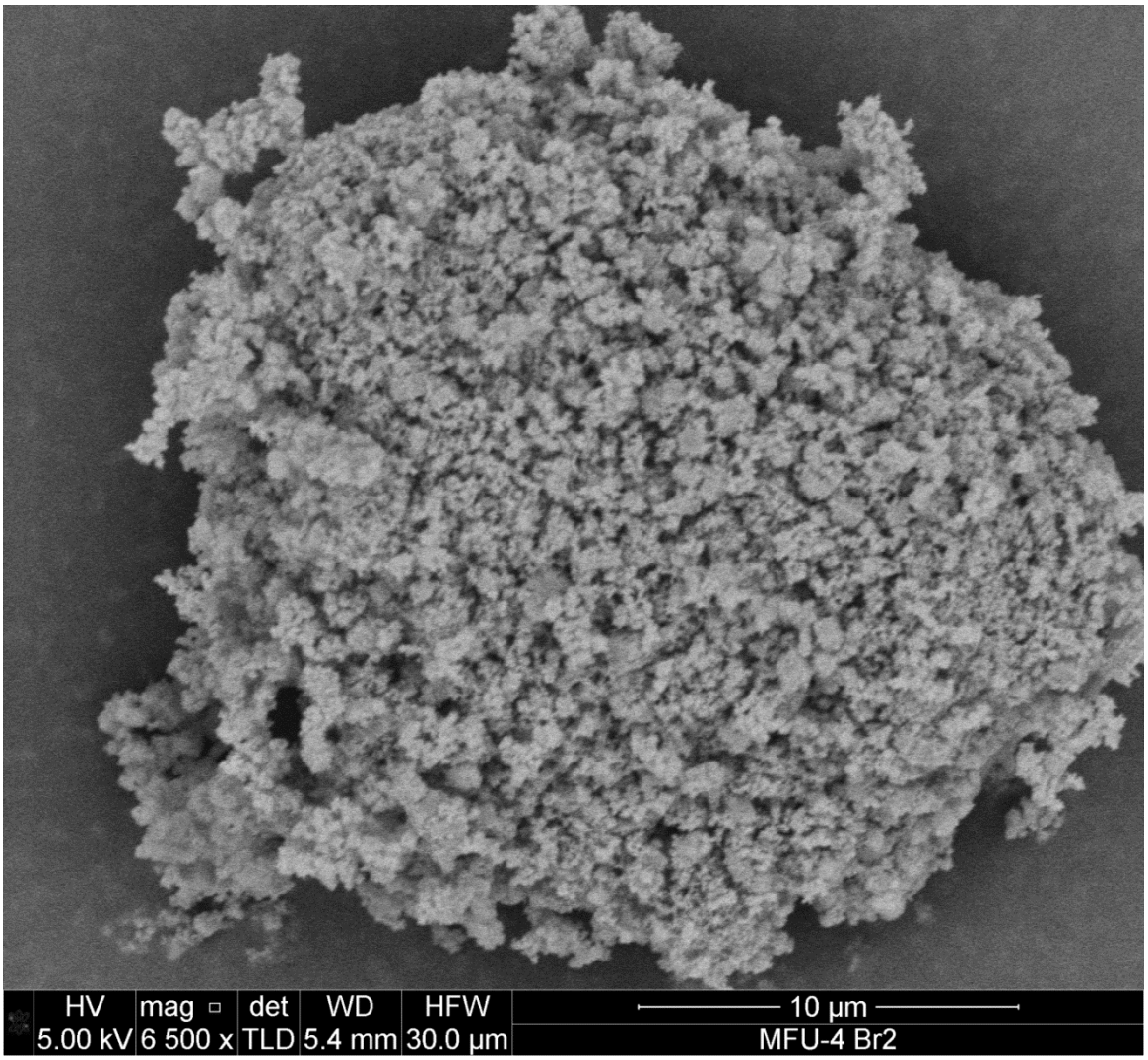

Figure 3.12: SEM image of the MFU-(Zn, Br)_T2 sample revealing that the grains have grown together during synthesis or form agglomerates. [87]

3.1.5. MFU-4 *large*

MFU-4 *large*[84] is synthesized solvothermally by mixing $ZnCl_2$ and H_2-BTDD {H_2-BTDD= bis(1*H*-1,2,3-triazolo[4,5-*b*],-[4',5'-*i*]dibenzo[1,4]dioxin} in N,N-dimethylformamide. The solvent molecules are removed at 180°C in vacuum. The resulting framework structure contains A-pores with a diameter of 11.97 Å and B-pores with a diameter of 18.56 Å. The aperture is 9.13 Å. The framework structure is illustrated in Figure 3.13.

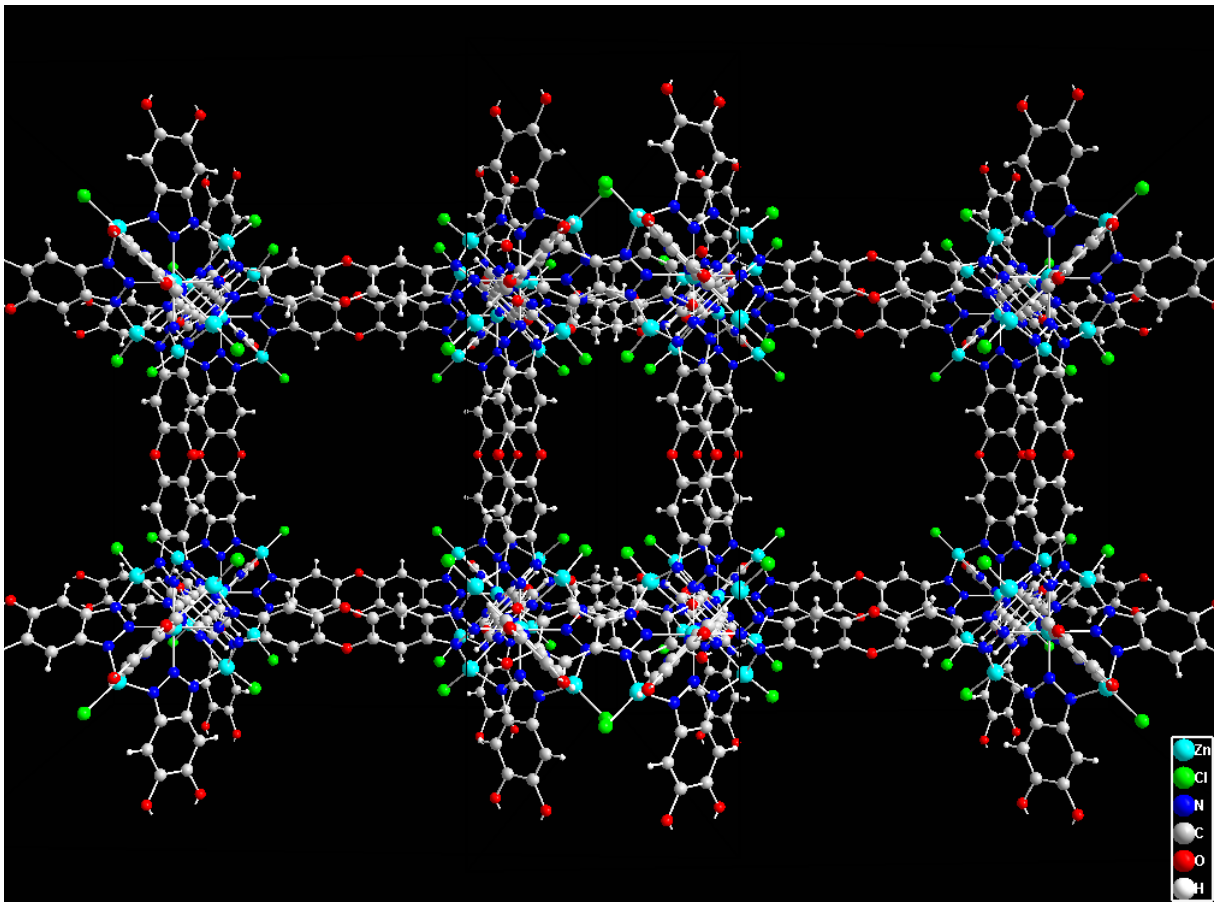

Figure 3.13: Structure of MFU-4 *large* based on powder XRD data. [97]

For this MFU-4 derivative a N_2 BET ssa can be measured, giving a value of 2750 m^2/g.[88] Hydrogen adsorption studies were performed on MFU-4 *large*. The isotherms measured between 77 K and 298 K are shown in Figure 3.14. The hydrogen uptake at 77 K is around 4 wt%. However, saturation is not reached at 20 bar and 77 K.

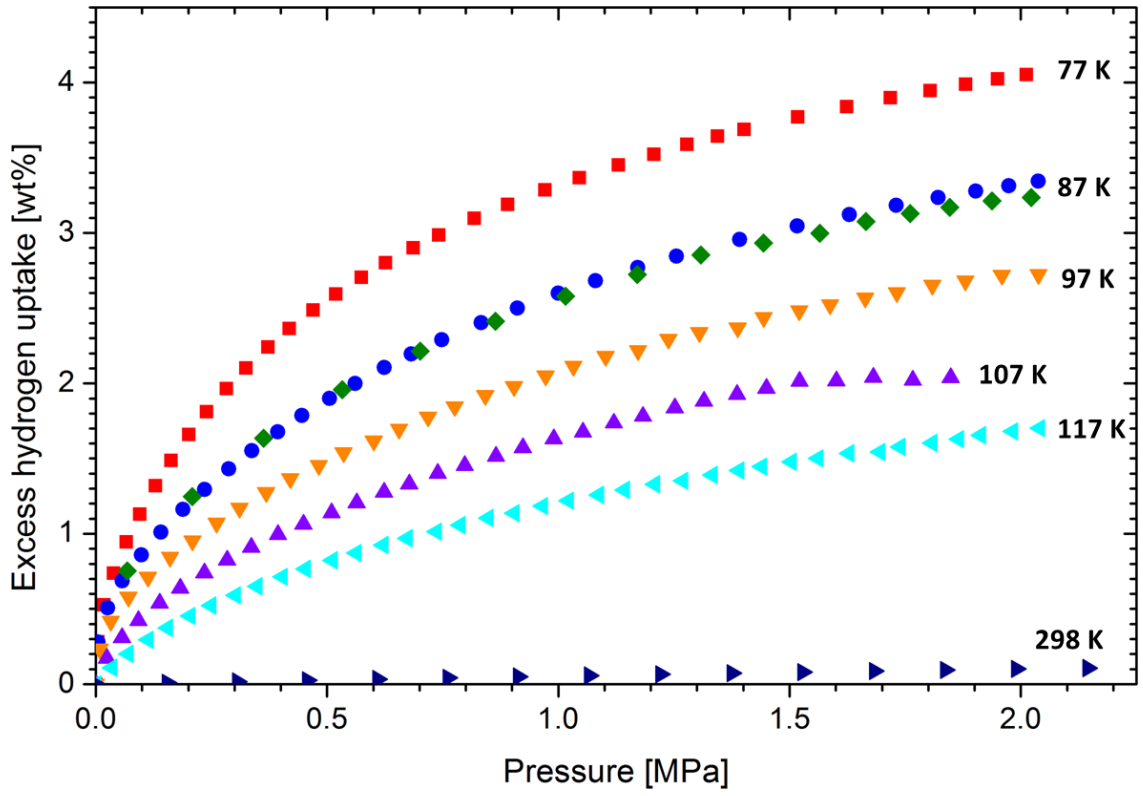

Figure 3.14: Hydrogen adsorption isotherms measured volumetrically for temperatures between 77 K and RT up to approximately 20 bar. [91]

TDS spectra of MFU-4 *large* were measured after exposure to pure hydrogen and deuterium gas at RT for different exposure pressures (see Figure 3.15). After exposure to 1 mbar, only one desorption signal centered around 55 K is visible. For higher loadings, a second signal occurs that is centered at 35 K. Selected desorption spectra are also published (see Figure 3.6).[88]

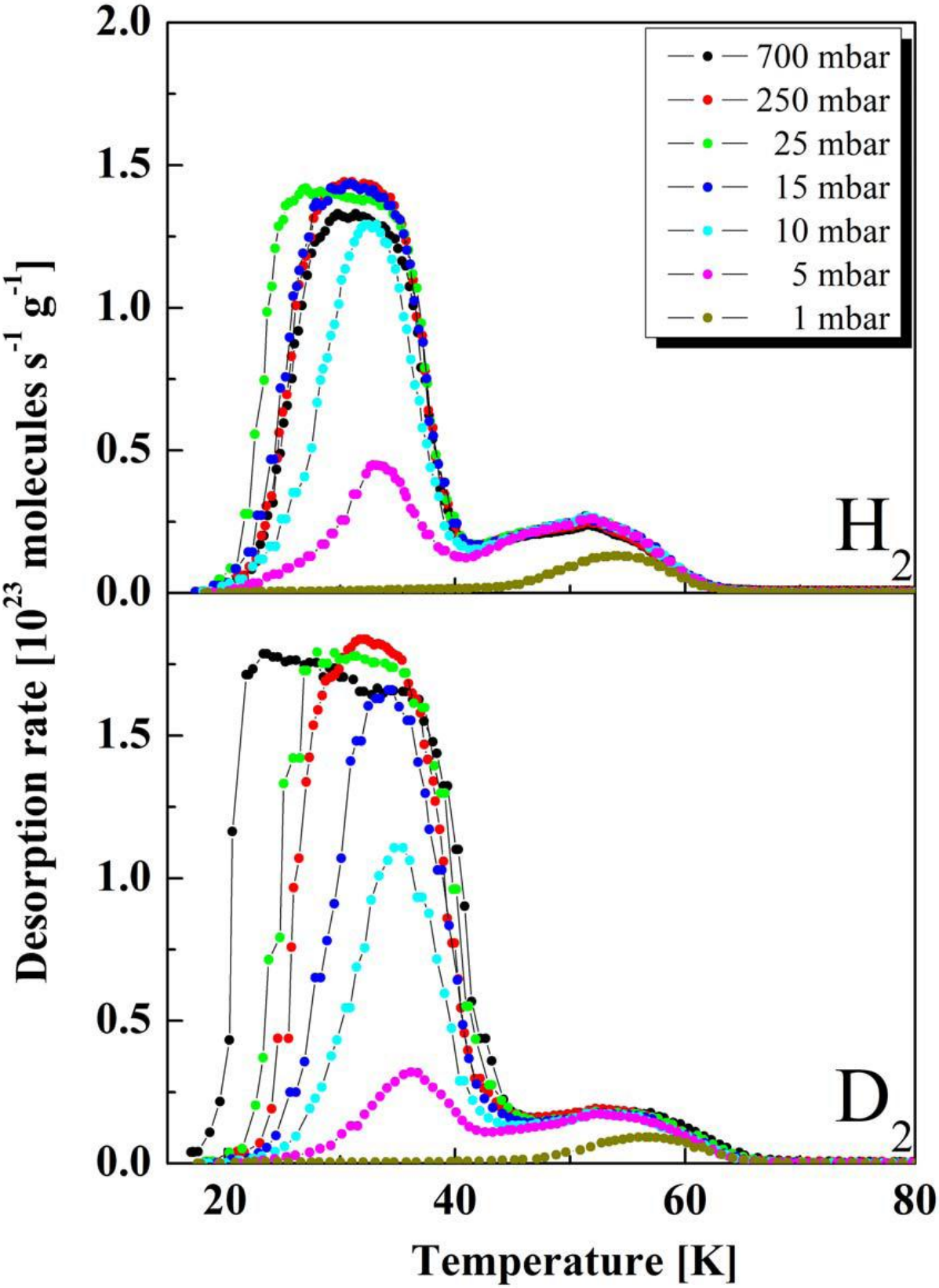

Figure 3.15: TDS spectra of MFU-4 *large* obtained after exposure to pure hydrogen and pure deuterium gas at RT. The spectra are recorded with a heating rate of 0.1 K/s.[83]

3.1.6. MOF-5

MOF-5 is one of the best studied MOF structures and the first representative of the isoreticular framework series; therefore also called IRMOF-1. The inorganic moieties are Zn-O-C clusters that are linked by benzene-based organic linkers, together forming a cubic structure.[14] It contains alternating pores of 12 Å and 15 Å in diameter that are formed by alternating orientation of the linker.[98] MOF-5 is synthesized by reacting zinc nitrate with terephthalic acid in N,N-diethylformamide.[98] The framework is thermally stable up to 470°C.[98]

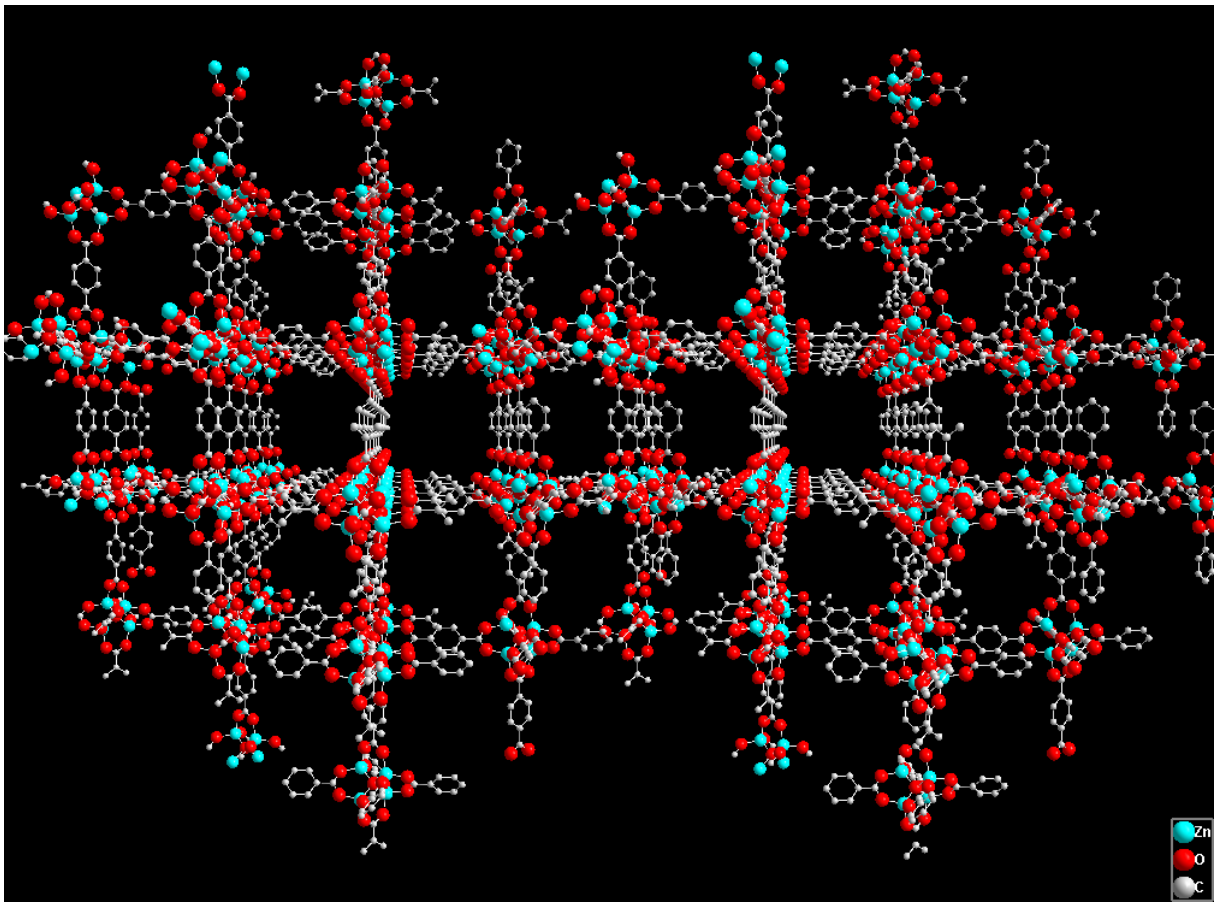

Figure 3.16: Structure of the MOF-5 framework.[99] The two different orientations of the benzene ring inside and outside the pore leads to the alternating pore size.

Hydrogen adsorption studies have been performed exhaustively. Exemplarily, hydrogen adsorption isotherms measured up to 80 bar are shown in Figure 3.17. The isotherms reveal that saturation is not fully reached at 80 bar. The hydrogen uptake at 77 K and 20 bar is slightly larger than for MFU-4 *large*. The ssa of MOF-5 is ~2300 m²/g.[73,91,100]

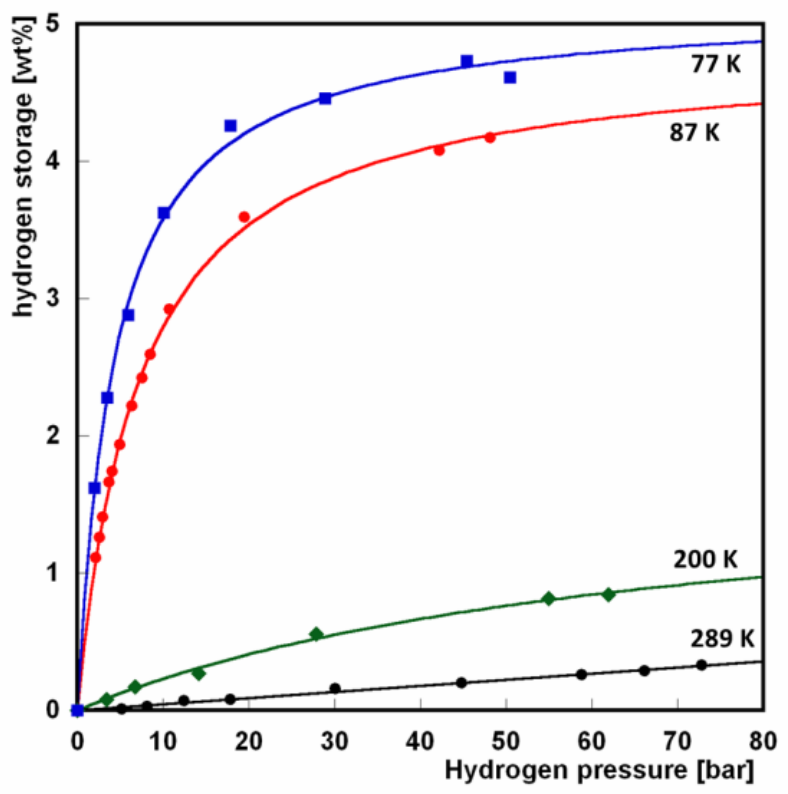

Figure 3.17: Hydrogen adsorption isotherms measured at 77 K, 87 K 200 K and 289 K up to 80 bar.[100]

A hydrogen desorption spectrum of MOF-5 after exposure to hydrogen at RT is published (see Figure 3.18).[73] The spectrum reveals an initial desorption signal attributed to liquefied hydrogen followed by two further desorption maxima centered around 30 K and 40 K. The adsorbed amount of hydrogen desorbs almost completely below 50 K.

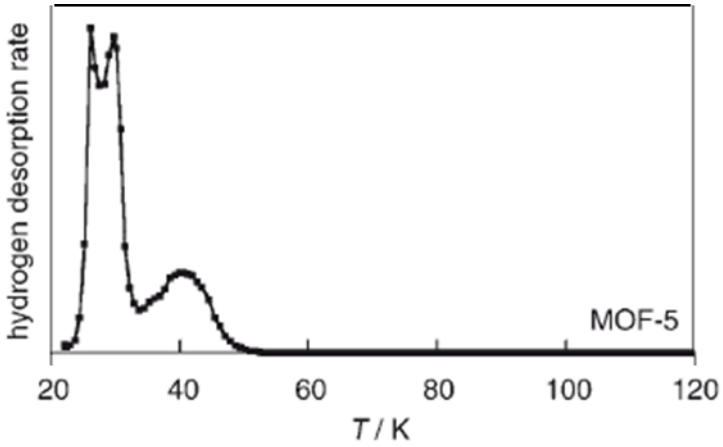

Figure 3.18: Hydrogen desorption spectrum of MOF-5 after gas exposure at RT.[73]

3.2. Experimental procedure

3.2.1. The TDS apparatus

The applied TDS device is in-house developed and in-house made. The construction is illustrated in Figure 3.19. The device can operate in the temperature range between 20 K and approximately 600 K. The sample chamber (yellow) is made of Cu and CuBe alloy. It can be heated by a heating spiral and cooled by LHe flow cryostat (blue) which is connected by a Cu heat exchanger (brown). A valve (beige) connects the sample chamber to the vacuum chamber with the mass spectrometer. The spectrometer is a Microvision Plus 100 D from Spectra. To ensure best heat contact, the sample holders (red) can be screwed tightly to the Cu block at the bottom of the sample chamber. A CrNi thermocouple and a platinum temperature sensor are glued each to the Cu block beneath the sample chamber and the bottom of the cryostat. In order to reach low temperatures, the cryostat and the sample chamber are surrounded by an insulation vacuum and additionally by a LN_2 shielding (pink).

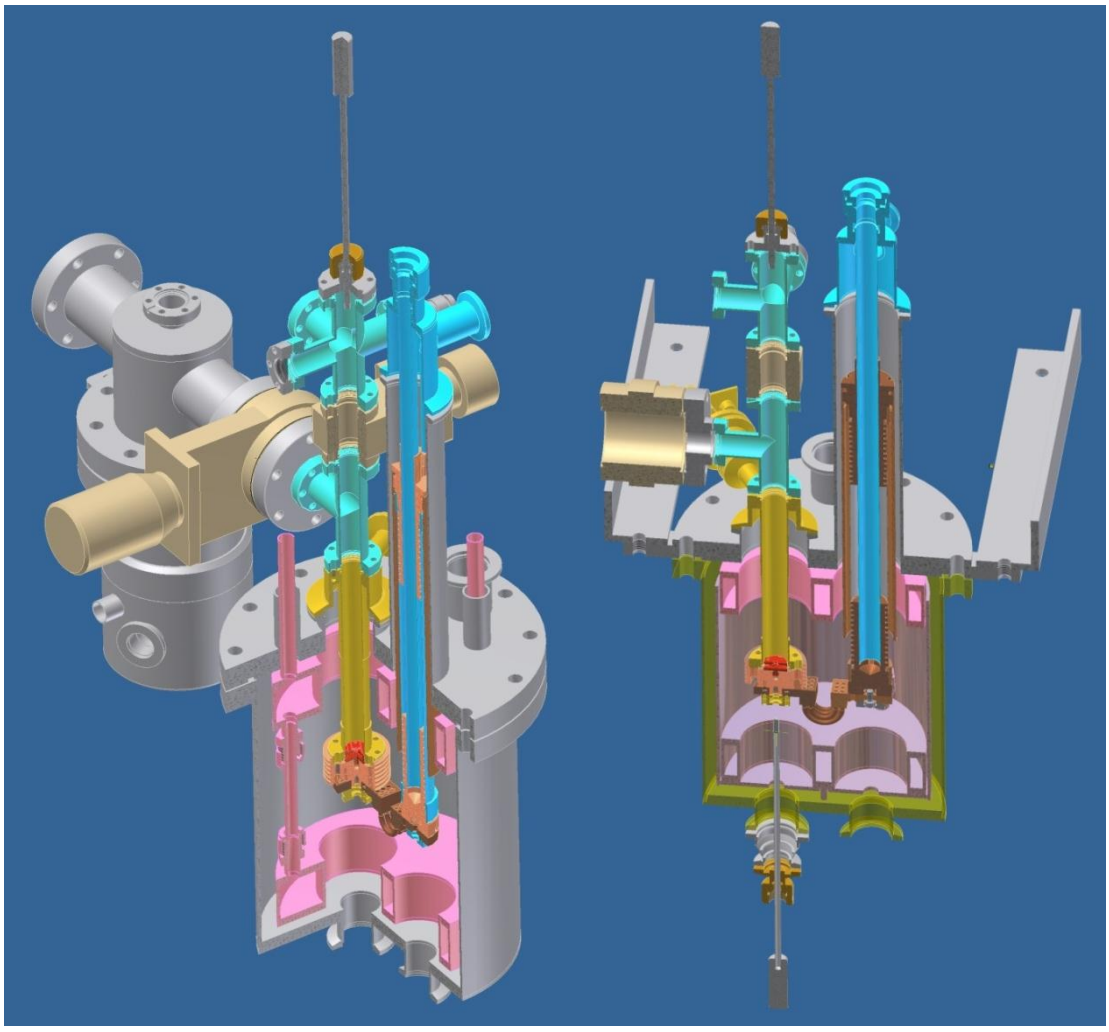

Figure 3.19: Construction of the applied in-house made TDS device.[101]

3.2.2. Calibration of the mass spectrometer signal

The mass spectrometer signal is calibrated in order to quantify the amount of hydrogen and deuterium that desorbs from the samples. The calibration substance was a solid piece of $Pd_{95}Ce_5$ of approximately 0.5 g. This alloy is a solid solution alloy where cerium atoms substitute the palladium atoms in the lattice; thereby causing a lattice distortion. If the alloy is exposed to low hydrogen or deuterium gas pressure, the hydrogen isotopes absorb in these distorted regions without forming a Pd hydride.[102] In this case the hydrogen isotopes are more strongly stabilized in their positions compared to the hydride. Therefore, the loaded alloy can be handled under ambient conditions for a short period of time. The calibration procedure was performed as follows. The PdCe alloy was etched prior to the calibration procedure by aqua regia and heated to 500 K-600 K under vacuum in order to remove hydrogen atoms absorbed during the etching process. Afterwards, the alloy was weighted and loaded in the sample chamber of the TDS device with 150 mbar pure H_2 or D_2 at 350 K for 1.5 h to 2.5 h. After loading the sample had to reach RT and was weighted again. The mass difference before and after loading is equal to the amount of gas that was taken up by the alloy. Subsequently, a desorption spectrum from RT to 500 K/600 K was recorded with a heating rate of 0.1 K/s (see Figure 3.20). After the degasing procedure and the cooling to RT, the alloy is weighted again. For the calculation of the calibration constants the described procedure was repeated 1-2 times and the obtained values were averaged. The calibration constants were determined repeatedly every few months but especially after changing the mass spectrometer setting, repair work on the spectrometer or exchange of filament. Exemplarily, one desorption curve of the calibration alloy is shown for each isotope.

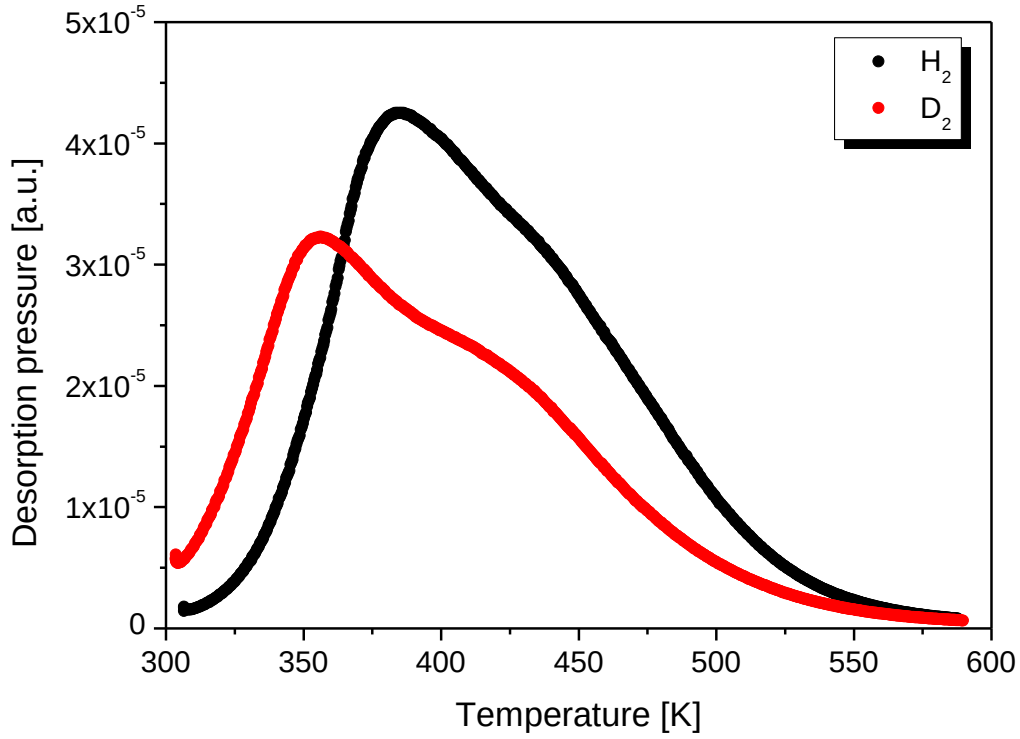

Figure 3.20: Hydrogen and deuterium desorption curves of the calibration alloy after exposure to the pure gases at 350 K for 2 h.

3.2.3. Running a measurement

After placing the sample (3-8 mg) in the device, it is activated at the adequate activation temperature (see Table 3.1) under vacuum and the chamber is baked if necessary. After approximately two hours of activation the valve to the sample chamber was opened in order to check the status of the activation. The activation procedure was stopped when the pressure in the sample chamber was adequately low. The MFU-4 derivatives were delivered solvent free, i.e. MFU-4(Zn, Cl) and MFU-4(Co, Cl) had already been heated at 280°C, MFU 4(Zn, Br) at 325°C and MFU-4 *large* at 150°C under vacuum in order to remove the solvent completely. After placing the samples in the TDS device, the samples were heated again in order to remove adsorbed water (see Table 3.1).

Table 3.1: Activation temperature after placing the samples in the TDS device

Sample	Takeda 3A	MFU-4(Zn, Cl)	MFU-4(Co, Cl)	MFU-4(Zn, Br)	MFU-4 *large*	MOF-5
$T_{act.}$ [K]	500	420	420	500	420	473

The optimum vacuum pressure in the sample chamber is in the range of 10^{-9} mbar. For quantum sieving experiments the sample is first cooled to the chosen exposure temperature and afterwards loaded with pure gas or an isotope mixture. The isotope gases are mixed in the gas supply pipe, i.e. before contact to the sample. The gas purity was 5.0 for hydrogen and 2.8 for deuterium. After exposure to the gas atmosphere for the selected exposure time (usually 1.5 h if no other value is given in the text), the sample is cooled to 20 K before pumping the remaining gas off. The heating rate in all experiments is 0.1 K/s and the measurement mode of the mass spectrometer is the so-called fast scan. The standardly recorded masses are 1, 2, 3, 4, 18 and 28 amu. The temperate data in the spectra are the values given by the Pt temperature sensor at the sample side.

3.2.4. Accuracy and experimental errors

The inaccuracy of the temperature measurement leads to inexact peak positions. The accuracy of the temperature measurement is determined by the accuracy of the data given by the temperature sensors and a possible temperature gradient between the positions of the temperature sensor at the directly heated Cu block and the sample. Neither the CrNi thermocouple nor the platinum sensor is ideal for low temperature measurements but they cannot be replaced by low temperature sensors because they cannot endure temperatures well above RT that need to be reached for sample activation and calibration. In order to estimate the error in temperature a FeAu thermocouple was glued at the upper part of the powder sample holder which can be considered as the worst possible error of the temperature because it includes a possible temperature gradient between the sample position and the location where the permanent temperature sensor are installed. The maximum difference between the platinum and the FeAu thermocouple was 5 K. This value was recorded at a sample temperature well below 20 K. Above 20 K the difference between the temperature given by the FeAu thermocouple and the permanent temperature sensors was smaller. As the peak positions are not of particular interest for the quantum sieving experiments, the inaccuracy in temperature has no severe influence on evaluation of the experimental data. However, it is important to note that at 50 K the PID values of the heating system change leading to a momentary deviation from the linear temperature rise; thereby causing a slight pressure instability in the some TDS spectra. Thus, any deviation in the course of the TDS spectra at 50 K is attributed to an experimental error rather than a sample effect. The most relevant source of error is the inaccuracy in the calibration

constants which directly affects the selectivity value. Outgassing of the loaded calibration alloy during weighing and pumping is the largest and most important experimental error. Apart from the error in the calibration constants, the measurement of the selectivity is very precise. If a measurement is repeated under the same experimental conditions for the same sample, the selectivity only varies slightly by around ±0.1.

4. Experimental results

4.1. Takeda 3A

The CMS Takeda 3A was exposed to a 10 mbar 1:1 H_2/D_2 mixture for 1.5 h for exposure temperatures between 30 K and 140 K. The resulting TDS spectra are shown in Figure 4.1. The desorption spectra for the different exposure temperatures are also compared for each isotope separately in Figure 4.2. The desorption spectra for all exposure temperatures exhibit a large initial desorption signal up to approximately 30 K for hydrogen and 50 K for deuterium. These pronounced signals are not fully visible on the chosen scale of the y-axis. A second desorption signal occurs from 30 K-100 K for hydrogen and 50 K-125 K for deuterium. A third desorption maximum centered around 170 K only occurs after gas exposure above 30 K. According to the pore size distribution of Takeda 3A (see chapter 3.1.1), only the desorption maximum around 170 K can be attributed to the 3 Å nanopores of the sample and therefore, only the area under this third desorption signal is used in order to calculate the gas uptake and the corresponding selectivity given in Table 4.1.

The uptake in the nanopores after exposure to a gas mixture rises with increasing exposure temperature. The maximum hydrogen uptake is reached after exposure to the mixture at 100 K whereas the maximum deuterium uptake is observed after exposure at 90 K. For exposure temperatures exceeding 100 K/90 K, the uptake decreases again. The selectivity drops linearly for exposure temperatures between 30 K and 100 K (see Figure 4.3). For exposure temperatures between 100 K and 140 K, the selectivity remains rather constant between 1.6 and 1.9.

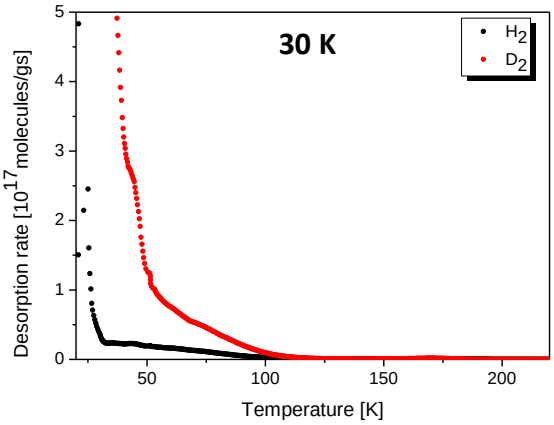
30 K
H2
D2
Desorption rate [10^17 molecules/gs]
Temperature [K]

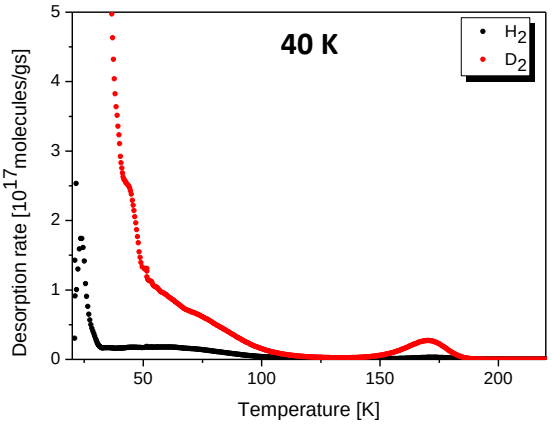
40 K
H2
D2
Desorption rate [10^17 molecules/gs]
Temperature [K]

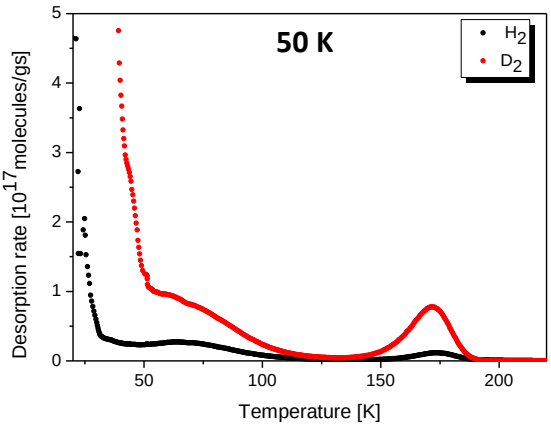
50 K
H2
D2
Desorption rate [10^17 molecules/gs]
Temperature [K]

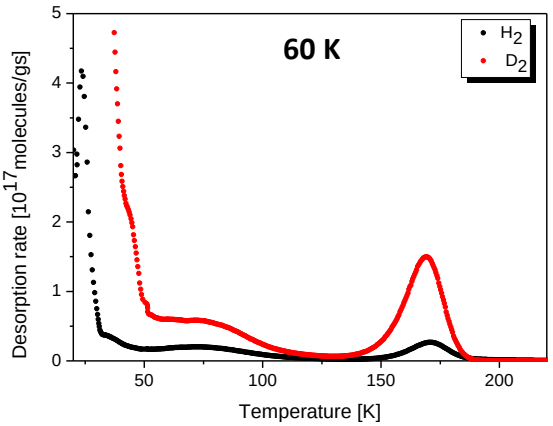
60 K
H2
D2
Desorption rate [10^17 molecules/gs]
Temperature [K]

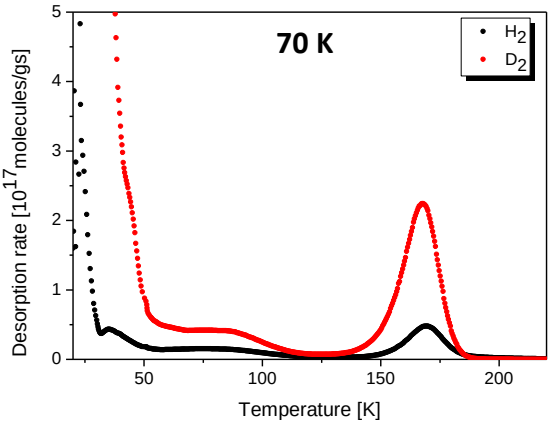
70 K
H2
D2
Desorption rate [10^17 molecules/gs]
Temperature [K]

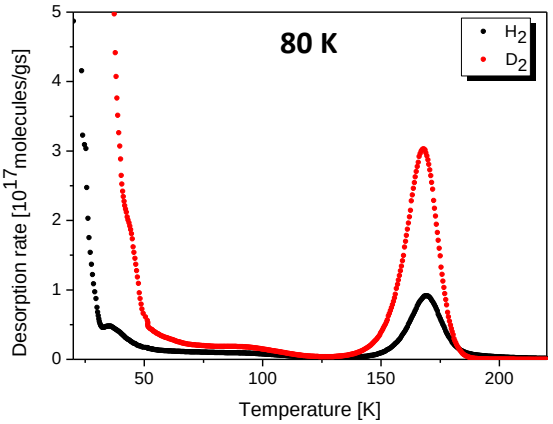
80 K
H2
D2
Desorption rate [10^17 molecules/gs]
Temperature [K]

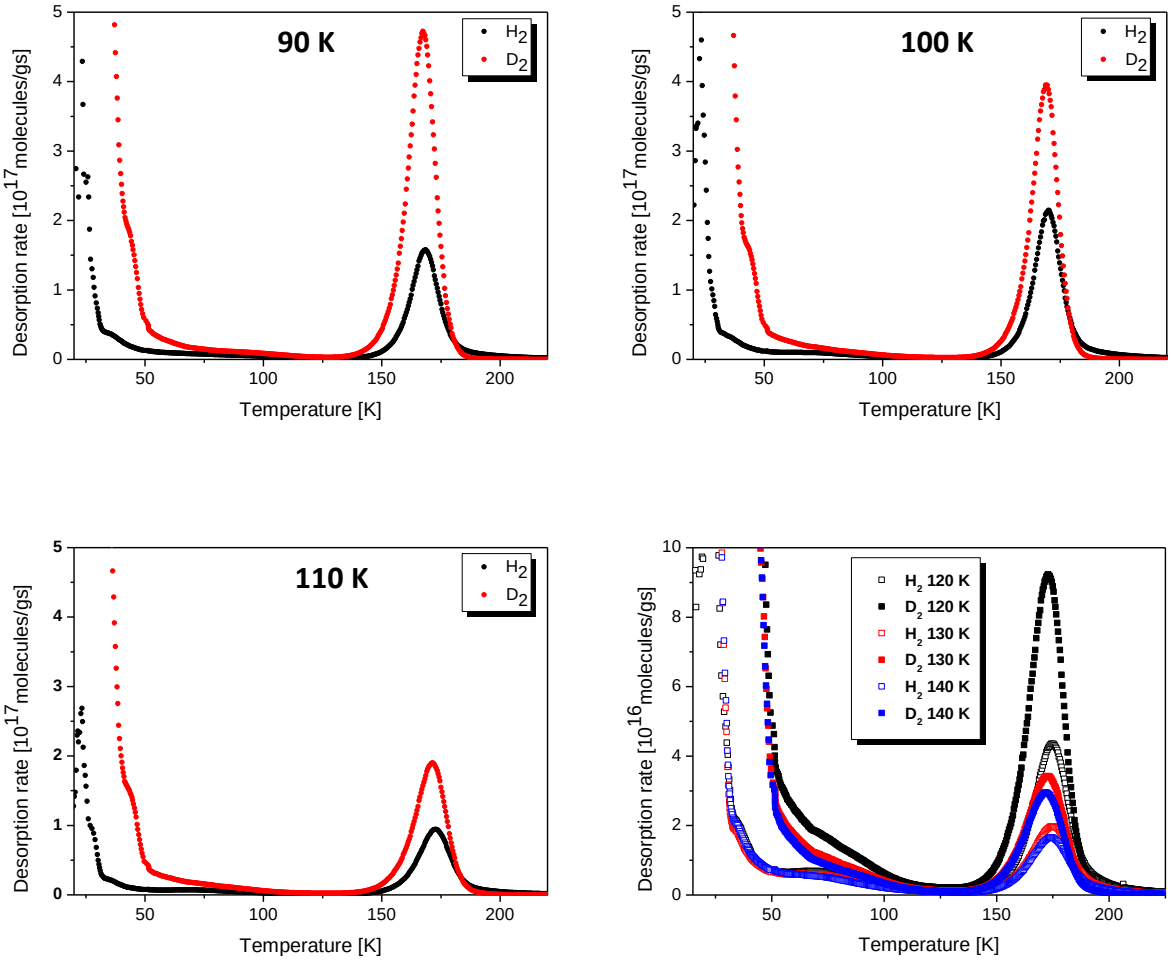

Figure 4.1: TDS spectra of Takeda 3A after exposure to a 1:1 isotope mixture for 1.5 h at 30-140 K. The spectra taken for the exposure temperatures of 30 K-110 K are shown in single pictures with the same scale on the y-axis for better comparison. Owing to the small uptake above 110 K, the spectra obtained after exposure at 120 K-140 K are shown separately in one image.

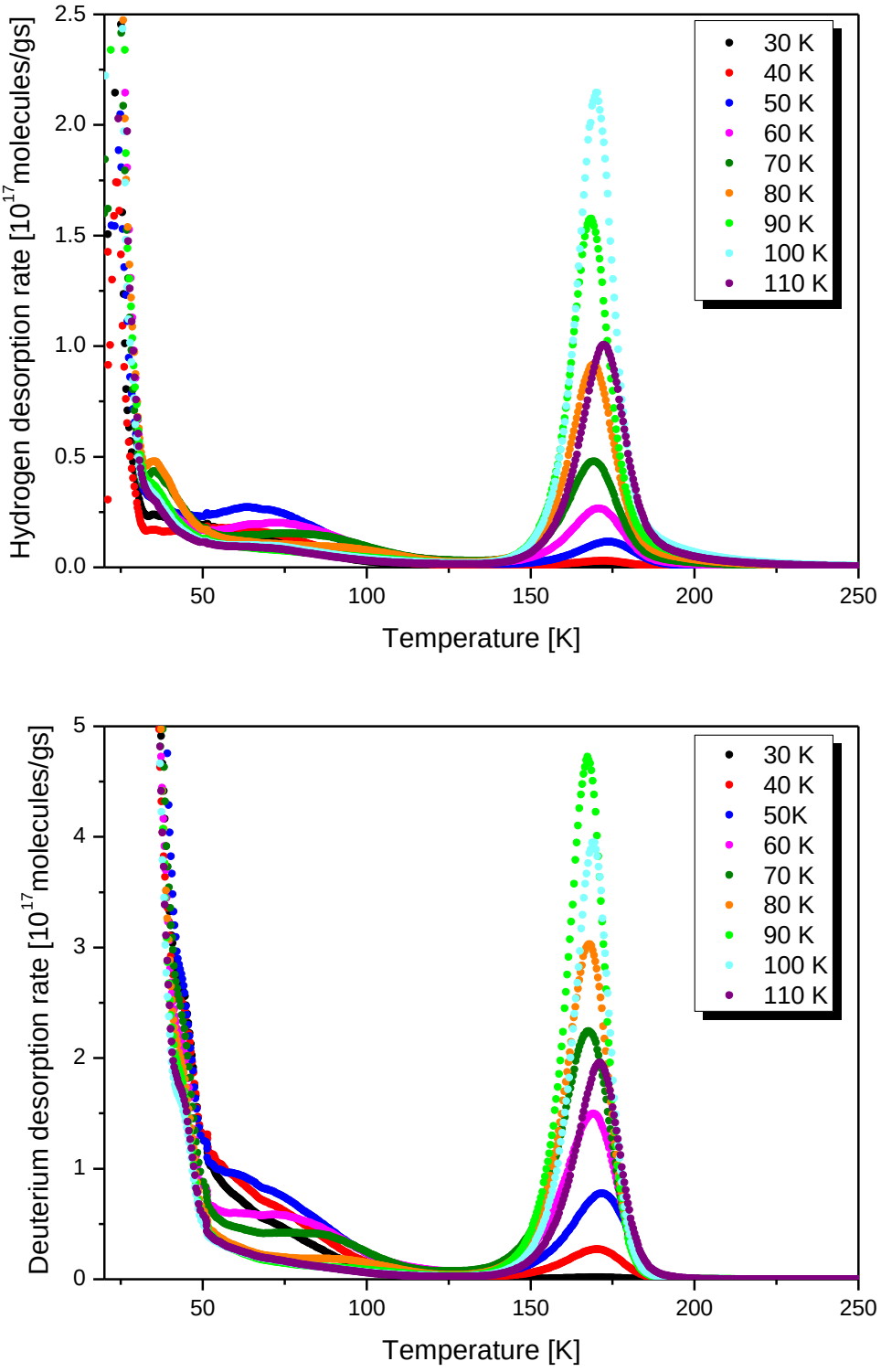

Figure 4.2: Comparison of the hydrogen (top) and the deuterium (bottom) desorption curves measured on the basis of 1:1 isotope mixtures at different exposure temperatures.

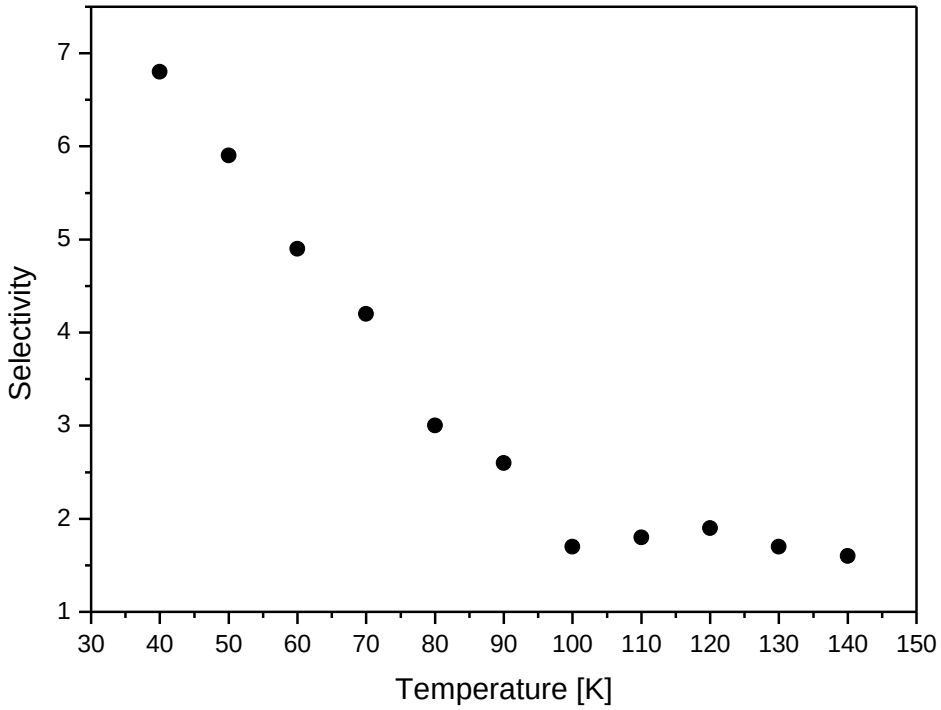

Figure 4.3: Molar selectivity of the nanopores in Takeda 3A as a function of the exposure temperature. The selectivity decreases linearly with temperature from 30 K to 100 K subsequently becoming constant ~1.6-1.9.

Table 4.1: Hydrogen and deuterium uptakes in the nanopores as well as the corresponding molar selectivity of Takeda 3 after exposure to a 10 mbar 1:1 isotope mixture at 40-110 K.

Texp [K]	40	50	60	70	80	90	100	110
H_2 [mg/g]	0.003	0.010	0.021	0.035	0.058	0.088	0.114	0.060
D_2 [mg/g]	0.041	0.117	0.207	0.293	0.343	0.464	0.378	0.220
S_{molar}	6.8	5.9	4.9	4.2	3.0	2.6	1.7	1.8

Takeda 3A was not only exposed to isotope mixtures. For an exposure temperature of 40 K it was also exposed to 10 mbar pure hydrogen and pure deuterium gas for 1.5 h. Thus, it was measured under the same measurement conditions as before except for the application of pure gases instead of an isotope mixture. The desorption spectra after exposure to the pure gases are shown in Figure 4.4. The gas uptakes in the 3 Å nanopores are 0.005 mg/g and 0.035 mg/g for hydrogen and deuterium, respectively. The corresponding molar D_2/H_2 ratio is 3.5.

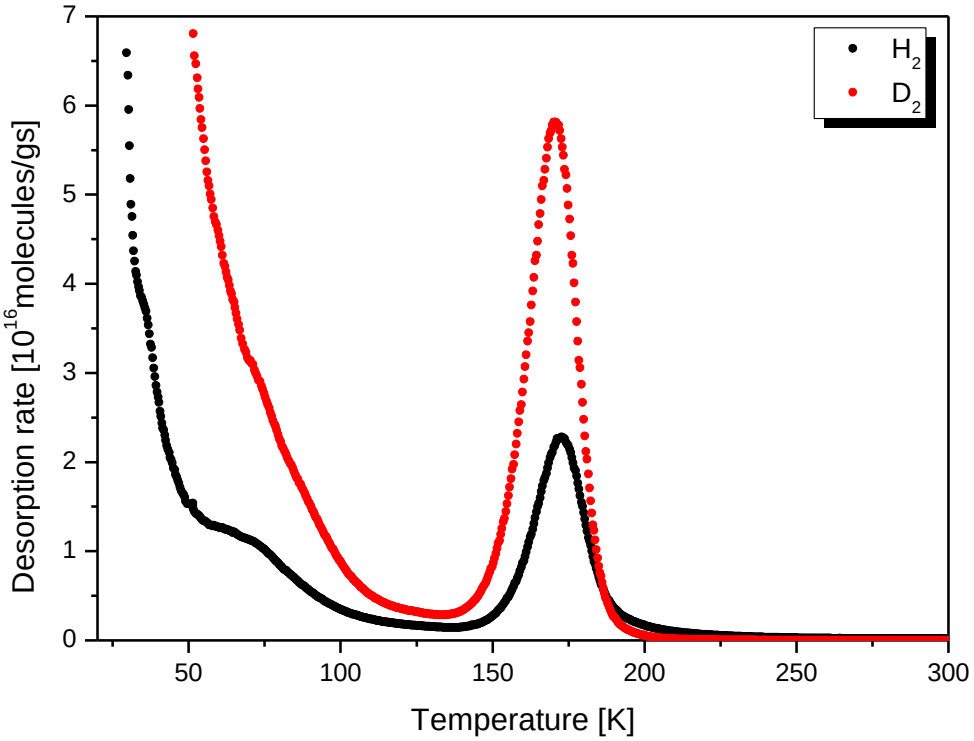

Figure 4.4: Desorption spectra of Takeda 3A after exposure to 10 mbar pure hydrogen and deuterium for 1.5 hours at 40 K.

4.2. MFU-4(Zn, Cl)

Figure 4.5 shows the desorption spectra for MFU-4(Zn, Cl) obtained after exposure to 10 mbar 1:1 isotope mixtures for 1.5 h at 30 K, 40 K and 50 K. The desorption spectra obtained after gas exposure at 30 K and 40 K exhibit a pronounced initial deuterium signal up to 50 K. Such a low temperature desorption signal does not occur for hydrogen. For exposure temperatures exceeding 30 K, an additional desorption signal reaching from roughly 50 K to 100 K can be found for both isotopes. Assuming that solely this high temperature desorption signal between 50 K-100 K results from the nanopores, the gas uptake and the molar selectivity can be calculated by integration over the high temperature

desorption signal (see Table 4.2). After gas exposure at 50 K, the desorption spectra of both isotopes are dominated by the high temperature desorption signal whereas the initial signal at ~25 K became marginal.

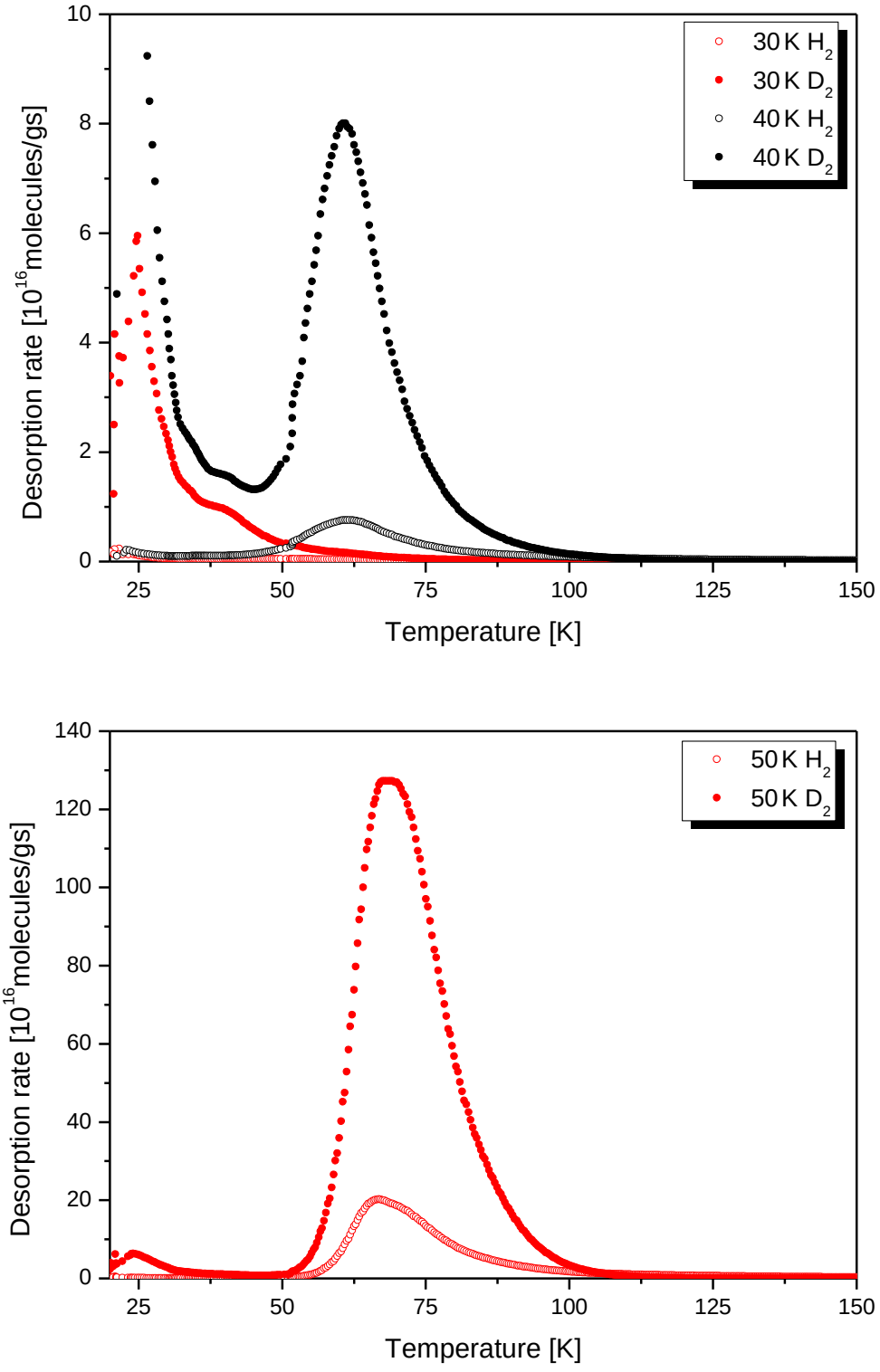

Figure 4.5: Desorption spectra of MFU-4(Zn, Cl) after exposure to a 1:1 isotope mixture for 1.5 hours at 30 K and 40 K (top) as well as 50 K (bottom).[103]

Figure 4.6 shows the desorption spectra after exposing MFU-4(Zn, Cl) to 10 mbar and 20 mbar 1:1 H_2/D_2 mixtures at 60 K and a 10 mbar mixture at 70 K for different exposure times. The uptake values in the micropores and molar selectivity values are also given in Table 4.2.

Table 4.2: Gas uptake in the micropores and molar selectivity values of MFU-(Zn, Cl) obtained for different exposure conditions. For the exposure temperatures of 40 K and 50 K, the uptake values are additionally given per weight in order to allow a comparison to Takeda 3A.

	H_2 uptake [molec/uc]	D_2 uptake [molec/uc]	S_{molar}
40 K 10 mbar 90 min	0.09 (0.007 mg/g)	0.62 (0.098 mg/g)	6.9
50 K 10 mbar 90 min	1.74 (0.137 mg/g)	10.12 (1.590 mg/g)	5.8
60 K 20 mbar 60 min	12.9	47.6	3.7
60 K 20 mbar 30 min	7.5	37.3	5.0
60 K 10 mbar 15 min	4.2	31.5	7.5
70 K 10 mbar 15 min	6.6	9.3	1.4
70 K 10 mbar 5 min	3.7	10.2	2.8

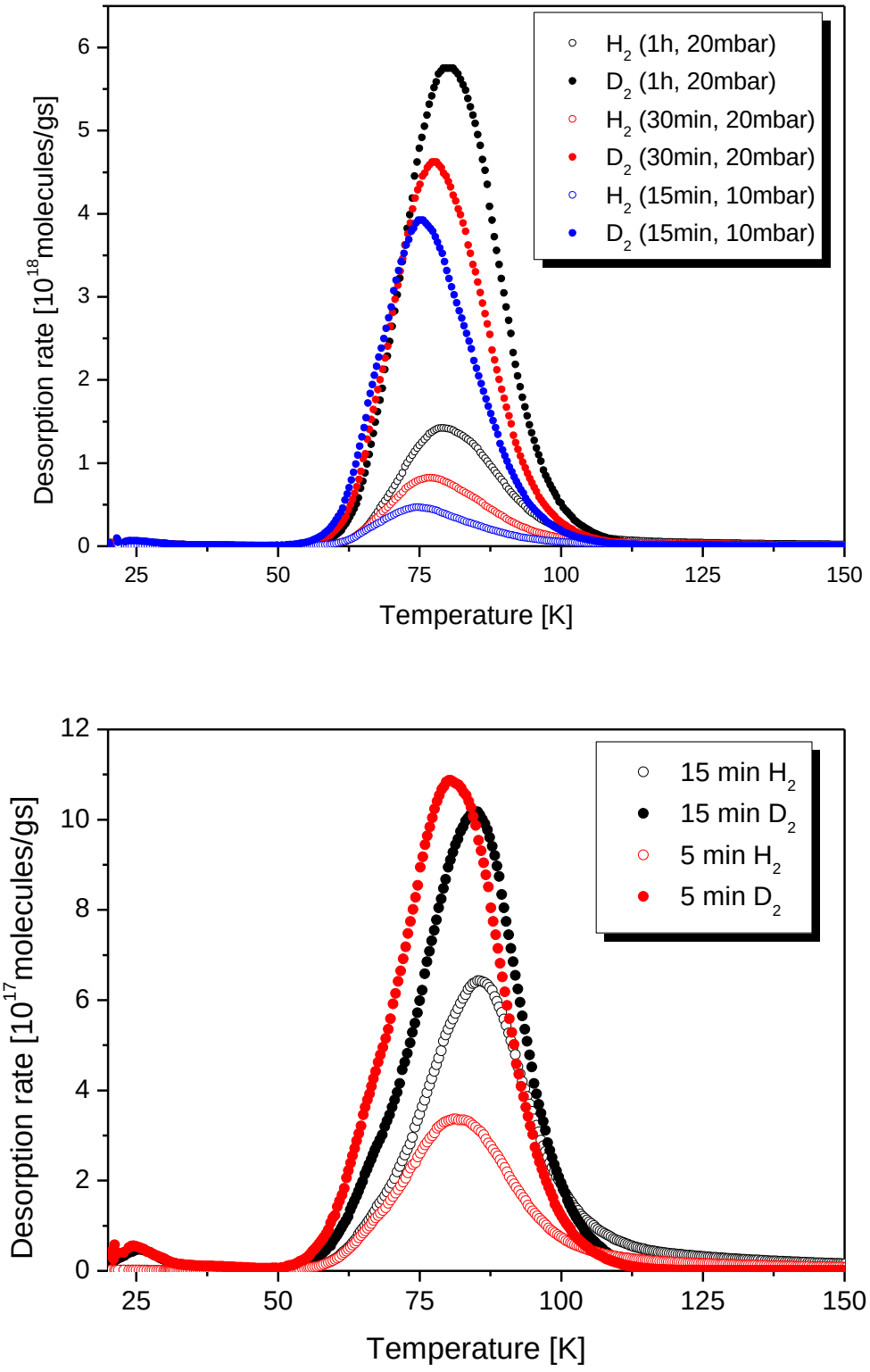

Figure 4.6: Desorption spectra of MFU-4 after loading with a 10mbar/20 mbar 1:1 isotope mixture at 60 K (top) and 10 mbar at 70 K (bottom) for different exposure times.[103]

MFU-4(Zn, Cl) was also exposed to 10 mbar pure hydrogen and deuterium gas at RT (see Figure 4.7). After exposure at RT, two different cooling procedures were performed. The first cooling procedure refers to direct cooling from RT to 20 K within 20 min. The second procedure corresponds to stepwise cooling, i.e. the sample is first cooled from RT to 70 K, held there for 15 min and subsequently cooled to 20 K. Comparing the gas uptakes after direct cooling and stepwise cooling yields that the gas uptakes increase for the stepwise cooling from 1 to 3 and 2.2 to 8 hydrogen and deuterium molecules per unit cell, respectively. Therefore, the molar D_2/H_2 ratios are 2.2 and 2.7 for the direct and the stepwise cooling, respectively.

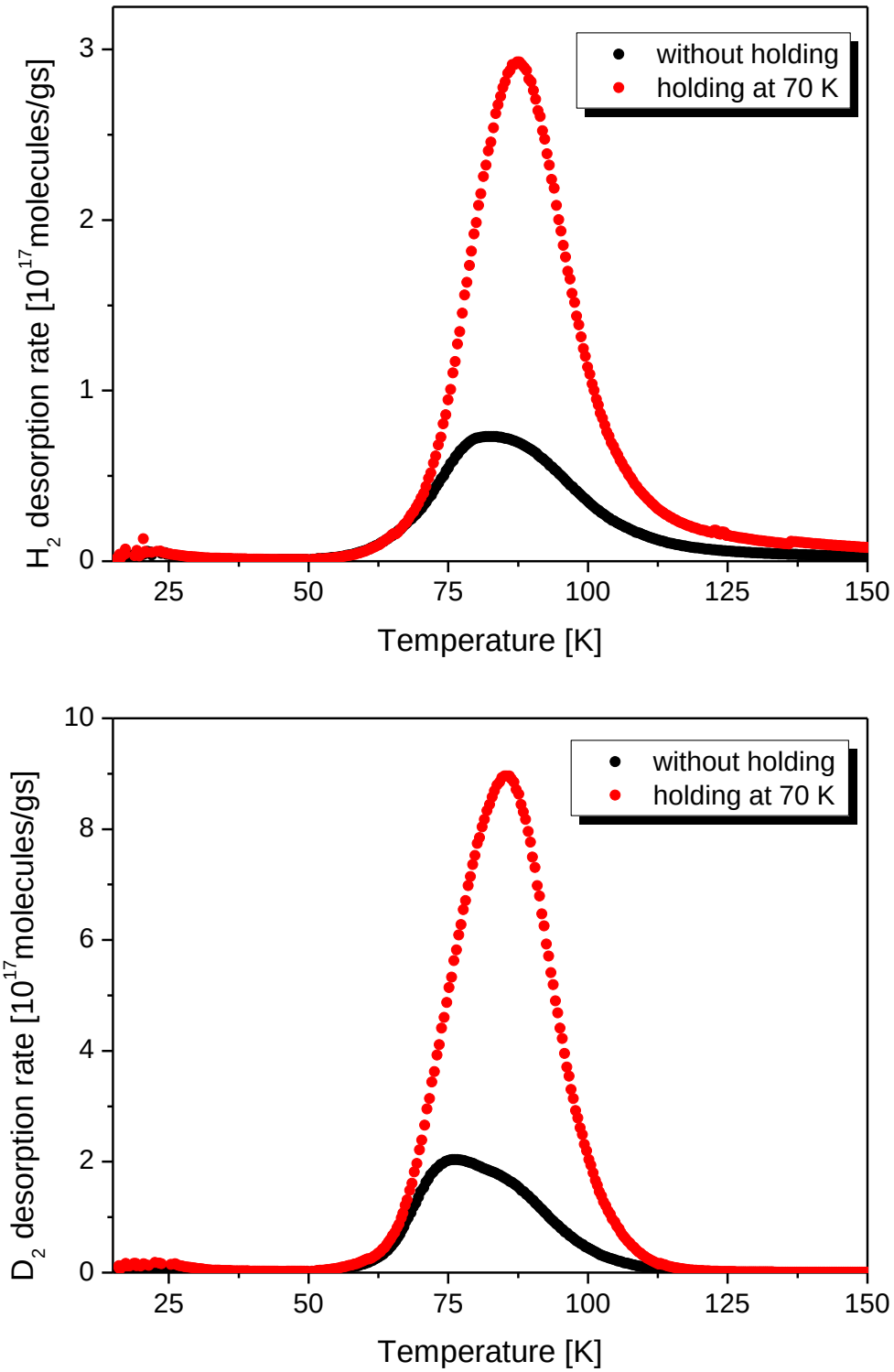

Figure 4.7: Hydrogen (top) and deuterium (bottom) desorption spectra obtained for two different cooling procedures. MFU-4(Zn, Cl) is exposed to 10 mbar pure gas for 15 min. Afterwards two different cooling procedures to 20 K are applied. The first cooling procedure corresponds to direct cooling from RT to 20 K within 20 min. The second procedure corresponds to cooling from RT to 70 K and keeping the sample at 70 K for 15 min before cooling to 20 K.

4.3. MFU-4(Co, Cl)

Figure 4.8 presents the hydrogen and deuterium desorption spectra obtained after exposure to a 10 mbar 1:1 isotope mixture at 30 K and 40 K for 1.5 h. The desorption spectra of both isotopes show a desorption peak from 20 K to 30 K which is only weak in intensity. A second desorption signal, also occurring for both isotopes, reaches from roughly 30 K to 100 K. The instability in the desorption pressure at 50 K can be attributed to a temporary instability in the temperature program (see chapter 3.2.4). Integration over the desorption signal between 30 K and 100 K yields the gas uptake and the selectivity.

Table 4.3: Hydrogen and deuterium uptake as well as the molar selectivity of MFU-4(Co, Cl)

Texp [K]	H_2 [mg/g]	D_2 [mg/g]	H_2 [molecules/SC]	D_2 [molecules/SC]	Smolar
30	2.39	18.87	29	116	4.0
40	4.68	18.64	57	115	2.0

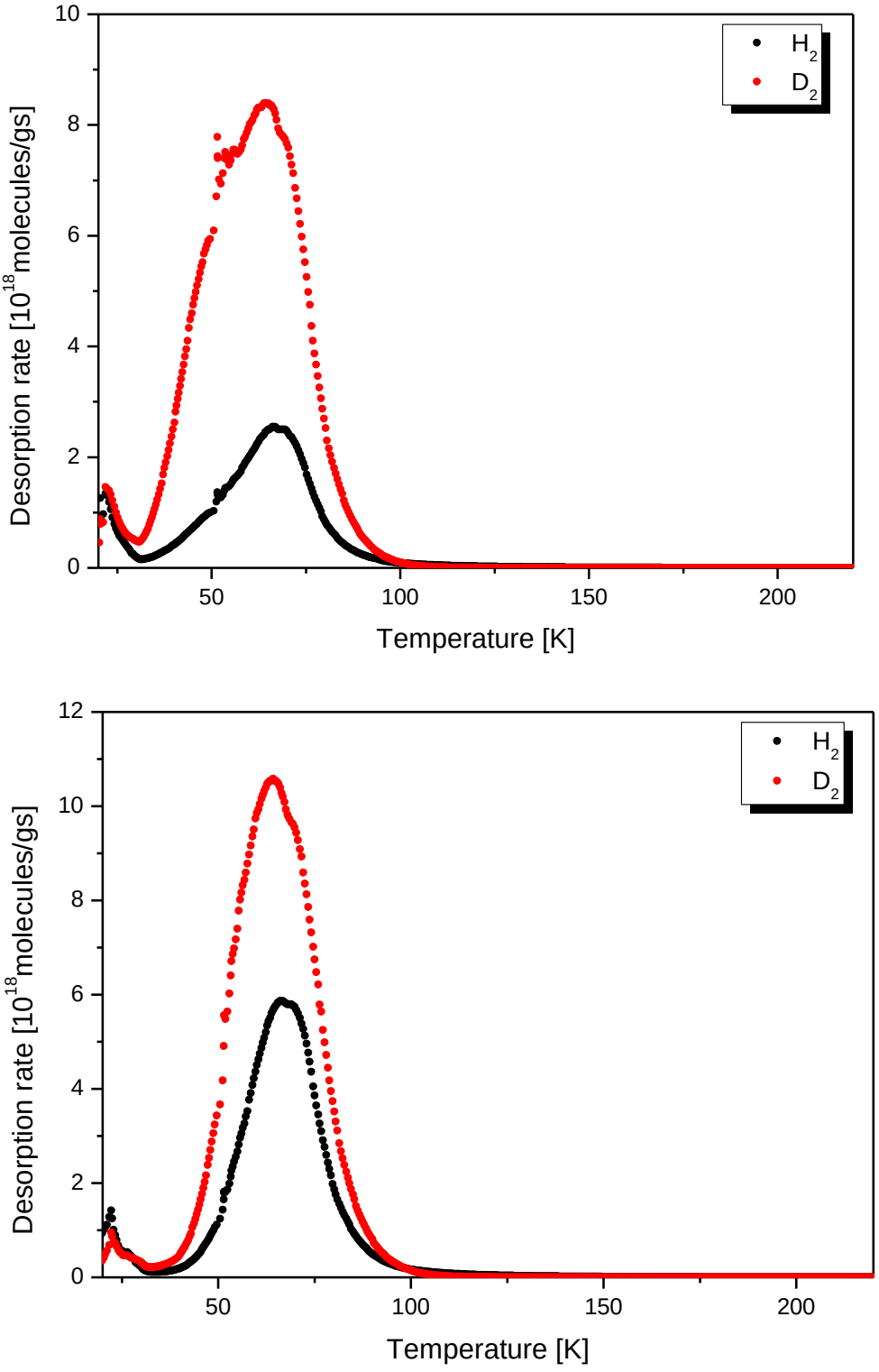

Figure 4.8: Desorption spectra of MFU-4(Co, Cl) after exposure to a 10 mbar 1:1 isotope mixture at 30 K (top) and 40 K (bottom) for 1.5 hours. The instability in the spectra at 50 K is due to an experimental error (see chapter 3.2.4).

4.4. MFU-4(Zn, Br)_T1

In contrast to the previous samples, MFU-4(Zn, Br)_T1 was not exposed to a 10 mbar but a 50 mbar 1:1 isotope mixture for 1.5 h for exposure temperatures between 60 K and 110 K. The reason for the increased exposure pressure is found in the larger kinetic barrier formed by the bromine window. An exposure pressure of 10 mbar is not enough to reveal the desorption signal resulting from the nanopores. The desorption spectra obtained after exposure to a 50 mbar 1:1 mixture are shown separately for each isotope in Figure 4.9.

Hydrogen exhibits only a weak low temperature desorption signal between 20 K and 25 K. After gas exposure at 60 K and 70 K, the hydrogen desorption spectra exhibit one desorption signal at higher temperature which is located around 77 K and 87 K, respectively. If MFU-4(Zn, Br)_T1 is exposed to the gas mixture at higher exposure temperatures than 70 K, the spectra exhibit two high temperature desorption maxima. The first one is centered around 77 K and its intensity and area is rather constant for all spectra exhibiting the two high temperature desorption signals. The second desorption maximum shifts from 98 K to 110 K, 114 K and 115 K after exposure at 80 K, 90 K, 100 K and 110 K, respectively. The second high temperature desorption peak is most pronounced after exposure at 90 K. However, its intensity and area decreases for exposure temperatures exceeding 90 K.

The deuterium desorption spectra for all exposure temperatures show a pronounced signal at 25 K. Two more desorption maxima occur at 34 K and 47 K that are rather equal in intensity and area for all exposure temperatures. Only the spectrum obtained after gas exposure at 70 K exhibits slight deviations in the course of the low temperature desorption signals. After gas exposure at 60 K and 70 K, the deuterium desorption spectra possess only one high temperature desorption maximum centered at 77 K and 86 K. Exposing MFU-4(Zn, Br)_T1 to the isotope mixture at 80 K or higher temperatures, two desorption maxima occur at higher desorption temperatures. The first rather constant signal is centered at 75 K. The second maximum shifts from 99 K to 110 K and 112 K with rising exposure temperature. This signal decreases significantly with rising exposure temperature.

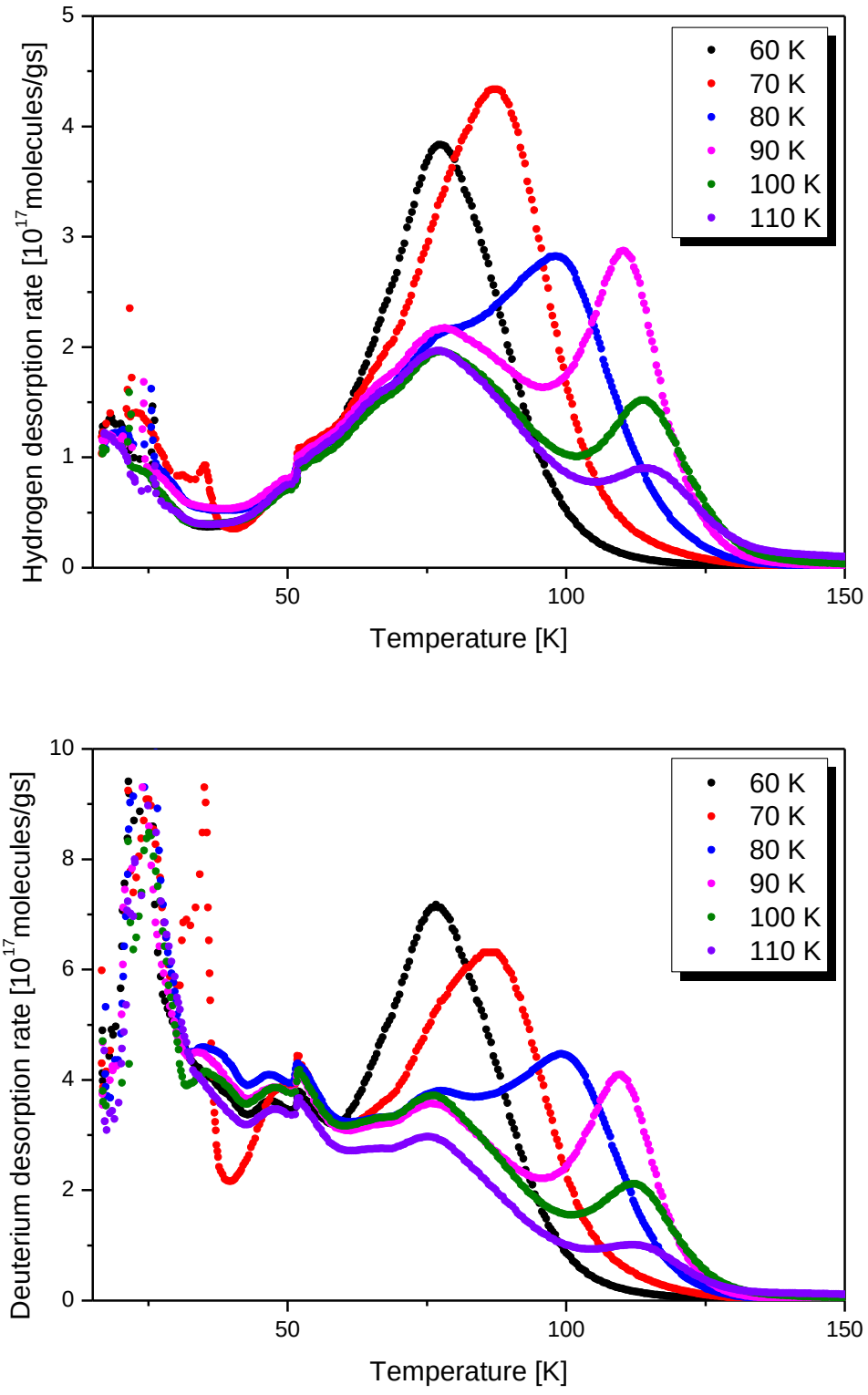

Figure 4.9: Hydrogen (top) and deuterium (bottom) TDS spectra of MFU-4(Zn, Br)_T1 after exposure to a 50 mbar 1:1 H_2/D_2 mixture for 1.5 h at different temperatures.

MFU-4(Zn, Br)_T1 was also exposed to a 10 mbar 1:1 H_2/D_2 mixture for exposure times of 1.5 h and 2.5 h at 90 K. These results are compared to the spectra obtained after exposure to 50 mbar for 1.5 h (see Figure 4.10). The hydrogen desorption spectra after exposure to 10 mbar gas mixture are equal for both exposure times. However, after exposure to 50 mbar, the two hydrogen desorption signals significantly increase in intensity. The deuterium desorption spectra after exposure to the 10 mbar mixtures show slight deviations in the signal intensity below 100 K but rather the same peak intensity and area for the high temperature peak centered at 110 K. This peak increases noticeably in intensity after exposure to a 50 mbar mixture, i.e. when the sample is exposed to higher gas pressure.

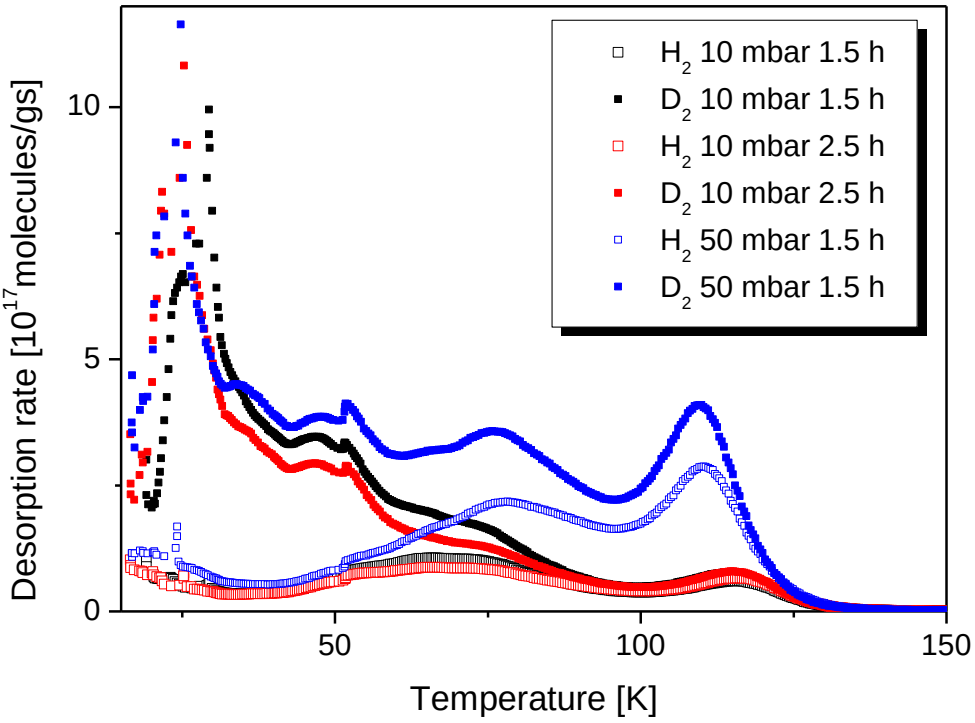

Figure 4.10: Desorption spectra of MFU-4(Zn, Br)_T1 after loading with a 10 mbar mixture at 90 K for two different exposure times. The data are compared to the results obtained after exposure to a 50 mbar mixture for 1.5 h.

MFU-4(Zn, Br)_T1 was also exposed to pure hydrogen gas at higher pressures, i.e. at 150 mbar and 500 mbar (see Figure 4.11). The desorption signal below 25 K is comparable for all exposure pressures. The desorption signal starting from 100 K increases significantly when the loading pressure is increased.

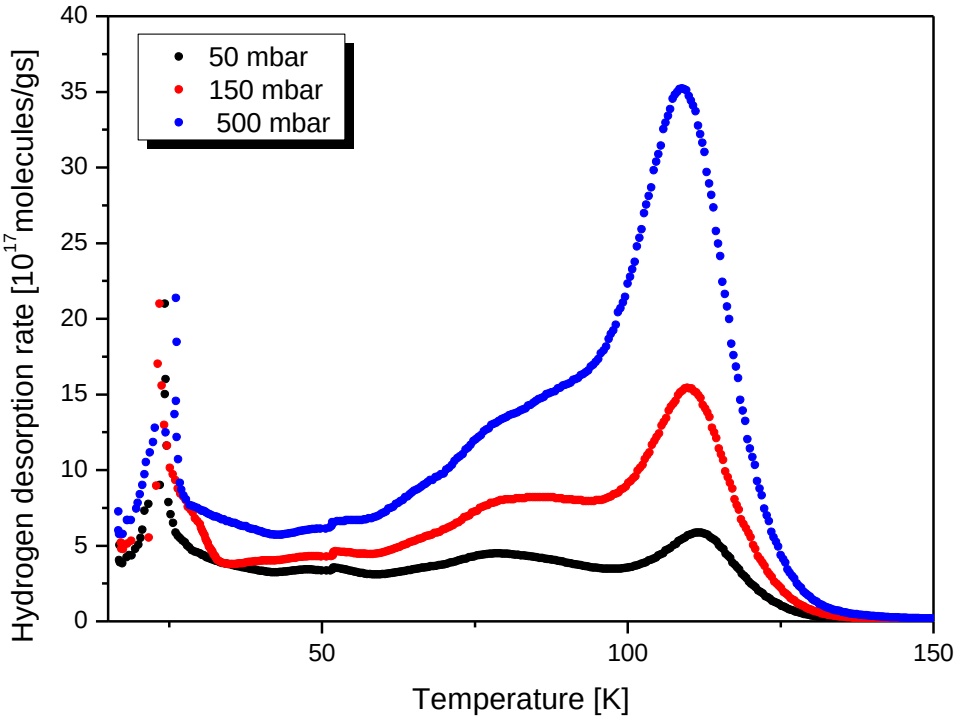

Figure 4.11: Desorption spectra of MFU-4(Zn, Br)_T1 after exposure to pure hydrogen for 1.5 h and 90 K.

4.5. MFU-4(Zn, Br)_T2

MFU-4(Zn, Br)_T2 was measured under the same measurement conditions as MFU-4(Zn, Br)_T1 but the exposure temperatures were exceeded up to 130 K (see Figure 4.12). After exposure to the gas mixture at 60 K, the desorption spectra of both isotopes exhibit one desorption signal of very low intensity centered around 85 K. An additional desorption shoulder at higher desorption temperatures can be found after gas exposure at 70 K and 80 K. For exposure temperatures between 90 K and 130 K, only one desorption signal can be found again. The maximum of this signal shifts with increasing exposure temperature from 119 K to 132 K. The intensity of the desorption signal increases up to an exposure temperature of 110 K. For exposure temperatures exceeding 110 K, the signal intensity decreases with rising exposure temperature.

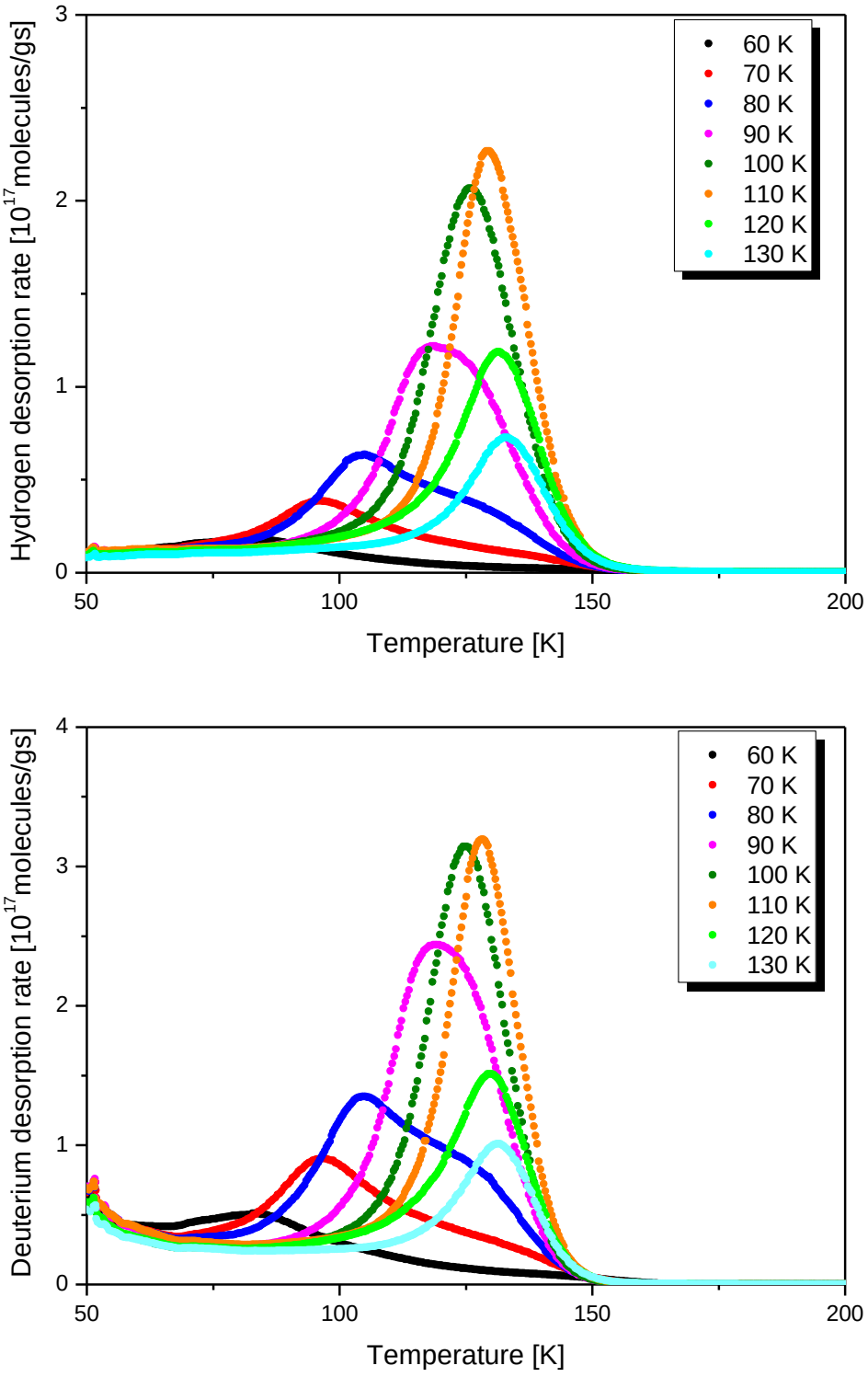

Figure 4.12: Hydrogen and deuterium desorption spectra of MFU-4(Zn, Br)_T2 after exposure to a 50 mbar 1:1 isotope mixture for 1.5 h at different exposure temperatures.

The gas uptake in the micropores and the corresponding selectivity values are calculated by integration over the whole desorption spectra for all exposure temperatures (see Table 4.4). For the exposure temperature of 60 K no values are given as the peak can hardly be separated from the background.

Table 4.4: Hydrogen and deuterium uptake as well as the molar selectivity measured for MFU-4(Zn, Br)_T2 at different exposure temperatures.

T_{exp} [K]	70	80	90	100	110	120	130
H_2 [mg/g]	0.06	0.09	0.13	0.18	0.17	0.11	0.07
D_2 [mg/g]	0.26	0.38	0.49	0.49	0.46	0.30	0.19
H_2 [molec/uc]	0.9	1.4	2.0	2.7	2.6	1.7	1.1
D_2 [molec/uc]	1.9	2.9	3.7	3.7	3.5	2.2	1.5
S_{molar}	2.1	2.1	1.9	1.4	1.3	1.3	1.4

The kinetics of the gas uptake at exposure temperatures of 80 K (two peaks) and at 110 K (single peak spectrum) were studied by applying different exposure times, namely. 45 min and 90 min (Figure 4.13). For an exposure temperature of 80 K, the gas uptake increases from 0.77 H_2 and 1.56 D_2 per unit cell to 1.4 H_2 and 2.9 D_2 per unit cell after exposure to the mixture for 45 min and 90 min, respectively. However, two desorption signals occur for both exposure times. For exposure at 110 K the uptake also increases with rising exposure time from 2.2 H_2 and 2.7 D_2 to 2.6 H_2 and 3.5 D_2 per unit cell. Additionally the influence of exposure pressure was studied. TDS spectra after exposure to 500 mbar pure hydrogen at 110 K were performed for the two different exposure times. The results (see Figure 4.15) exhibit desorption curves of equal shape and magnitude. The uptake values are 38 and 39 H_2 per unit cell. For an exposure temperature of 80 K, the TDS spectra after exposure to 10 mbar and 50 mbar isotope mixture are compared revealing very weak desorption signals after exposure to only 10 mbar of gas (see Figure 4.14).

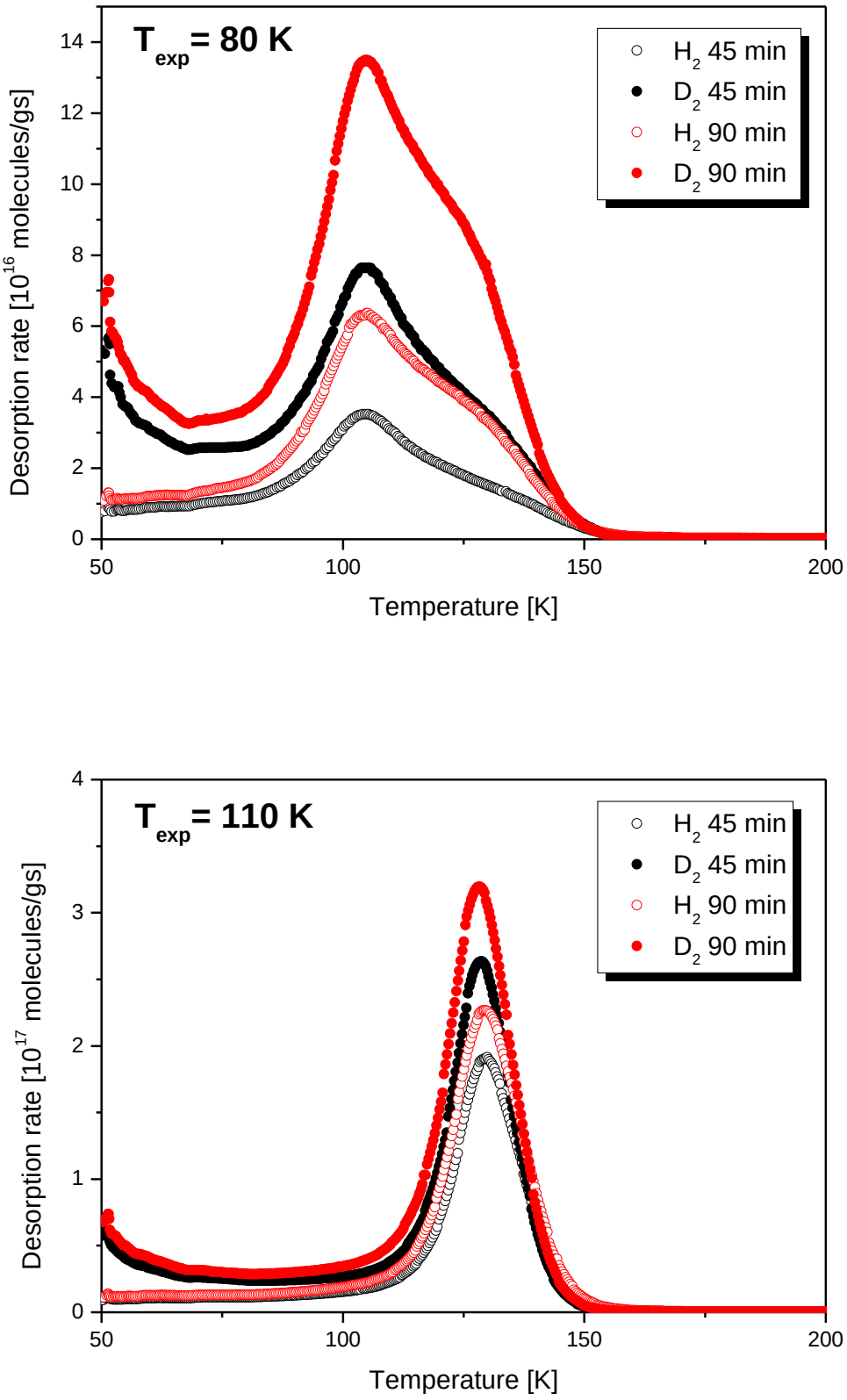

Figure 4.13: Thermal desorption spectra of MFU-4(Zn, Br)_T2 obtained after exposure to a 50 mbar 1:1 isotope mixture for 45 min and 90 min at 80 K (top) and 110 K (bottom).

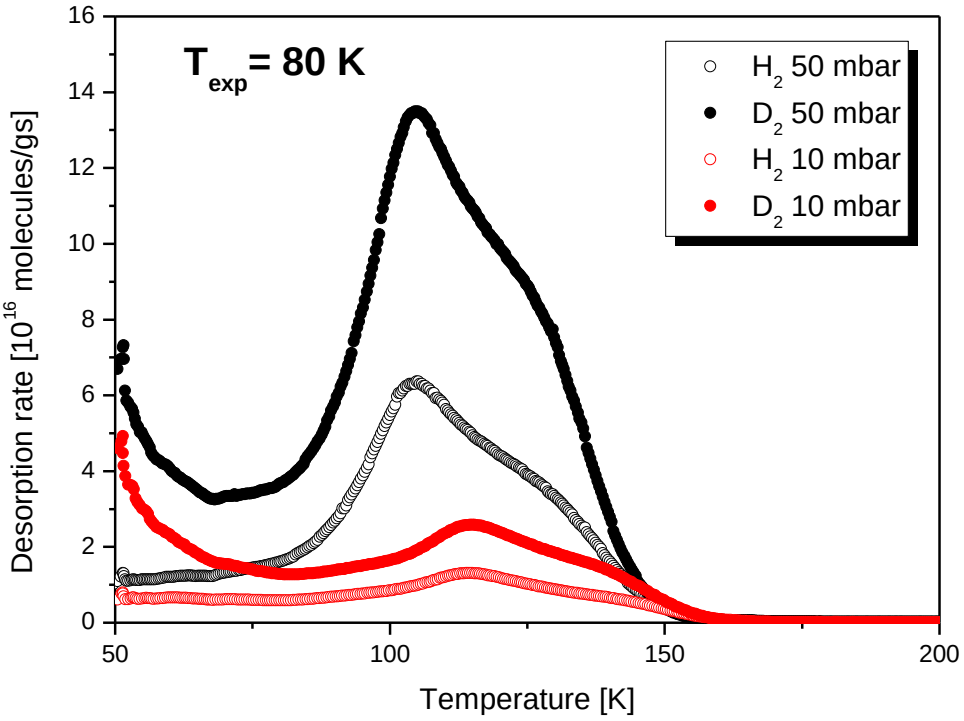

Figure 4.14: TDS spectrum of MFU-4(Zn, Br)_T2 after exposure to a 10 mbar 1:1 isotope mixture for 1.5 h compared to the spectra obtained under the same exposure conditions but a pressure of 50 mbar.

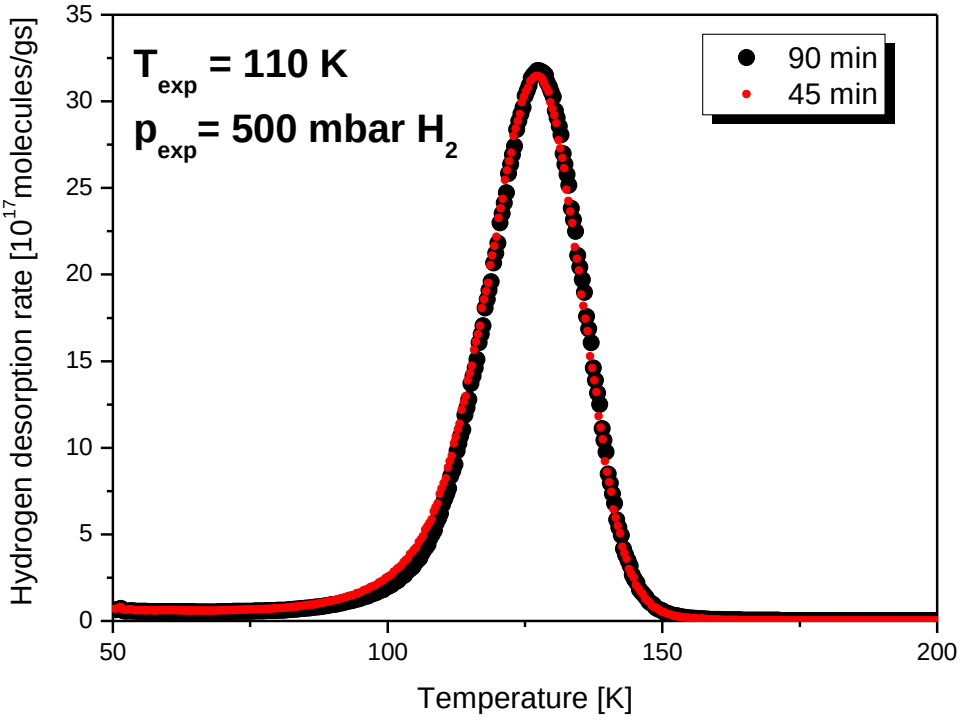

Figure 4.15: Desorption spectrum after exposing MFU-4(Zn, Br)_T2 to 500 mbar pure hydrogen gas at 110 K for 45 min and 90 min.

4.6. MFU-4 *large*

MFU-4 *large* was exposed to 10 mbar pure hydrogen and deuterium as well as a 10 mbar 1:1 isotope mixtures at RT and at 40 K. The exposure times are 15 min and 90 min for exposure at RT and 40 K, respectively.

RT exposure of pure gases results in spectra with two desorption maxima and an additional small desorption shoulder located below 25 K. The first desorption signal is centered around 30 K and exhibits a higher intensity than the following signal with a maximum located around 45 K. The shapes of the hydrogen and the deuterium spectrum are equal but the deuterium spectrum is shifted to slightly higher desorption temperatures with respect to the hydrogen spectrum (see Figure 4.16). The gas uptake calculated by integration over both peaks yields 210 D_2 and 194 H_2 per unit cell, i.e. 10 mg/g hydrogen and 23 mg/g deuterium. Thus, the molar D_2/H_2 ratio after pure gas exposure at RT is 1.08.

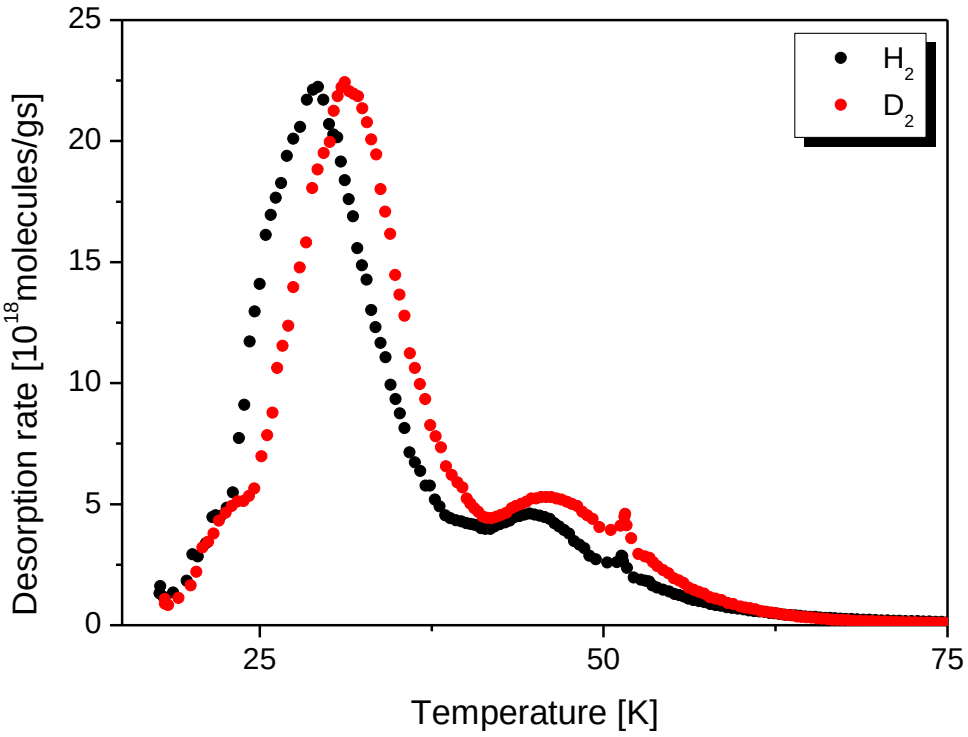

Figure 4.16: Hydrogen and deuterium desorption spectra after exposing MFU-4 *large* to 10 mbar pure gas at RT for 15 minutes.

Exposing MFU-4 *large* to the 1:1 mixture at RT yields desorption spectra presented in Figure 4.17. The desorption maximum centered at 30 K is slightly more pronounced for hydrogen whereat the signal centered at 45 K is more pronounced for deuterium.

Instabilities in the desorption spectra occur at 30 K and 50 K whereat the instability at 50 K can be attributed to the heating control (see chapter 3.2.4). The calculation of the uptake results 108 H_2 and 117 D_2 per unit cell (integration over both peaks). The molar selectivity is equal to the molar D_2/H_2 ratio after pure gas exposure at RT, i.e. it is 1.08.

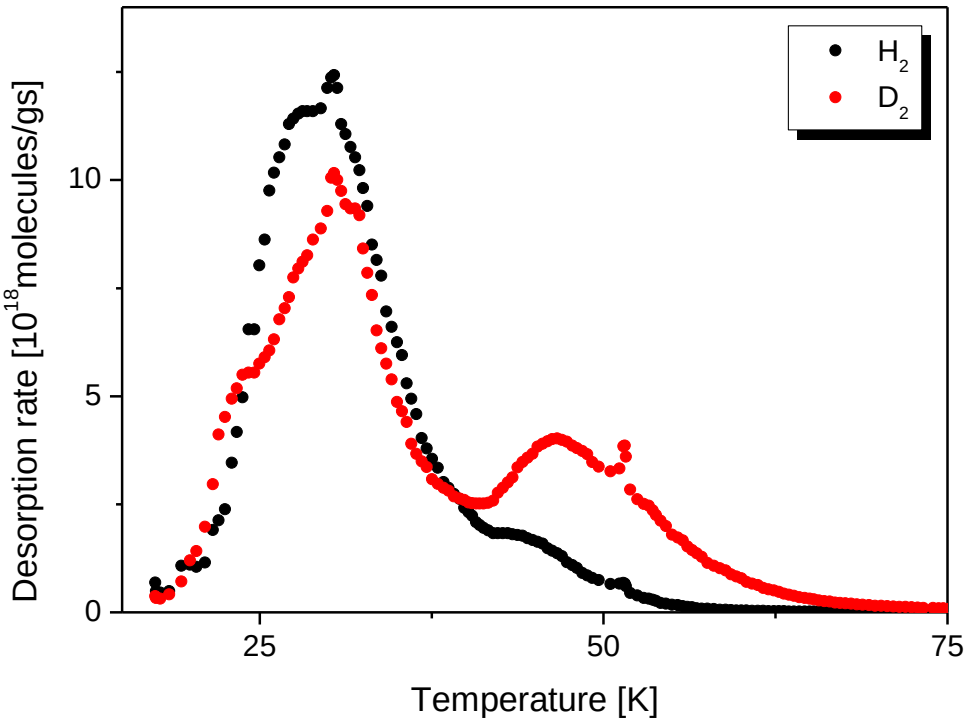

Figure 4.17: Desorption spectra of MFU-4 *large* after loading with a 10 mbar mixture at RT for 15 minutes.

Pure gas exposure at 40 K yields desorption spectra with a two peaks for both isotopes (see Figure 4.18). The first desorption signal ranges from 20 K to 40 K. The second desorption signal ranges from 40 K to 60 K. The shapes of the desorption spectra are equal for two isotopes but the deuterium uptake is larger. The calculated uptakes (integration over both peaks) are 360 H_2 per unit cell (19 mg/g) and 569 D_2 per unit cell (61 mg/g) yielding a molar H_2/D_2 ratio of 1.6.

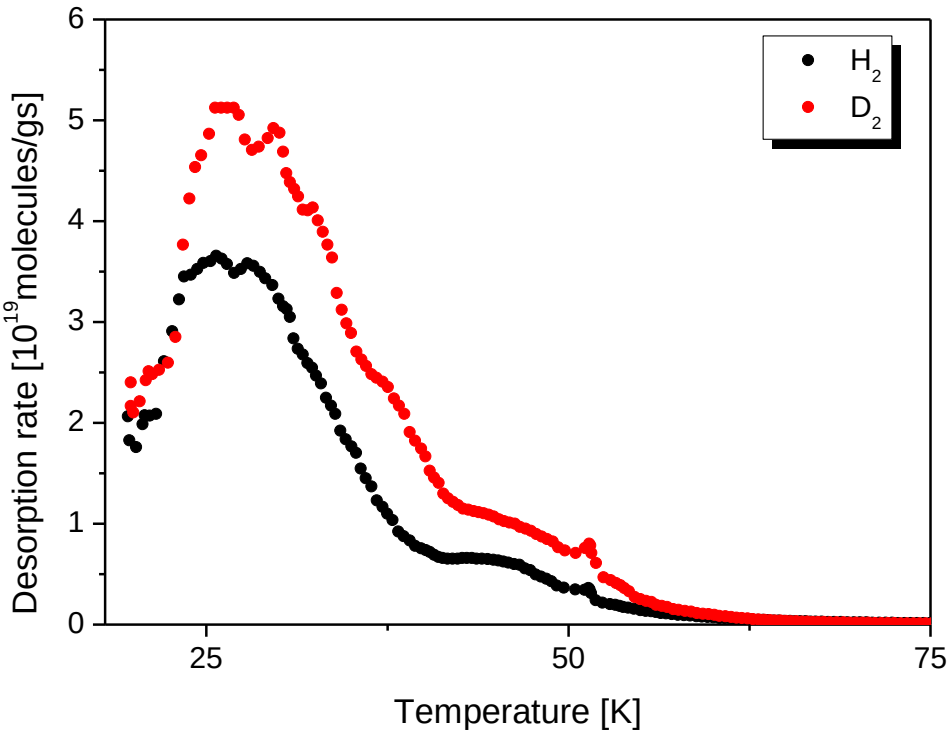

Figure 4.18: Desorption spectra of MFU-4 *large* after exposure to 10 mbar pure hydrogen and deuterium at 40 K for 1.5 h.

Exposing MFU-4 *large* to a 1:1 mixture at 40 K leads to severe differences of the desorption spectra for the two isotopes. The hydrogen desorption spectrum shows only one low temperature desorption signal ranging from 20 K to 50 K. The desorption spectrum of deuterium possesses the same low temperature signal but two additional maxima at higher desorption temperatures. These additional deuterium desorption maxima are centered at 34 K and 46 K. The uptake values (integration over the whole spectrum) are 191 H_2 and 318 D_2 per unit cell yielding a molar selectivity of 1.7.

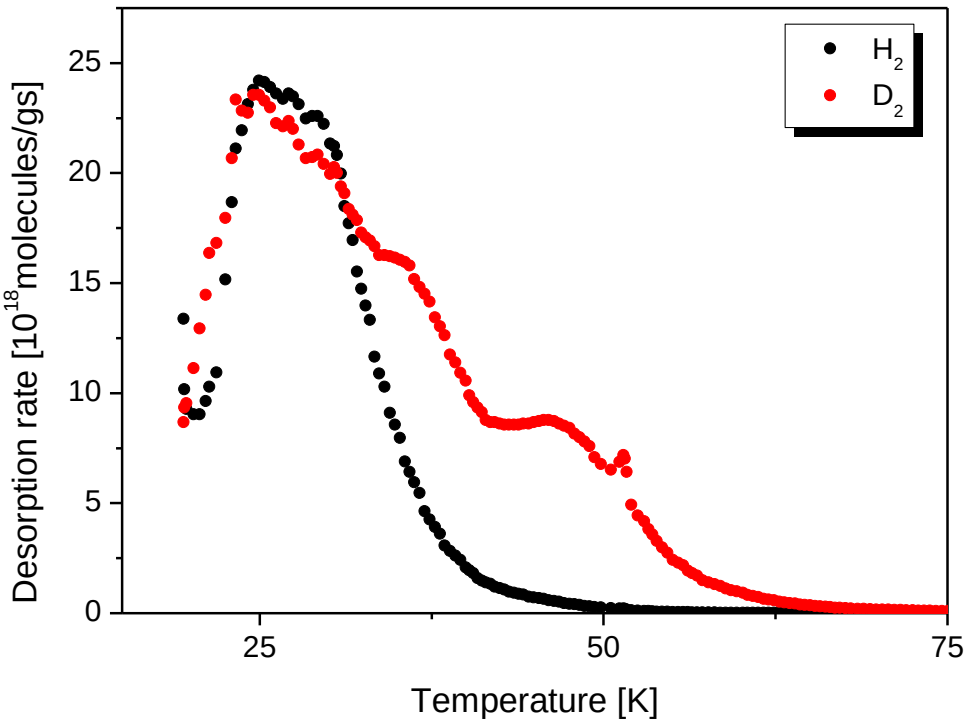

Figure 4.19: Desorption spectra of MFU-4 *large* after exposure to a 1:1 H_2/D_2 mixture at 40 K for 1.5 h.

For sample exposure to a 10 mbar 1:1 mixture at 40 K, the results of two different exposure times, namely 15 min and 90 min, are compared (see Figure 4.20). In principle the spectra do not change noticeably with decreasing exposure time. Just slightly more liquid forms after exposure for 15 min compared to the exposure for 90 min. 191 H_2 and 286 D_2 per unit cell are adsorbed after exposure for 15 min. Therefore the selectivity of 1.5 is equal to the value obtained after 90 min exposure within the measurement accuracy.

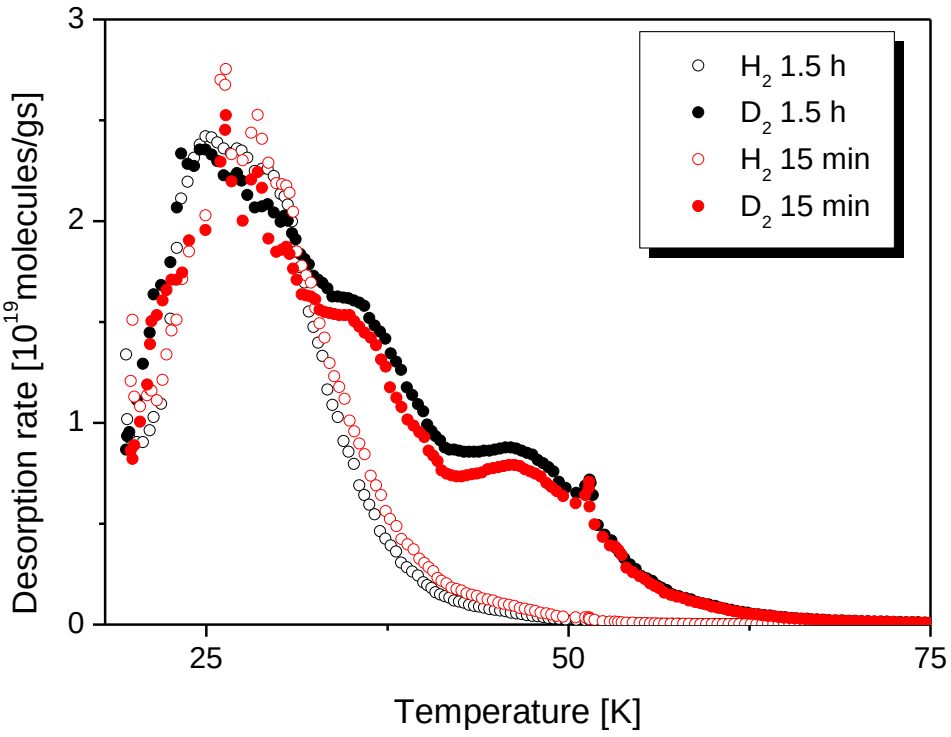

Figure 4.20: Desorption spectra of MFU-4 *large* after exposure to a 10 mbar H_2/D_2 mixture at 40 K for 15 minutes and 1.5 h.

MFU-4 *large* was also tested with 50 mbar 1:1 mixtures exposed for 15 min and 1.5 h at 40 K. The results are shown in Figure 4.21. The hydrogen spectra exhibit only one signal centered around 25 K. The deuterium spectra exhibit a signal ranging from measurement start at 20 K to approximately 30 K which is dominated by liquid formation. A desorption shoulder attaches to this signal at the high temperature side. A third deuterium desorption signal extends roughly from 40 K to 60 K. Furthermore, the desorption spectrum does not change with exposure time. The gas uptakes after loading a 50 mbar 1:1 mixture at 40 K are 44 H_2 and 258 D_2 as well as 32 H_2 and 273 D_2 per unit cell after 15 minutes and 1.5 h exposure, respectively. The selectivity values are 5.9 and 8.5 after 15 min and 90 min exposure.

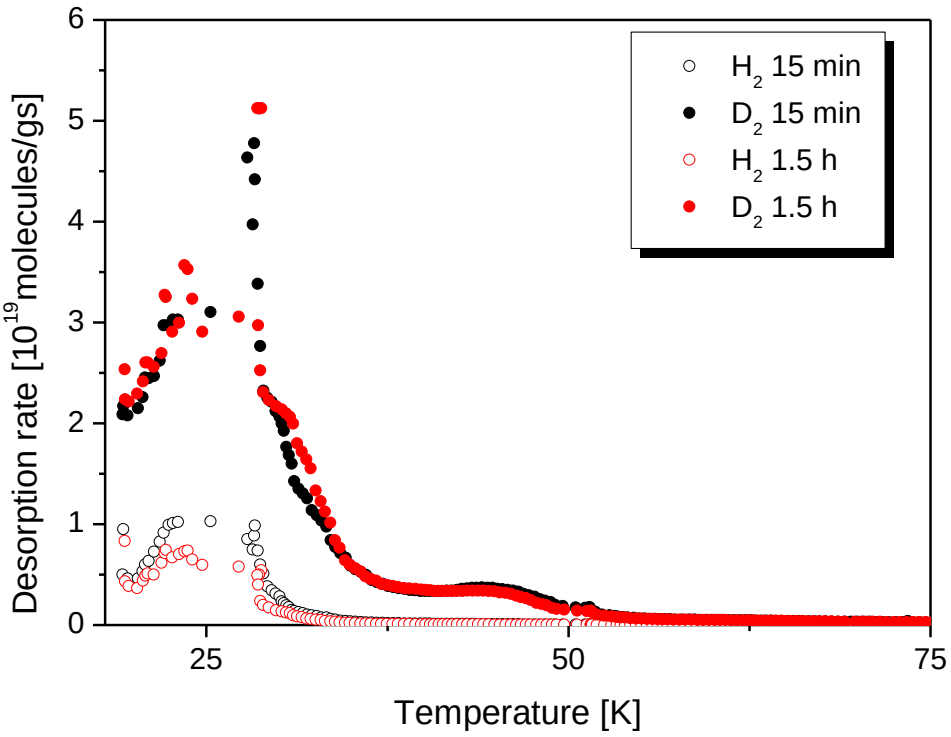

Figure 4.21: Hydrogen and deuterium desorption spectra obtained after loading a 50 mbar 1:1 mixture at 40 K for 15 min and 1.5 h. A pronounced signal from liquid deuterium occurs at 25 K.

MFU-4 *large* was exposed to a 5 mbar 1:1 mixture at 40 K for 15 min. The results are shown in Figure 4.22. For the exposure to low pressure, only one desorption signal seems to occur for both isotopes. It is characterized by a remarkable increase in desorption pressure up to 25 K and a subsequent uniform decline in desorption rate. Additional desorption maxima are not found for this low loading pressure of 5 mbar. The gas uptakes are estimated yielding 75 H_2 and 115 D_2 per unit cell. The selectivity is therefore 1.5.

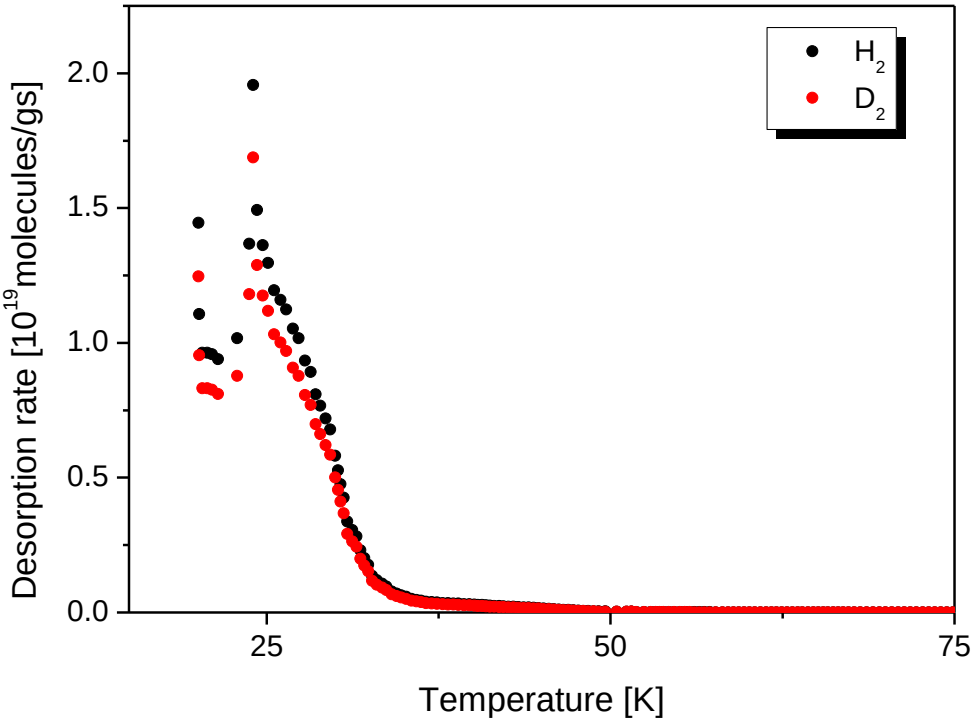

Figure 4.22: Desorption spectra of MFU-4 *large* after exposing the sample to a 5 mbar 1:1 mixture at 40 K for 15 min. The high temperature desorption signal is hardly visible.

A partial desorption experiment was performed after exposure to a 10 mbar 1:1 mixture at 40 K for 1.5 h. The result can be seen in Figure 4.23. The partial desorption experiment is characterized by two desorption runs. The first run starts from 20 K and ends at 41.5 K. Afterwards the sample is immediately cooled back to 20 K and the second desorption run ranging from 20 K to the final temperature is conducted. In the first desorption run hydrogen and deuterium desorb but in the second run mainly deuterium desorbs. In the second run 2.8 H_2 and 48.4 D_2 per unit cell are desorbed, resulting in a selectivity of 17.3.

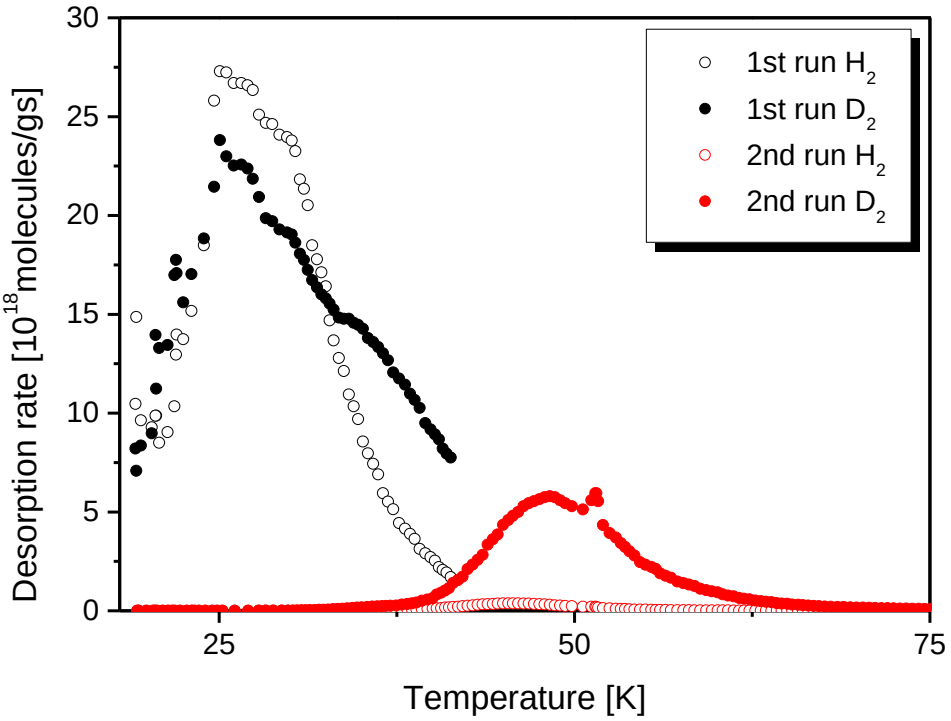

Figure 4.23: Partial desorption of MFU-4 *large* after exposure to a 10 mbar mixture at 40 K for 1.5 h. In the first desorption run the sample temperature is increased from 20 K to 41.5 K. Afterwards the sample is cooled back to 20 K. Then a second desorption run is performed from 20 K to the final temperature. Obviously hydrogen desorbs almost completely in the first desorption run. Therefore the second desorption run yields mainly deuterium.

The desorption spectra of MFU-4 *large* are also recorded for different gas compositions. In Figure 4.24 the spectra after exposure to 90/10 and 80/20 H_2/D_2 mixtures are compared to the results obtained for a 1:1 mixture and the pure gas exposure (see also Table 4.5)

All spectra presented in Figure 4.24 are obtained for exposure conditions of 10 mbar gas for 1.5 h at 40 K. For the mixtures with a hydrogen excess, the low temperature desorption peak ranging from 20 K to 40 K is more pronounced for hydrogen. The high temperature desorption signal centered at 45 K is dominated by deuterium desorption even in case of hydrogen excess. In case of hydrogen excess the hydrogen desorption extends to higher desorption temperatures.

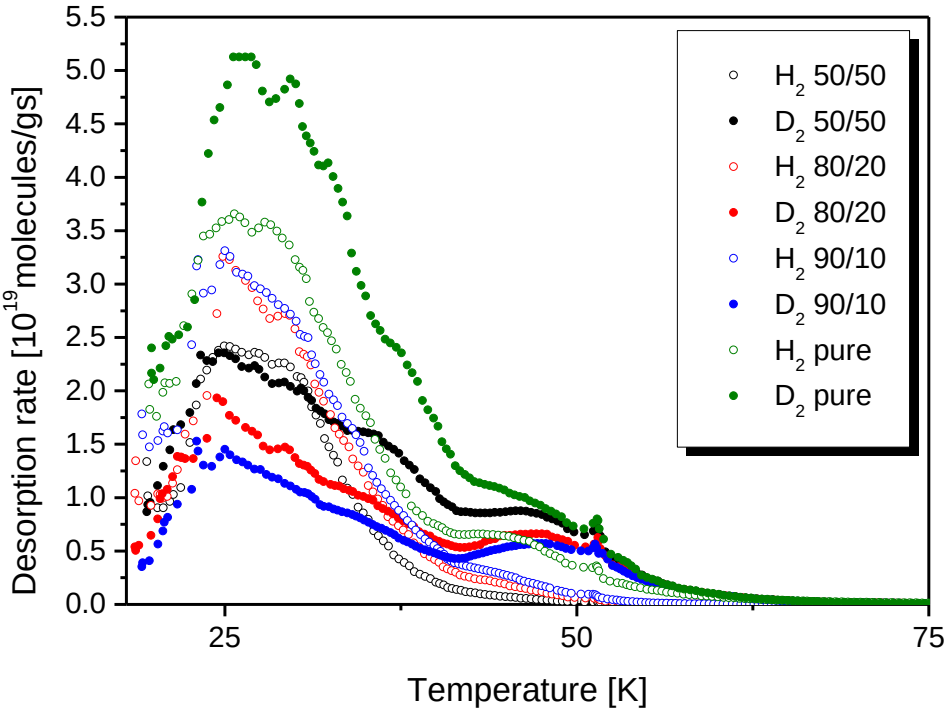

Figure 4.24: Desorption spectra of MFU-4 *large* recorded after exposure to H_2/D_2 atmospheres with different H_2/D_2 ratios reaching from 50/50 to 90/10. Pure gas experiments are shown for completeness. The sample was exposed to the different atmospheres at 40 K for 1.5 h.

MFU-4 *large* was exposed to the 10 mbar 1:1 H_2/D_2 mixture at 80 K for 1.5 h. The results are compared to the spectra obtained after exposure to the same gas atmosphere at 40 K. At 80 K the desorbed amount is smaller compared to the exposure at 40 K and therefore a liquid signal is observed. The gas uptakes after exposure to 80 K are 76 H_2 and 152 D_2 per unit cell. The integral selectivity (integration over the whole spectrum) is therefore 2.0. In contrast to the spectrum obtained after exposure at 40 K, the hydrogen desorption spectrum after gas exposure at 80 K also exhibits a desorption shoulder attaching the initial desorption signal. However, the high temperature desorption signal up to 50 K is dominated by deuterium.

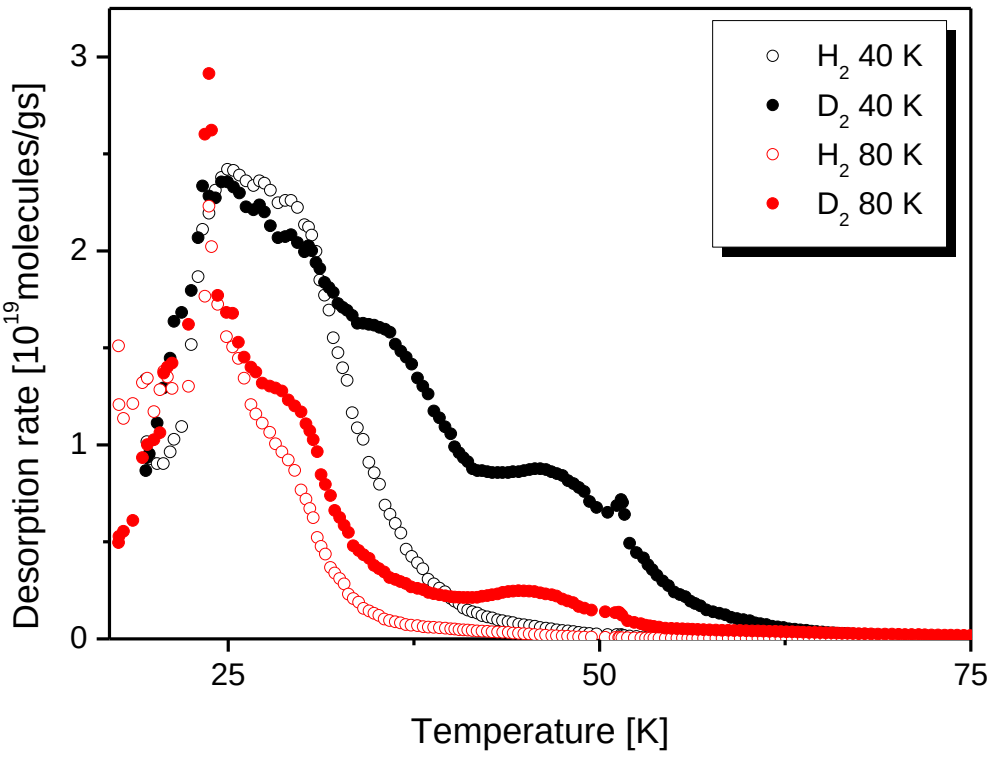

Figure 4.25: Desorption spectra after exposure to a 1:1 isotope mixture for 1.5 h at 80 K compared to the values obtained after exposure at 40 K.

The experimental results presented in Figure 4.24 and Figure 4.25 are also evaluated quantitatively in more detail in Table 4.5. An integral uptake (integration over the whole spectrum) and the uptake of the strong adsorption sites (integration over the high temperature signal) are calculated for the desorption data obtained after gas exposure at 40 K. For the measurement performed after gas exposure at 80 K, only the results after integration over the strong adsorption sites are given because the spectra exhibit a considerable liquid signal at low desorption temperatures.

Table 4.5: Hydrogen and deuterium uptake values obtained after exposure to 10 mbar pure gases or H_2/D_2 mixtures of different compositions. The integral values refer to an integration over the whole spectrum, i.e. all adsorption sites. The uptake at the strong sites is a result of an integration over the signal from ~42 K onwards.

	pure gas	90/10 mixture	80/20	50/50	80 K
H_2 per unit cell integral	360	268	229	191	-
D_2 per unit cell integral	569	167	215	318	-
H_2 per unit cell strong sites	46	16	10	3	3
D_2 per unit cell strong sites	73	49	54	59	20
fraction of strong sites occupied by D_2	100%	75%	84%	95%	87%

4.7. MOF-5

TDS spectra of MOF-5 were recorded after exposure to 10 mbar pure hydrogen and deuterium gas as well as a 1:1 H_2/D_2 mixture at 40 K for 30 min (see Figure 4.26).

After pure gas loading, the desorption spectra of the two isotopes are similar and exhibit a smooth initial increase in desorption pressure, subsequently followed by a desorption maximum centered at 30 K and 32 K for hydrogen and deuterium, respectively. A desorption shoulder extends up to roughly 70 K. 643 D_2 and 463 H_2 desorb per unit cell, i.e. the D_2/H_2 ratio is 1.4. These uptake values correspond to approximately 124 mg/g D_2 and 44.6 mg/g H_2.

Exposing MOF-5 to a 1:1 H_2/D_2 mixture, yields desorption spectra of different shapes for the two isotopes. Only one desorption maximum centered at 30 K is found for hydrogen. However, the deuterium spectrum exhibits three desorption signals in the desorption temperature range between 25 K and 70 K. 331 D_2 and 267 H_2 desorb per unit cell (integral values). These uptake values correspond to 63.8 mg/g deuterium and 25.7 mg/g hydrogen.

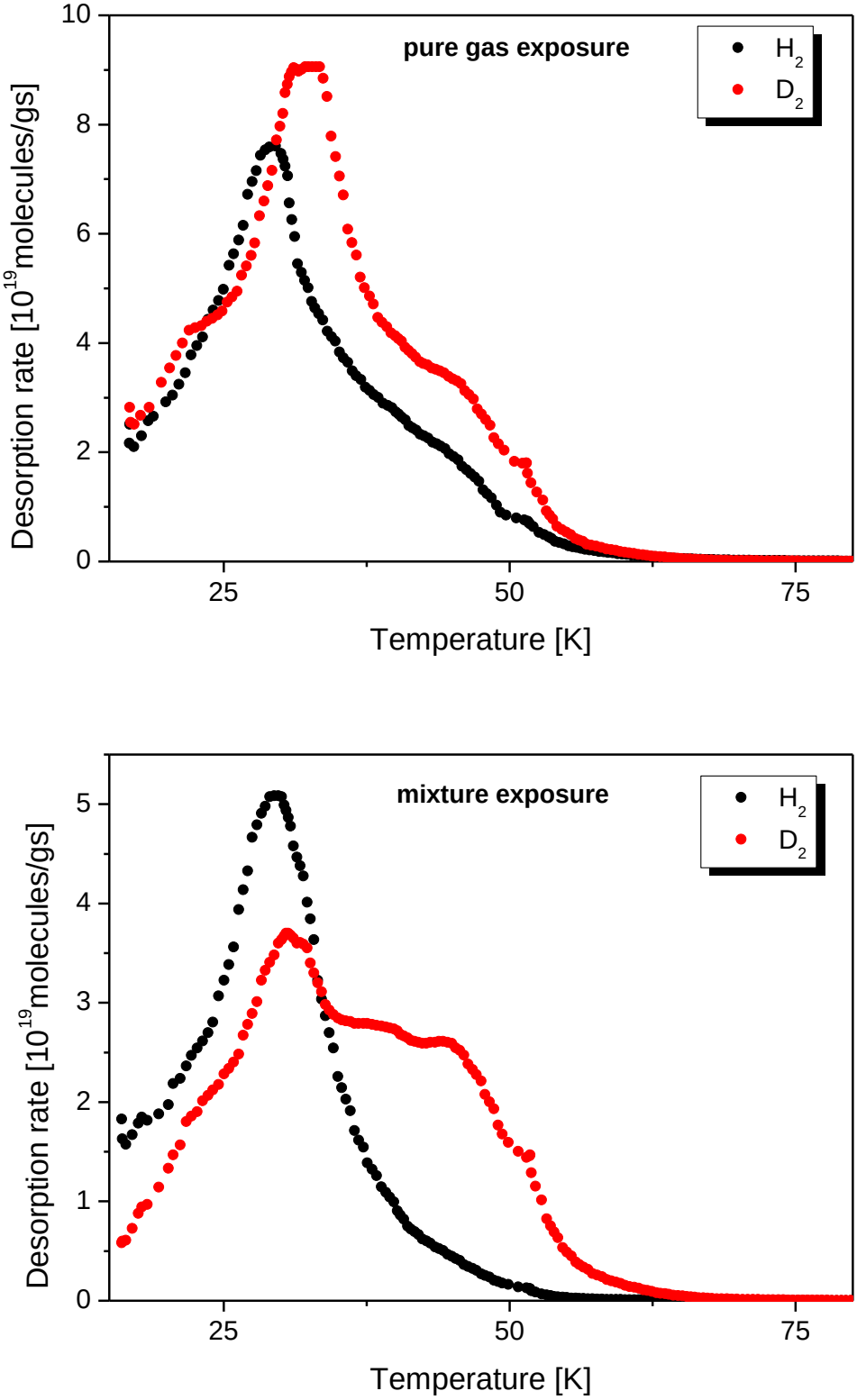

Figure 4.26: Thermal desorption spectra after exposing MOF-5 to 10 mbar pure hydrogen and pure deuterium at 40 K for 30 min (top) and after exposure to a 10 mbar 1:1 isotope mixture for 30 min (bottom).

Partial desorption was performed for MOF-5 after exposure to a 10 mbar 1:1 isotope mixture at 40 K for 30 min (see Figure 4.27). The first desorption run is performed from 20 K to 35 K. Subsequently the sample is immediately cooled back to 20 K and the second desorption run from 20 K to the final temperature is started. The second desorption run yields 89 D_2 and 13 H_2 per unit cell, thereby giving a molar selectivity of 6.8.

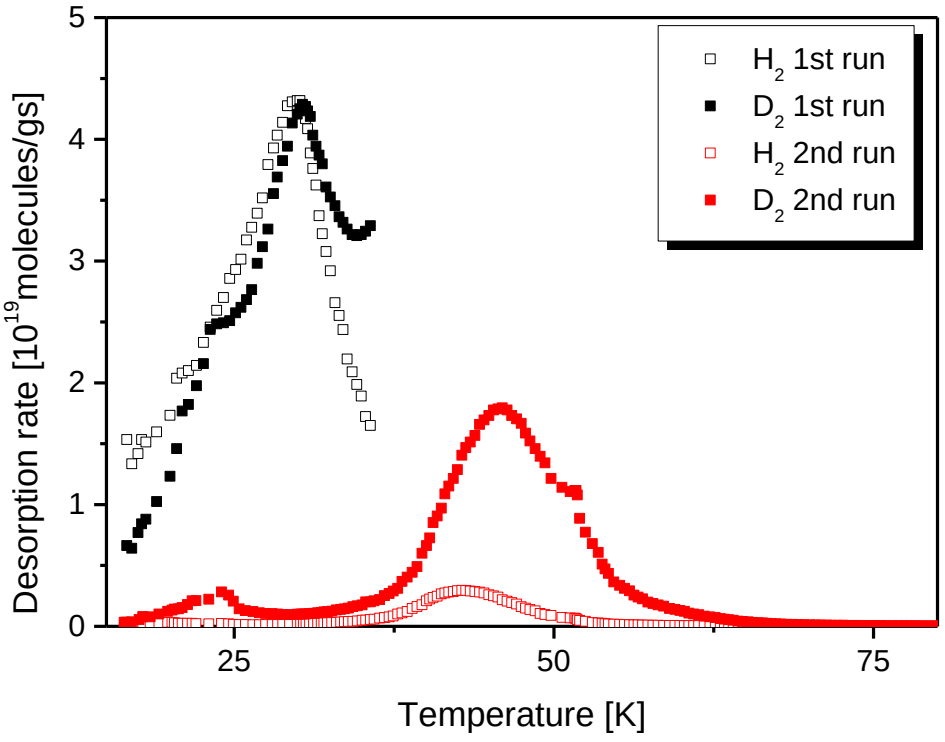

Figure 4.27: Partial desorption of MOF-5 after exposure to a 10 mbar 1:1 isotope mixture at 40 K for 30 min. The first desorption run is performed between 20 K and 35 K.

5. Discussion

Up to now, the separation capability of nanoporous materials has only been estimated roughly by the molar D_2/H_2 ratio obtained by pure gas adsorption experiments that are usually performed at 77 K. The selectivity was not accessible in these experiments and was therefore calculated theoretically or estimated semi-experimentally by applying IAST to the pure gas adsorption isotherms. The current work describes the first experimental selectivity values obtained by applying isotope mixtures in low-temperature TDS experiments.

The H_2/D_2 selectivity was determined for the following samples:

1) Takeda 3A, a carbon molecular sieve for which quantum sieving effects in the sense if inverse kinetics were shown by QENS.[54] Additionally, adsorption isotherms for hydrogen and deuterium are available (see chapter 2.2.3).[55]
2) MFU-4(Zn, Cl), MFU-(Co, Cl) and MFU-4(Zn, Br) that are representatives of the isoreticular MFU-4 framework series. They possess the same framework topology and therefore pore topology with bimodal pore size distribution but slightly different sizes of the pores and pore apertures. As these three MFU-4 sample possess pore apertures of 3 Å or smaller, i.e. apertures comparable to the kinetic diameter of hydrogen, they are termed small-pore MFU 4 derivatives in the following.
3) MFU-4 *large* and MOF-5 which possess apertures and pores far above the kinetic diameter of hydrogen.

5.1. Hydrogen isotope adsorption in Takeda 3A

Takeda 3A was loaded with 10 mbar 1:1 H_2/D_2 mixtures for 1.5 h at different exposure temperatures (30 K-140 K) in order to measure the selectivity as a function of exposure temperature (see Figure 4.1). For exposure temperatures exceeding 40 K, the hydrogen and deuterium spectra exhibit three desorption signals. The first signal is a large initial desorption signal ranging from measurement start to approximately 25 K for hydrogen and 50 K for deuterium. The second signal extends from roughly 25 K-100 K and 50 K-125 K for hydrogen and deuterium, respectively. The third desorption maximum occurs at a desorption temperature of approximately 170 K. As discussed in chapter 3.1.1, Takeda 3A possesses a broad pore size distribution of mesopores and micropores. Therefore the first low temperature desorption signal can be attributed to adsorption and condensation in the mesopores. The second signal is a result of adsorption in the micropores of various sizes.

Only the third high temperature desorption signal centered around 170 K is thought to be attributed to the characteristic 3 Å nanopores. However, the TDS spectra of Takeda 3A is dominated by the two low temperature desorption signals because the adsorption in the nanopores is very small for the chosen exposure conditions (<0.05 wt %). The third high temperature desorption signal does not occur after exposure at 30 K, suggesting that no hydrogen isotope can penetrate the 3 Å nanopores of Takeda 3A at 30 K at least for the chosen exposure time of 90 min.

In principle the desorption spectra in this work are consistent with literature results (see chapter 3.1.1) where also low temperature desorption signals and a characteristic peak at elevated temperatures is found after pure gas exposure at RT. However, the signal attributed to the 3 Å pores is found at slightly higher temperatures in this work. This might be caused by differences in heat contacts or different accuracies in the temperature measurement. The TDS spectra in literature show a large intensity of the high temperature peak whereas the present work exhibits a low intensity of the high temperature peak with respect to the low temperature signals. These differences in intensity are only due to the differences in loading conditions i.e. gas exposure at low temperature and pressure in the current work.

In the following, only the adsorption and the selectivity in the nanopores will be discussed. The gas uptake increases with rising exposure temperature until a maximum uptake is reached at 90 K and 100 K for deuterium and hydrogen, respectively. This observation strongly indicates that hydrogen isotope adsorption is kinetically limited up to approximately 100 K, i.e. the presence of a substantial diffusion barrier as a prerequisite for quantum sieving is fulfilled in Takeda 3A. The selectivity decreases linearly with increasing exposure temperatures in the range from 40 K to 100 K. For exposure temperatures between 100 K and 140 K, the selectivity is found to remain fairly constant around 1.6-1.9. The decreasing selectivity with rising exposure temperature up to 100 K is consistent with QENS measurements which revealed a higher diffusivity of deuterium whereat the difference in isotope diffusivity decreases with increasing temperate and reaching an equal value for hydrogen and deuterium at 100 K.[54] However, even at an exposure temperature of 100 K and above, the deuterium uptake still exceeds the hydrogen uptake in the performed TDS experiments and therefore the selectivity remains larger than 1.

There are three possibilities that might explain why the selectivity does not drop to definite 1:

I) The first possibility is that the determined calibration constants for the mass spectrometer signal are not accurately enough.

II) The second possibility is related to the experiment itself. It is assumed that the results of the TDS experiment reflect the adsorption state at the exposure temperature and that the cooling to 20 K just freezes this adsorption state. However, after gas exposure at 100 K or higher, a large temperature window has to be crossed which might change the adsorption state. During the cooling from 100 K/140 K to 20 K, additional deuterium might be adsorbed.

III) A third possible explanation is a high deuterium concentration at the surface due to its lower ZPE value which might impede hydrogen adsorption. As the adsorbed amount and therefore the penetration rate are low, the deuterium concentration on the powder particle surface barely changes with time. Thus, not many adsorption sites at the surface become vacant, i.e. available for hydrogen. In that case, hydrogen could not equalize the concentration within the chosen exposure time of 1.5 h and the selectivity values of 1.6-1.9 would just be due to non-equilibrium and direct competition for the adsorption sites between hydrogen and deuterium.

The influence of direct competition in the presence of an isotope mixture (case III) can be estimated if the sample is measured under the same conditions except for the application of pure gases. Therefore Takeda 3A was also exposed to 10 mbar pure hydrogen and deuterium gas at 40 K for the same exposure time. The selectivity in the presence of the mixture is about twice the molar D_2/H_2 ratio of the pure gases. In the presence of the mixture, the hydrogen and deuterium uptakes are 0.003 mg/g and 0.041 mg/g, respectively. For pure gases the uptakes are 0.005 mg/g and 0.035 mg/g. Thus, the hydrogen uptake is larger in the presence of pure gas whereas the deuterium uptake is larger in the presence of the mixture. However, the gas uptake is marginal in both cases (< 0.05 wt%) and the deuterium uptake exceeds the hydrogen uptake noticeably for the mixture and the pure gas experiments. Nevertheless, the selectivity is 6.8 and the D_2/H_2 ratio only 3.5 for the same measurement conditions.

One can conclude that three contributions could yield the higher deuterium uptake compared to the hydrogen uptake in the presence of pure gases and the isotope mixture as well as the higher selectivity compared to the D_2/H_2 ratio.

1) **Non-ideal behavior of the isotope mixture:**

   The higher selectivity compared to the D_2/H_2 ratio suggests that the isotope mixture does not behave like in an ideal solution. Competitive adsorption obviously enhances the selectivity.

2) **Preferred adsorption of deuterium:**

   Deuterium is preferentially adsorbed due to its lower ZPE value. The results of Zhao[55] suggest D_2/H_2 ratios smaller than 1.1 at 77 K. But at 40 K deuterium will be preferred even more. In order to reveal this influence, the D_2/H_2 ratio measured by Zhao at 77 K is compared to the selectivity measured by TDS after exposure to the mixture at 80 K.

3) **Kinetic effect:**

   The results of the QENS measurements[54] state that the diffusivity of deuterium must be noticeably larger at 40 K (see Figure 2.13). Therefore the isotopes will penetrate the framework at different rates in the TDS experiments. Thus, the selectivity is a function of exposure time.

The influence of 2) and 3) are discussed in the following:

2) The TDS spectra obtained after exposure to a 10 mbar 1:1 isotope mixture for 1.5 h at 80 K yield a molecular selectivity of 3.0. This selectivity value is much larger than the molar D_2/H_2 ratio (~1.06) calculated on the basis of isothermal pure gas adsorption experiments at 77 K up to 1 bar[55] (see chapter 2.2.3 and Figure 2.12). However, the molar D_2/H_2 ratios are equilibrium values that are reached after several hours. The selectivity measured after gas exposure for 90 min is a non-equilibrium value which is always larger than the equilibrium value due to the higher penetration rate of deuterium.

3) The paper of Zhao also indicates higher rate constants of adsorption and desorption for deuterium in Takeda 3A at 77 K (see Figure 5.1). A maximum difference in the adsorption/desorption rate constants for the isotopes is found at low pressure and surface coverage.

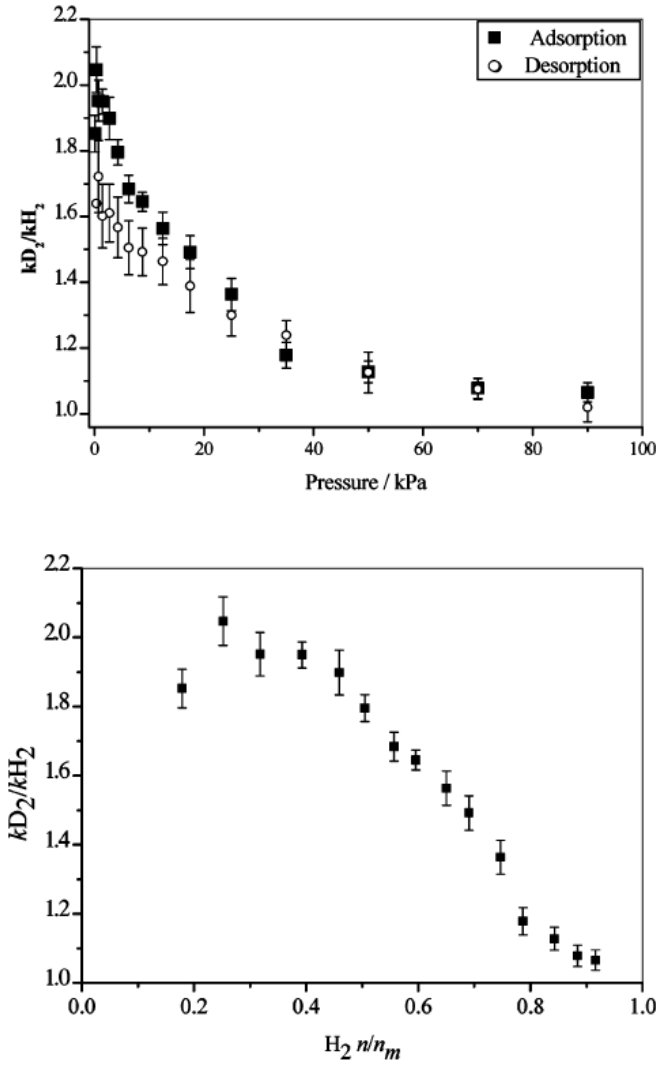

Figure 5.1: Ratio of the rate constants of adsorption (closed symbols) and desorption (open symbols) as a function of pressure at 77 K (top) and the rate constants of adsorption as a function of surface coverage at 77 K (bottom).[55]

One can therefore conclude for the mixture based TDS experiment that the higher adsorption rate of deuterium leads to its enrichment in the adsorbed state for short exposure times. With elapsing exposure time, an increasing amount of hydrogen will adsorb tending to reach the equilibrium adsorption ratio. However, as diffusion is slow at low temperatures in Takeda 3A, the establishment of adsorption equilibrium needs probably more time than 90 min. TDS experiments with different exposure times were not measured for Takeda 3A but for MFU-4(Zn, Cl).

For Takeda 3A and the measured selectivity values by low temperature TDS experiments, two main conclusions can be drawn. Firstly, the mixture does not behave like an ideal solution. Therefore, the selectivity in the presence of a mixture is larger compared

to the D_2/H_2 ratio after pure gas exposure. Secondly, the measured selectivity values are larger than the D_2/H_2 ratios obtained by isotherm measurements because TDS exploits the kinetic nature, i.e. the inverse kinetics of the quantum sieving phenomenon, and therefore non-equilibrium selectivity values are obtained for the chosen exposure conditions.

5.2. Hydrogen isotope adsorption in MFU-4(Zn, Cl)

A comprehensive study combining the experimental results presented in this chapter and the theoretical results presented in chapter 5.3 can be found in literature.[103] In the present work the experimental and theoretical results are discussed separately. This chapter only presents the experimental results obtained by TDS. In chapter 5.3 the results of theoretical approaches by the group of Prof. Heine are presented and correlated to the experimental results.

As MFU-4(Zn, Cl) is a representative of the isoreticular MFU-4 family, it possesses the characteristic framework topology of alternating small and large pores arranged in alternating manner. The pores are connected by an aperture which is smaller than the small pore itself. Therefore, any molecule diffusing into the MFU-4 framework has to pass the large and the small pore and additionally the aperture between them. As the aperture in MFU-4(Zn, Cl) is only 2.5 Å, molecules like nitrogen with a kinetic diameter of 3.64-3.8 Å[104] are excluded from adsorption whereas smaller molecules like water (d_{kin}=2.641 Å)[104] and hydrogen (d_{kin}=2.827-2.89 Å)[104] can still penetrate.[88] Thus, MFU-4(Zn, Cl) exhibits a pronounced gating effect which could be exploited for quantum sieving. The small pore of 3.88 Å and the aperture could act as separation gates whereas the large pore of 11.94 Å offers a large surface area for storing gas.

TDS spectra are recorded after exposure to a 10 mbar 1:1 isotope mixture at 30 K, 40 K and 50 K for 1.5 h. The exposure conditions of MFU-4(Zn, Cl) are therefore equal to those applied to Takeda 3A in order to allow a direct comparison of the two samples. After gas exposure at 30 K, no gas is adsorbed in the MFU-4(Zn, Cl) framework. Only a low temperature deuterium desorption signal resulting from the surface and the void volume between the powder particles occurs. This signal is a result of the cooling to 20 K. After exposure at 40 K and 50 K, hydrogen and deuterium adsorb inside the framework. The corresponding desorption maximum is located around 75 K-80 K. MOFs with a bimodal pore structure where pores are connected by apertures larger than the gas molecule exhibit two desorption maxima. But in MFU-4(Zn, Cl) the aperture and the A-pore are too small to allow

an independent desorption from the small and the large pore (gating effect) and therefore only one desorption maximum is observed. The uptake drastically increases by rising the exposure temperature from 40 K to 50 K. The hydrogen uptake increases by a factor of nearly 20 whereat the deuterium uptake increases by a factor of more than 15. The noticeable increase in gas uptake suggests strongly accelerated diffusion above 40 K and therefore an opening of the pore aperture.

The TDS spectra obtained after exposure to the isotope mixture at cryogenic temperatures are consistent with literature spectra measured after exposure to pure hydrogen at RT (see chapter 4.2).

For exposure temperatures of 60 K and 70 K, the H_2/D_2 selectivity of MFU-4(Zn, Cl) is also measured as a function of exposure time. Owing to the larger gas uptake at 60 K for long exposure times, the exposure pressure was increased from 10 mbar to 20 mbar in order to ensure a constant gas composition. The desorption spectra obtained after exposure at 60 K for different exposure times converge at the low temperature side, indicating that the desorption process is diffusion limited because the extension of the peak to the high temperature side is a measure for the penetration depth of the adsorbed molecules. For short exposure times only the near surface regions of the powder grains contain adsorbed molecules. For long exposure times the molecules are able to penetrate deeper into the grains. The molecules adsorbed deeper inside need more time to diffuse to the surface and desorb there in the TDS experiment. Thus, these molecules are detected with a time and therefore a temperature delay. The selectivity decreases with increasing exposure time revealing I) inverse kinetics, i.e. the characteristic feature of quantum sieving and II) that the measured selectivity values are non-equilibrium values.

Exploiting the kinetic preference of deuterium yields a maximum selectivity of 7.5 after gas exposure at 60 K for 15 min.

After gas exposure at 70 K, the desorption spectra do no longer converge at the low temperature side. One can therefore assume that the diffusion limitations of the adsorption process become marginal. This hypothesis is strengthened by the fact that the selectivity drops even faster after exposure to a 10 mbar mixture at 70 K, reaching a value of 1.4 already after 15 min exposure. Also the uptake after exposure at 70 K for 15 min is decreased compared to the exposure at 60 K for 15 min. A decrease in gas uptake as soon as the selectivity converges to 1 was already observed in Takeda 3A. Additionally, also the high

pressure adsorption isotherms measured from 77 K to RT find a continuous decline in uptake with rising exposure temperature (see Figure 3.5).

Knudsen diffusion, the predominant diffusion mechanism in porous materials at low pressure, is not observed in MFU-4(Zn, Cl) because Knudsen diffusion would lead to faster diffusion of the lighter isotope according to[105]

$$D_K = 97r\sqrt{\frac{T}{M}}. \qquad (5.1)$$

D_K is the Knudsen diffusion coefficient, r is the pore radius and M is the molecular weight. In microporous materials the diffusion is not only determined by the collisions of the diffusing particles with the pore walls but additionally influenced by the interaction between adsorbent and adsorbate. In that case theoretical work predict that the diffusion is slower and the Knudsen diffusion coefficient represents an upper boundary.[106]

Summing up, inverse kinetics and therefore kinetic quantum sieving was shown in MFU-4(Zn, Cl). Based on this observation, the dependence of the selectivity on exposure time can be explained. If MFU-4(Zn, Cl) is exposed to an isotope mixture within the scope of a TDS experiment, both isotopes will adsorb but they will penetrate the framework at different rates. The hydrogen diffusivity is more strongly reduced due to quantum sieving. Therefore, deuterium penetrates first and enriches in the MOF framework. In the course of time, an increasing amount of hydrogen diffuses into the framework and tends to alleviate the D_2/H_2 ratio until the equilibrium value is reached. At 70 K the kinetic barrier becomes marginal and therefore the selectivity converges to 1 even for short exposure times.

5.3. Theoretical approach to quantum sieving in MFU-4(Zn, Cl)

Quantum sieving in MFU-4(Zn, Cl) was investigated theoretically by the group of Prof. T. Heine (Jacobs University, Bremen). Details about their calculations can be found in the supporting information of the joint publication. [103]

5.3.1. Penetration of the barrier

The aperture formed by the four chlorine atoms results in a barrier of approximately 100 meV due to electrostatic repulsion.[103] Therefore neither hydrogen nor deuterium should be able to penetrate. The minimum energy path corresponds to a hydrogen alignment in-line with the two of the four chlorine atoms (see Figure 5.2). The reason for the in-line orientation of the hydrogen atom is attributed to its dipoles. The electron density and

therefore the negative charge is concentrated in the middle in order to form the bond. The nuclei, carrying positive charge, repel each other. Thus, the hydrogen molecule possesses two dipoles, together forming an electrical quadrupole (Figure 5.2). This leads to an oriented passing of hydrogen though the pore aperture, i.e. it aligns its positive ends into the direction of the electron shells of the chlorine atoms.

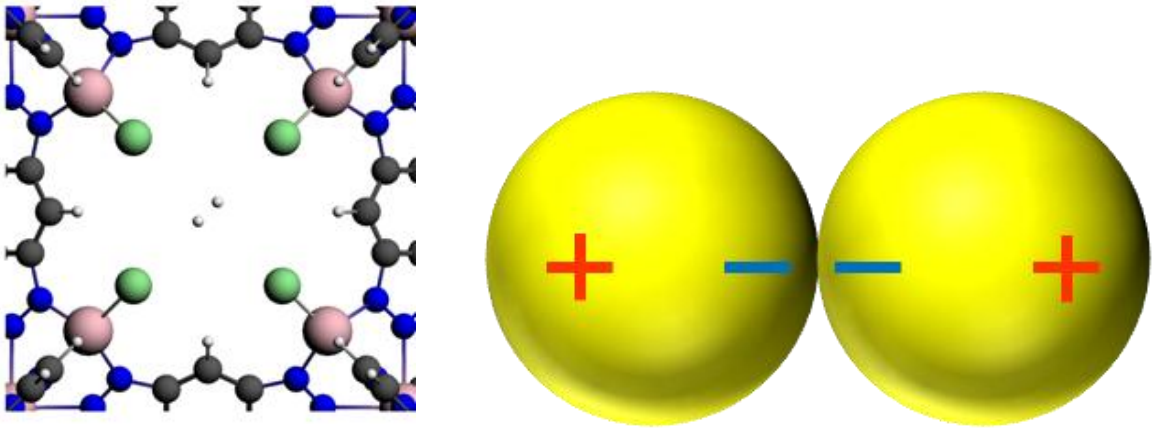

Figure 5.2: Detail of the MFU-4(Zn, Cl) structure showing the pore aperture formed by four chlorine atoms with a hydrogen molecule that passes the aperture along the minimum energy path, i.e. it passes in-line with two of the four chlorine atoms (left).[107] The right image sketches the two dipoles of a hydrogen atom, together forming an electrical quadrupole.

5.3.2. Phonon excitations

Despite the theoretical calculations yield a negligible penetration rate due to the large penetration barrier, TDS experiments revealed a small uptake at 40 K and strongly increasing uptake if the exposure temperature is raised to 50 K. Calculating the full phonon spectrum of MFU-4(Zn, Cl) by DFT yields that the first phonons are observed between 41 and 380 cm^{-1}.[103] These modes are all related to displacement of the chlorine/zinc bonds. Their bonds bend and twist as illustrated in Figure 5.3. These movements strongly affect the pore aperture, i.e. the aperture is increased in size. As the effective aperture size is rising, the energy barrier for penetration is lowered. Therefore, hydrogen and deuterium can penetrate rather easily above 45 K, thereby leading to a strong increase in the experimentally determined uptake at 50 K compared to exposure at 40 K.

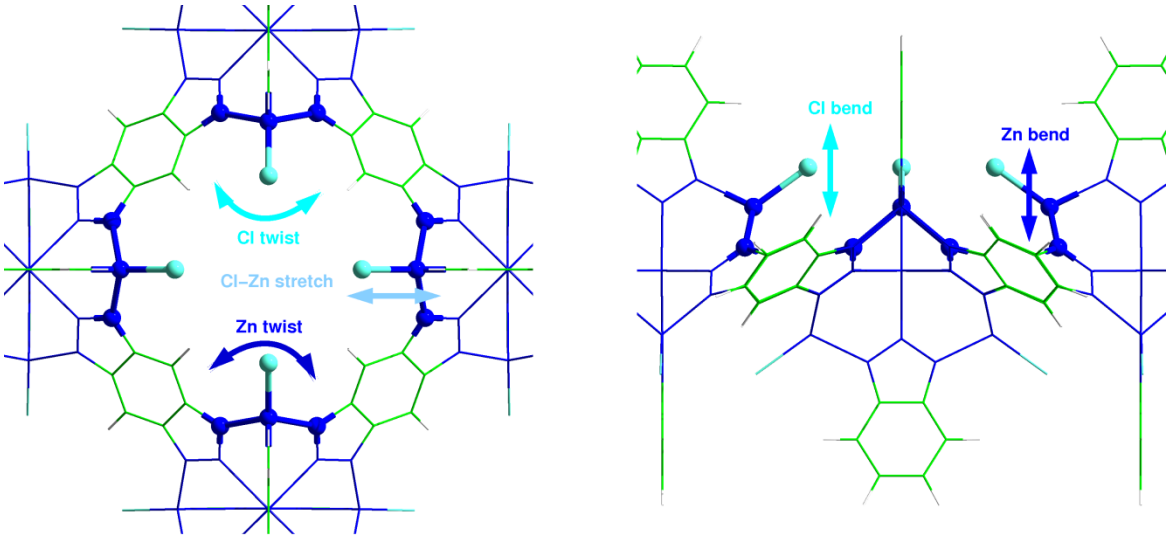

Figure 5.3: Illustration of the opening of the pore aperture by optical phonons in the range of 41-380 cm^{-1}. The twisting and stretching of the Cl bonds increases the effective size of the pore window. It is important to note that the terminology of the "twisting" and "bending" movements are based on the movement of all four Cl atoms relative to each other and not just related to a single bond.[103]

The experimentally observed increase in uptake with rising exposure temperature is very sharp. Actually, the uptake increases by a factor of up to twenty when rising the exposure temperature from 40 K to 50 K. According to solid state theory, the phonons are bosons and therefore follow the Bose-Einstein statistics (for higher temperatures the Boltzmann statistics also describe the phonon energy distribution satisfyingly). Therefore, the onset should be rather smooth. However, in MFU-4 (Zn, Cl) the optical phonons occur already at low temperatures and there are many modes. Additionally, all these phonons refer to soft modes, i.e. they lead to significant displacements. It is important to note that these phonons occur in a rather complex framework and therefore affect not only the chlorine and zinc atoms. The real impact of these phonons can only be visualized and understood when taking the whole framework into account. Therefore, the discussed phonons should not be mixed up with movements in a simple chemical structure.

A sudden opening is not only observed in MFU-4(Zn, Cl). Also other porous materials are known for temperature[108-110] or pressure[111] triggered opening which has to distinguished from a structural breathing of the framework. Both effects lead to a sudden gas uptake and/or gas release of a structure that has been closed before, i.e. did not allow any guest molecules to enter or leave the pores. However, the cause of the two effects is very different. Breathing is related to structural changes observable in XRD. The gate opening,

sometimes just termed “gating” or “opening”, is either related to induced flexibility in the adsorbent or the gain in kinetic energy of the adsorptive which then possesses the required activation energy to overcome a barrier like a narrow entrance. In Mn-Formate, a MOF structure possessing 1D zigzag channels with an aperture of 3.64 Å, an opening effect for nitrogen and argon adsorption was shown.[109] The TDS profiles of Mn-Formate obtained after nitrogen adsorption at different temperatures reveal increasing gas uptakes from 83 K to 143 K followed by a decrease in uptake for higher adsorption temperatures (see Figure 5.4).

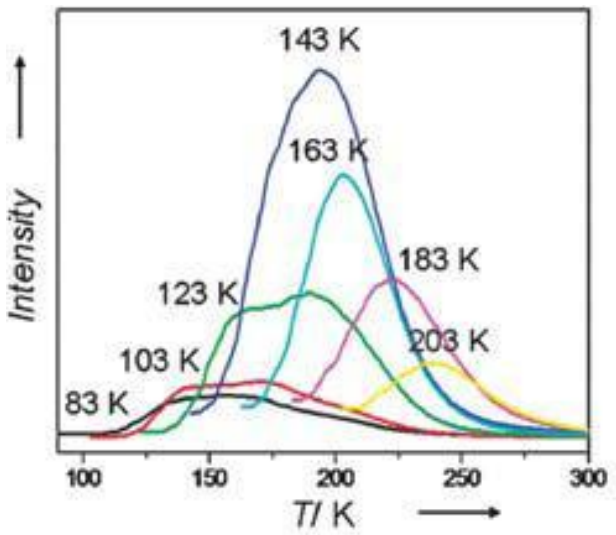

Figure 5.4: TDS profiles of Mn-Formate after exposure to nitrogen at different exposure temperatures.[109] Reproduced by permission of the Royal Society of Chemistry.

The TDS spectrum of Mn-Formate exhibits a similar trend as the H_2- and D_2-TDS spectra of Takeda 3A and MFU 4(Zn, Cl). The uptake increases up to a certain temperature and decreases afterwards. The authors ascribe this behavior either to increasing energy of the nitrogen molecules and/or to an opening of the aperture due to lattice vibrations. As the authors cannot prove one of the two proposed mechanism, they suppose that both effects might play a role.[109] However, the dominant mechanism could depend on the investigated material. Temperature-triggered adsorption was also observed in type A zeolite that cannot be assumed to be flexible.[108] These authors suggest that the increase in kinetic energy of the gas molecules allows them to overcome the barrier and to penetrate the zeolite. In a Cu-based organic-inorganic hybrid material the gating effect could be shown for nitrogen and CO_2 adsorption.[110]

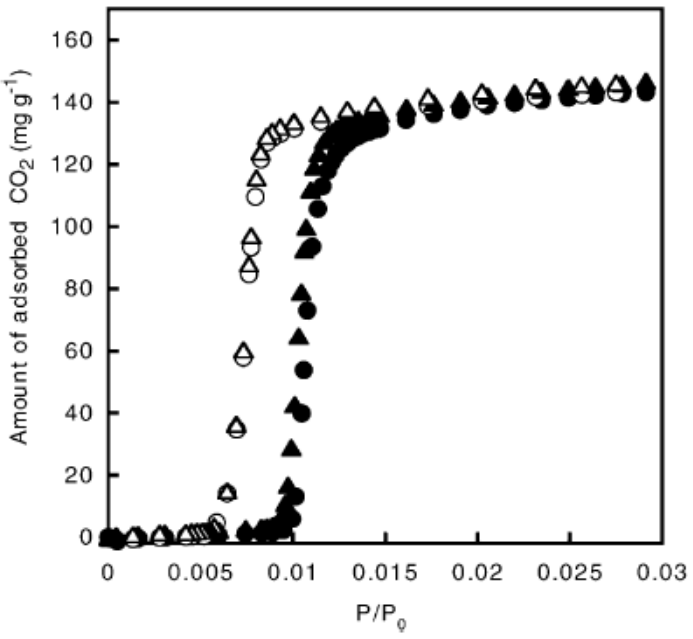

Figure 5.5: The CO_2 adsorption isotherms of the Cu-based hybrid material measured at 273 K. Closed and open symbols refer to adsorption and desorption, respectively. The different symbols denote different adsorption runs performed in order to evidence the reproducibility of the gate opening.[110]

The CO_2 adsorption isotherms of the Cu-based hybrid material exhibit a sudden onset in gas adsorption at a relative pressure of 0.01. A hysteresis, formed by the adsorption and desorption branch, is commonly observed for structures that exhibit gate opening.[111,112] The TDS spectrum of water displays a very sharp desorption signal. The authors also attribute the sudden desorption of water to the gate opening. Their proposed mechanism suggests that the gate is opened by bending vibrations of the bonds that restrict the gate. However, they admit to have no proof for their model. The H_2 and D_2 desorption spectra of MFU-4(Zn, Cl) exhibit the same sharp onset in desorption as the Cu-based material for water. For both materials the lattice vibrations are a possible and reasonable cause for the gate opening. For MFU-4(Zn, Cl) the assumption can be supported by the calculated phonon spectrum.

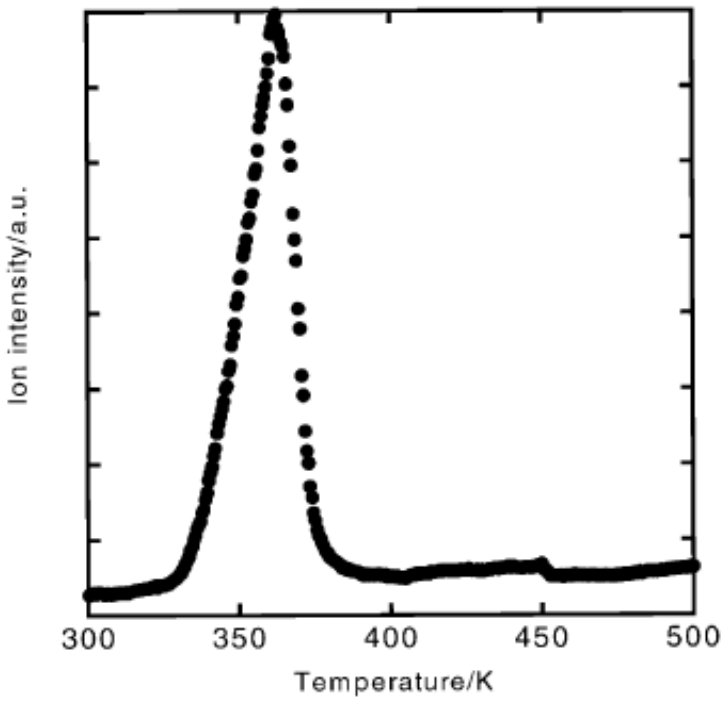

Figure 5.6: TDS spectrum of water removed from the Cu-based hybrid material.[110]

5.3.3. Adsorption in the framework

Density profiles for pure hydrogen and pure deuterium gas are calculated by QLDFT for an average inverse gas density of $8.512*10^{-4}$ m³/mol and 77 K. Subtraction of the density profiles, i.e. $n(D_2)$-$n(H_2)$, yields the adsorption probability density presented in Figure 5.7. This illustration suggests that the deuterium tends to be located at the pore walls and the pore aperture whereas hydrogen tends to stay in the center of the pore. Deuterium forms a dense adsorption layer on the pore wall whereas hydrogen still resembles a gas. Based on the adsorption probability densities one can draw another picture of the time-dependent H_2/D_2 isotope adsorption process in MFU-4(Zn, Cl) compared to the one presented in chapter 5.2 which was mainly based on the difference in penetration rate due to the higher diffusivity of deuterium compared to hydrogen. Considering the density profiles, deuterium is adsorbed in the first step as it enriches at the powder particles surface due to its lower ZPE value. Therefore the surface is blocked for hydrogen molecules. Deuterium starts to penetrate the MFU-4(Zn, Cl) framework in the second adsorption step; thereby leaving vacant adsorption sites at the powder particle surface behind. Subsequently, they can be populated by hydrogen. As hydrogen and deuterium occupy different adsorption sites in the pores, adsorption equilibrium can be reached easily. Consequently, there are two important effects for hydrogen isotope adsorption in MFU-4(Zn, Cl), namely kinetic quantum sieving

and another non-kinetic ZPE effect. The higher density of deuterium in the pore window is attributed to the kinetic quantum sieving effect. The occupation of the surface by deuterium is also a result of its lower ZPE value but without kinetic character.

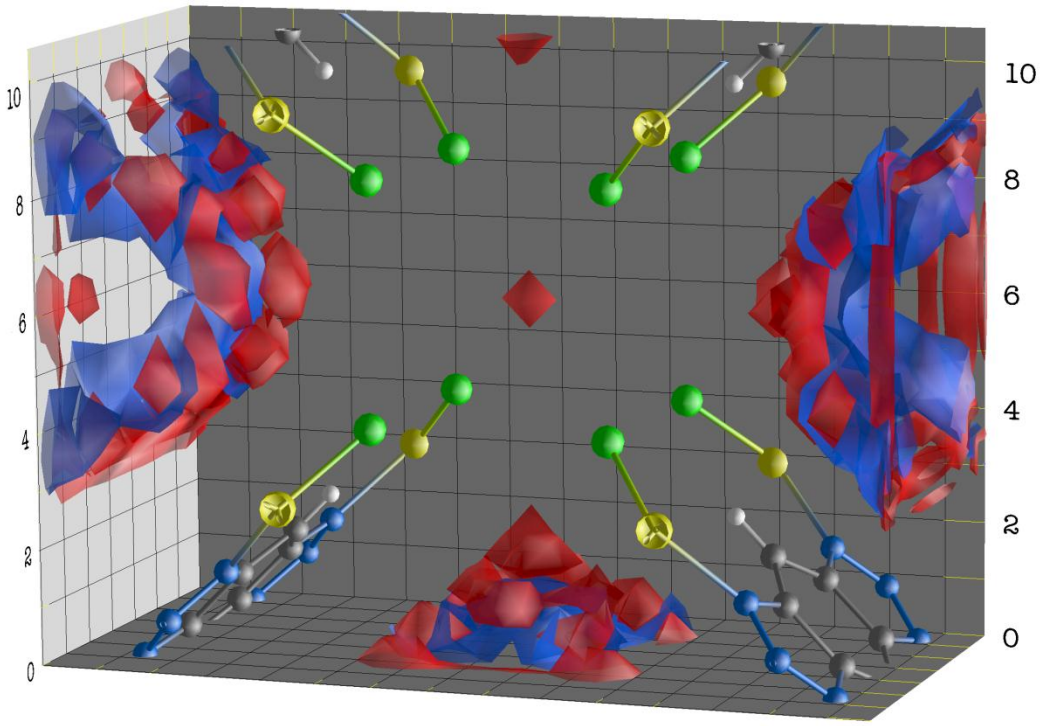

Figure 5.7: Detail of the MFU-4(Zn, Cl) framework showing the difference in adsorption probability densities at 77 K for hydrogen and deuterium in the pore aperture and its vicinity. Blue areas indicate hydrogen excess and red areas deuterium excess. A comparison of the probability densities reveals that deuterium enriches at the pore walls and the aperture whereas hydrogen is located inside the pores. Thus, deuterium forms a rather dense quantum liquid at the inner surface whereas hydrogen remains in the center of the pore.[103]

The ZPE value for the quantum sieving, as discussed in chapter 2.2, is a result of the confinement. In the large pore, the molecule is not confined in the sense of a particle in a box. Here the ZPE value of the molecule is directly related to its degrees of freedom.

5.4. Comparing Takeda 3A to MFU-4(Zn, Cl)

Takeda 3A and MFU-4(Zn, Cl) separate H_2/D_2 mixtures by quantum sieving. However, they also exhibit remarkable differences in the TDS results which require a detailed comparison and discussion. The desorption spectra of the two samples obtained after exposure to the isotope mixture at 40 K are shown for each isotope individually in Figure 5.8. Comparing the low temperature desorption signal yields information about the presence of

pores of different sizes. The low temperature signal in Takeda 3A is much more pronounced due to the broad pore size distribution. In contrast, MFU-4(Zn, Cl) exhibits a well-ordered 3D framework structure containing only the two types of nanopores.

The onset of the desorption in MFU-4(Zn, Cl) is steep whereas it proceeds slowly in Takeda 3A. Assuming that the pore-opening-model for MFU-4(Zn, Cl) presented in chapter 5.3 is correct, one could think of a structure which is either open or closed. Up to the onset temperature, the pore structure of MFU-4(Zn, Cl) is closed. Around 45 K the pores open according to the calculated phonon spectrum. When the MFU-4(Zn, Cl) structure opens, the adsorbed gas is released in a sudden burst, yielding the experimentally observed strong increase in desorption rate.

The third and most obvious difference is related to the temperature of the desorption maxima. The desorption maximum related to the 3 Å nanopores in Takeda 3A occurs at much higher temperature compared to MFU-4(Zn, Cl), i.e. the temperature difference is ~100 K. This difference in the desorption temperature could also be related to the pore-opening model. The phonon-induced opening of the pore aperture facilitates the desorption as soon as the structure opens. The desorption spectra for different exposure temperatures in Takeda 3A do not give any hint to temperature induced pore opening. Even more important, the fitting of the QENS measurements performed by Nguyen indicated that the pore size decreases with rising temperature in Takeda 3A.[54] Therefore, the high desorption temperature and the slow increase in desorption rate could be related to pore contraction or a rather constant pore size. Additional results of this constant pore size are the low gas uptake and the slowly decreasing selectivity over a large temperature range. However, it is important to note that MFU-4(Zn, Cl) possesses a bimodal pore structure. The gas adsorbed in the large pore desorbs at relatively low temperature; thereby generating a gas atmosphere in the large pore that cannot be released due to the gating effect. Therefore, the gas pressure in the large pore increases with rising temperature. Finally, this backpressure could be large enough to kick out the molecules in the small pores, yielding a sudden desorption burst at comparably low desorption temperatures.

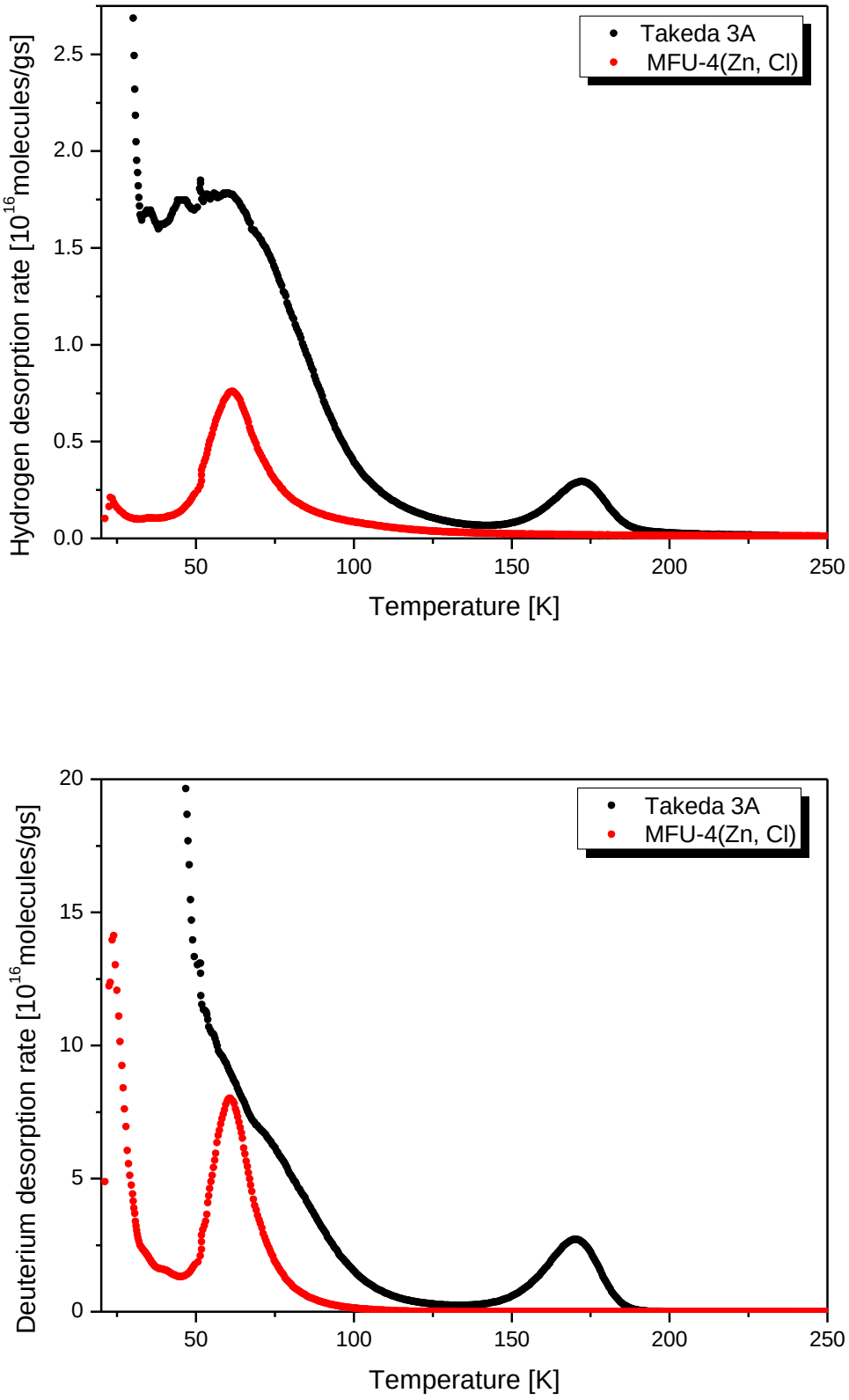

Figure 5.8: Desorption spectra of Takeda 3A and MFU-4(Zn, Cl) obtained after exposure to a 1:1 mixture at 40 K for 1.5 h. The desorption spectra are shown for each isotope separately. The hydrogen spectra are shown on the top and the deuterium spectra at the bottom.

5.5. Hydrogen isotope adsorption in MFU-4(Co, Cl)

Quantum sieving could be shown experimentally and theoretically in MFU-4(Zn, Cl). In order to reveal the influence on pore/aperture size on the selectivity, a second framework with the same topology but slightly larger pore/aperture size is investigated. The pore topology, not just the pore size, plays a crucial role for the magnitude of the kinetic quantum sieving effect.[36] As the MFU-4 family is a series of isostructural frameworks, the effect of topology is eliminated. Ideally, any differences in selectivity are then attributed to difference in pore size and aperture size.

Before starting the discussion of the quantum sieving in the MFU-4 derivatives, a short insertion on pore size determination might be helpful. The standard methods for experimental pore size determination[113] are mainly based on gas adsorption, e.g. CO_2, experiments. The resulting adsorption curves are either fitted by DFT or they are compared to experimental reference curves. But the small-pore MFU-4 derivatives MFU-4(Zn, Cl), MFU-4(Co, Cl) and MFU-4(Zn, Br) possess pore apertures comparable to the kinetic diameter of hydrogen and therefore an experimental pore size analysis by gas adsorption is not possible. Thus, the pore sizes are estimated on the basis of the framework structure determined by XRD. The pore size corresponds to the largest sphere that fits into the cavities. The aperture size is equal to the diagonal distance between the halogen atoms after subtracting twice the Van der Waals radius of the corresponding halogen atom. The atomic positions might change slightly with temperature and sample type, i.e. single crystal or powder.

MFU-4(Co, Cl) was measured under the same exposure conditions as the previous samples for the exposure temperatures of 30 K and 40 K. In contrast to the MFU-4(Zn, Cl) and Takeda 3A, MFU-4(Co, Cl) takes up hydrogen and deuterium even after gas exposure at 30 K. The adsorbed amount of deuterium is equal for both exposure temperatures, i.e. 116 and 115 molecules per unit cell. But the hydrogen amount increases from 29 to 57 molecules after exposure at 30 K and 40 K, respectively. Therefore, the selectivity decreases from 4.0 to 2.0 after mixture exposure at 30 K and 40 K, respectively.

The occurrence of adsorption in MFU-4(Co, Cl) even at 30 K as well as the 633 times larger hydrogen and 185 times larger deuterium uptake at 40 K compared to MFU-4(Zn, Cl) reveal that the pore aperture of ~3 Å forms no substantial barrier to hydrogen isotope diffusion. Therefore no high selectivity due to quantum sieving is observed. Owing to the

large gas uptake, it is assumed that the gas composition could have changed during the exposure which could have led to an additional decrease in selectivity due to hydrogen excess in the gas phase.

5.6. Hydrogen isotope adsorption in MFU-4(Zn, Br)

Two MFU-4(Zn, Br) samples were investigated. These samples are synthesized differently. MFU-4(Zn, Br)_T1 is synthesized via the solvothermal route whereas MFU-4(Zn, Br)_T2 is produced by the microwave-assisted method. XRD analysis performed by the group of Prof. Volkmer revealed that both samples exhibit the same X-ray pattern and therefore the same framework structure. However, the difference in synthesis yields powders with different grain size distributions as evidenced by SEM images (see Figure 3.10, Figure 3.11 and Figure 3.12). Two SEM samples of each MFU-4(Zn, Br) type were prepared and viewed in the SEM in order to ensure that the prepared SEM samples are representative for the whole powder. The results obtained by SEM were consistent. The SEM images revealed that MFU-4(Zn, Br)_T1 exhibits a bimodal grain size distribution. The larger grains are comparable in size to MFU-4(Zn, Cl), i.e. they are roughly in the range of 1-3 µm. The smaller grains are below 0.5 µm. However, the small grains exhibit the same cubic shape as the large ones. One can therefore assume that the small particles are not just fragments of large grains. MFU-4(Zn, Br)_T2 only consists of the small particles. Even the largest observed cubes are below 1 micron. The small grains of MFU-4(Zn, Br) agglomerate or have grown together during the synthesis forming large particles that reach several tens of microns in length.

The TDS results obtained after exposing MFU-4(Zn, Br)_T1 to 500 mbar hydrogen gas reveal that the desorption signal starting from 100 K is attributed to adsorption from the regular pore structure of the MOF. This signal cannot be found for a loading pressure of 10 mbar. Therefore, the up to now applied exposure pressure of 10 mbar is not suitable to investigate MFU-4(Zn, Br) even for an extended exposure times of 2.5 h. An exposure pressure of 50 mbar is a compromise. The selectivity values are dependent on exposure pressure and therefore a pressure increase up to 50 mbar makes a direct comparsion to the selectivity values of the other MFU-4 derivatives more difficult. However, the exposure pressure is still far below atmospheric pressure and therefore a comparison to the other MFU-4 derivaties is acceptable.

The need of a large exposure pressure to reach adsorption inside the framework suggests a substantially larger kinetic barrier in MFU-4(Zn, Br) compared to MFU-4(Zn, Cl).

The desorption spectra of MFU-4(Zn, Br)_T1 obtained for different exposure temperatures show that the desorption signal from the characteristic pore structure does not occur for exposure temperatures below 80 K. This observation suggests that MFU-4(Zn, Br) also exhibits a temperature induced opening of the aperture due to phonon excitations. In addition to the desorption signal from the characteristic pore structure, the desorption spectra of MFU-4(Zn, Br)_T1 exhibit several desorption signals at lower temperatures. In particular the deuterium desorption signals up to 50 K are attributed to the adsorption at the powder particle surface. The desorption signals observed for desorption temperatures between 50 K and 100 K might be caused by defects, e.g. degassing channels created when the solvent molecules escape through the narrow apertures, or adsorption in "grain boundary regions", i.e. imperfect crystal structure where two grains have grown together.

The desorption spectra of MFU-4(Zn, Br)_T2 obtained for different exposure temperatures reveal an accessibility of the inner pore structure above ~90 K. For this sample no noticable low temperature desorption signals are found, indicating that those found for MFU-4(Zn, Br)_T1 could only be due to imperfect framework structure. The smaller grains of MFU-4(Zn, Br)_T2 might contain fewer defect, e.g. solvent removal from the small grains might be easier. As MFU-4(Zn, Br)_T2 exhibits better desorption spectra, the uptake values and selectivity values are calculated for this sample. Despite the large exposure pressure of 50 mbar and the high exposure temperatures, the sample takes up only a few molecules per unit cell. The low gas uptake is a result of the large kinetic barrier. Although the sample exhibits a substantial kinetic barrier to hydrogen isotope diffusion, the selectivity is low, i.e. below 3, and the selectivity also tends to decrease with rising exposure temperature. The low selectivity could be attributed to the high opening temperature where the isotope diffusivities might not longer differ noticably.

MFU-4(Zn, Br)_T2 was exposed to isotope mixtures at 80 K and 110 K for different exposure times, namely 45 min and 90 min. At 80 K the gas uptake doubles when the exposure time is increased from 45 min to 90 min. For the exposure at 110 K, the uptake increases by 20-30% when the exposure time is increased. One can conclude that MFU-4(Zn, Br) opens the aperture gradually with rising temperature due to phonons. When

500 mbar instead of 50 mbar are applied, no time-dependence is found at 110 K. This observation suggests that the structure is open at 110 K and that the difference in uptake after exposure to 50 mbar is only due to the low pressure. Above the opening temperature the gas uptake in MFU-4(Zn, Br)_T2 decreases. The effect of decreasing uptake when the exposure temperature exceedes the temperature where the kinetic barrier vanishes, i.e. when the pore structure is open, has already been observed in MFU-4(Zn, Cl) where the uptake decreases above 60 K.

Selected TDS spectra of the two MFU-4(Zn, Br) samples are compared in Figure 5.9. The desorption temperatures of MFU-4(Zn, Br)_T2 are higher compared to MFU-4(Zn, Br)_T1. This could be explained by different thermal conductivities. When the gas pressure in the sample chamber does not contribute noticeably to the temperature conduction, the temperature is conducted from one powder particle to the next via particle contacts. Owing to the smaller grains in MFU-4(Zn, Br)_T2, much more contacts have to be crossed when heating the sample with the constant rate in the experiment. The sample temperature is therefore lower as indicated by the temperature sensors and the desorption seems to occur at higher temperatures.

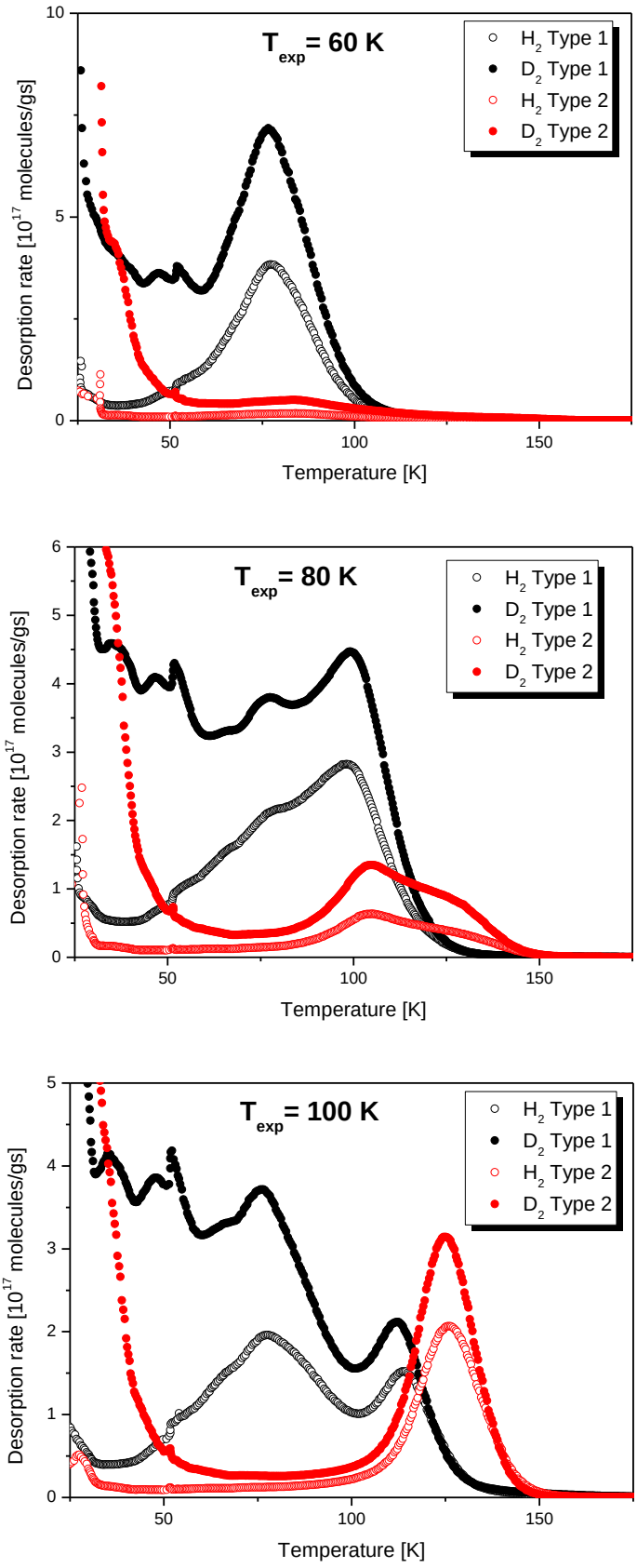

Figure 5.9: Comparison of the hydrogen and deuterium desorption spectra of MFU-4(Zn, Br)_T1 and MFU-4(Zn, Br)_T2 for the exposure temperatures of 60 K, 80 K and 100 K.

5.7. A comparison of a small-pore MFU-4 derivatives

Comparing the results obtained for MFU-4(Zn, Cl), MFU-4(Co, Cl) and MFU-4(Zn, Br) shows that effective isotope separation by quantum sieving in these small-pore MFU-4 derivatives is only possible in a very narrow size window of the aperture. A window of 2.5 Å performed well up to 60 K, i.e. as long as the pore aperture forms a kinetic barrier and is not largely opened by phonons. An aperture of 3 Å is critically large as it barely hinders hydrogen isotope diffusion even at low temperatures of 30 K. Therefore, the selectivity in MFU-4(Co, Cl) is low. The main idea behind MFU-4(Zn, Br) was to investigate whether high selectivity values can be reached at higher exposure temperatures by decreasing the size of the aperture, i.e. by increasing the kinetic barrier. It was shown that higher temperatures are required to open the structure; thereby making it accessible for gas adsorption. However, the selectivity is low at these high temperatures which might be due to the small difference in isotope diffusivity at elevated temperatures.

The discussion about the experimental and theoretical results obtained for MFU-4(Zn, Cl), showed that the main parameter for selectivity, i.e. window size, is subjected to change due to phonon excitations. The temperature induced flexibility leads to an opening of the structure that occurs at different temperatures in the MFU-4 derivatives.

Additionally, the aperture is changed chemically when chlorine is replaced by bromine. Therefore, the aperture is not only changed in size and the change in the chemical environment could have an additional influence on the selectivity.

5.8. Hydrogen isotope adsorption in MFU-4 *large*

The pore diameters in MFU-4 *large* are 11.97 Å and 18.56 Å. The alternating small and large pores are connected by a pore aperture of 9.13 Å.[88] Owing to the large pores and pore aperture in MFU-4 *large* compared to the kinetic diameter of hydrogen, the hydrogen and deuterium molecules adsorbed in the smaller and the larger pore can desorb independently. Therefore the desorption spectra of MFU-4 *large* exhibit more than one desorption maximum. The shapes of TDS spectra obtained after exposure to pure gases are in good agreement with literature data (see chapter 3.1.5).

As the aperture exceeds the kinetic radius of hydrogen considerably, no kinetic limitations of the hydrogen isotope adsorption and in particular no quantum sieving is expected in MFU-4 *large*. TDS experiments performed for exposure times of 15 min and 90 min reveal that no kinetic limitations occur even after gas exposure at 40 K. The spectra and the uptake do not change noticeably for the two exposure times. Only the desorption signal reaching from 23 K to 30 K is slightly sharper after exposure for 1.5 h compared to exposure for 15 min which is only due to a more stabilized adsorption layer for longer cooling times, i.e. the sample and the gas are thermally equilibrated.

The work of Chu et al.[56] (see also chapter 2.2.4) proposes that the maximum equilibrium H_2/D_2 ratio occurs at pore sizes where the maximum difference in the adsorption rate constants for the isotopes is already exceeded. Moreover, the heavier isotope should always be preferentially adsorbed even in the absence of kinetic barriers because of the lower ZPE value. Exposing MFU-4 *large* to the pure gases at RT and 40 K reveals that the uptake after gas exposure at RT is equal for the two isotopes (D_2/H_2=1.08) but larger for deuterium after exposure at 40 K (D_2/H_2=1.6). However, the larger deuterium uptake at cryogenic temperatures does not necessarily have to be ascribed to the difference in ZPE values. Another reason can be found in the different thermal de Broglie wavelengths λ_{dB} of the isotopes

$$\lambda_{dB} = \frac{h}{\sqrt{2\pi m k_B T}}. \qquad (5.2)$$

The thermal de Broglie wavelength can be considered as the required space for the adsorbing molecule. As shown in Figure 5.10 the thermal de Broglie wavelength is larger for hydrogen compared to deuterium for all temperatures. However, the difference in the thermal de Broglie wavelength decreases with rising temperature, i.e. the thermal de Broglie

wavelengths of the isotopes converge with rising temperature. Thus, at low temperature where the thermal de Broglie wavelength is much smaller for deuterium compared to hydrogen, the deuterium adsorption layer can be packed denser, yielding the higher deuterium uptake.

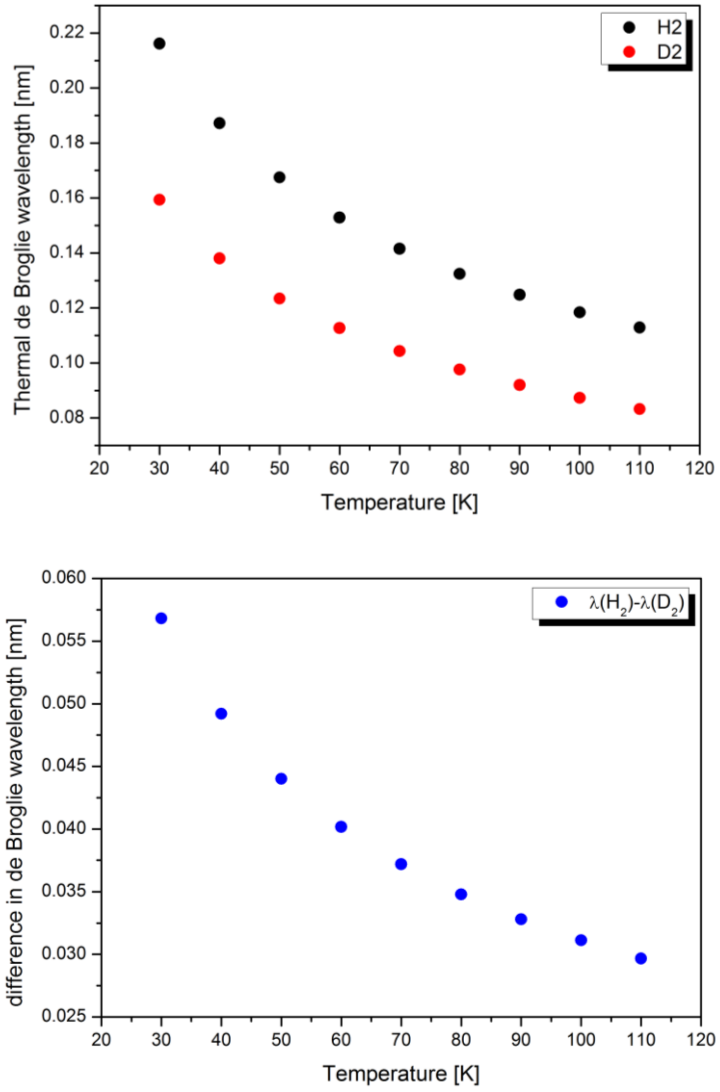

Figure 5.10: Thermal de Broglie wavelengths of hydrogen and deuterium for T=30 K-110 K (top) and the difference of their wavelengths (bottom).

Except for the higher deuterium uptake compared to the hydrogen uptake after exposure at 40 K, the desorption spectra of the two isotopes are very similar. Thus, the isotopes occupy the same adsorption sites.

In contrast to the spectra obtained for the pure gases, the shapes of the desorption spectra obtained after exposure to isotope mixtures exhibit significant differences. The molar D_2/H_2 ratios after pure gas exposure are equal to the corresponding selectivity values

within the measurement accuracy, i.e. 1.08 at RT exposure and 1.6/1.7 for exposure at 40 K. However, the isotopes populate different adsorption sites when mixtures are applied. After exposure to a mixture at RT, the high temperature desorption peak centered around 45 K is more pronounced for deuterium compared to hydrogen. After exposure to a mixture at 40 K, this high temperature desorption signal solely occurs for deuterium. One can conclude that deuterium tends to occupy the stronger adsorption sites and the extent of selective deuterium adsorption at the strong adsorption sites rises with decreasing adsorption temperature.

It seems that the deuterium desorption spectrum after exposure to the mixture at 40 K shows three maxima. The first one ranges from 20 K to 30 K, the second one from 30 K to 40 K and the third one from 40 K to 70 K. The experimental observation of three adsorption sites fits the theoretical results from the group of Prof. Heine obtained for pure hydrogen adsorption (see Figure 5.11 and Figure 5.12).

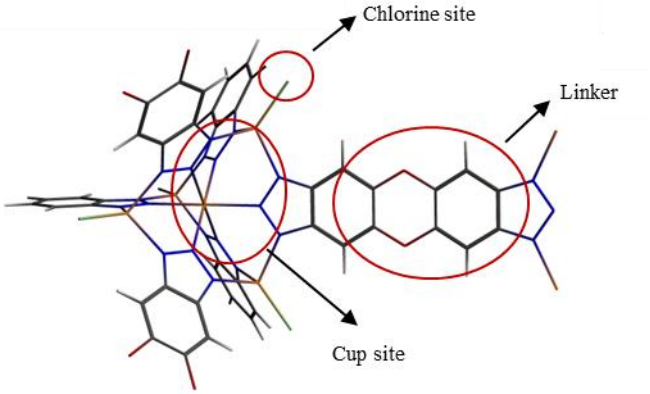

Figure 5.11: Theoretically obtained hydrogen adsorption sites in MFU-4 *large*. Color code: Zn-orange, C-grey, Cl-green, O-red, N-blue, H-grey. The adsorption sites are marked with red circles.[114]

On the cup site the hydrogen atom adsorbs at the central Zn atom. On the linker hydrogen adsorbs along the oxygen-oxygen axis. Additionally, hydrogen adsorbs in a T-shape with respect to the chlorine.

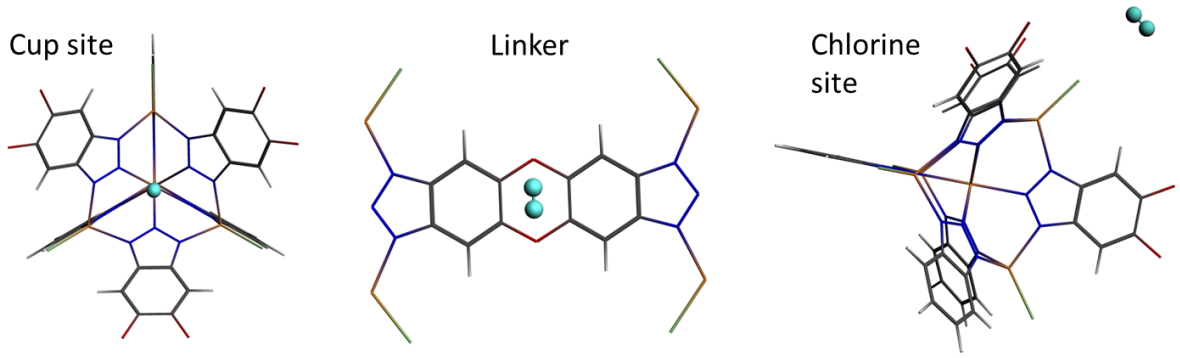

Figure 5.12: Hydrogen adsorbed at each of the three adsorption sites found in MFU-4 *large*.[114]

Summing up, no kinetic quantum sieving is found in MFU-4 *large*. The selectivity of 1.08 and 1.7 after exposure to the isotope mixture at RT and 40 K is due to the differences in ZPE values and/or de Broglie wavelengths which yield a larger amount of adsorbed deuterium with decreasing exposure temperature. However, the TDS results suggests that there are strong adsorption sites in MFU-4 *large* that are selective for deuterium which will be discussed in more detail in the following subchapter on the basis of partial desorption experiments. The selective deuterium adsorption at the strong adsorption sites might be due to the fact that the strongest adsorption sites are populated first when adsorption occurs. As deuterium adsorbs preferentially due to its lower ZPE value, it adsorbs first and therefore occupies the strongest adsorption sites. At low temperatures, no exchange between deuterium adsorbed at the strong sites with hydrogen molecules in the gas phase is expected.

5.9. Experimental hydrogen isotope separation with MFU-4 large

The desorption spectra after exposure to a 10 mbar 1:1 H_2/D_2 mixture at 40 K reveal only one desorption signal for hydrogen but three for deuterium. Hydrogen desorbs at low desorption temperatures up to approximately 40 K whereas the high temperature desorption signals are dominated by deuterium desorption. This allows a direct gas separation experiment by partial desorption. In this experiment the sample is degased in two runs. In the first run, reaching up to 41.5 K, hydrogen is released. After cooling back to 20 K, the second desorption run is performed up to the final desorption temperature (~RT). As hydrogen already degased in the first run, the second run yields mostly deuterium. The selectivity in the second run is 17.3. Thus, the strong adsorption sites in MFU-4 *large* separate H_2/D_2 isotope mixtures more efficiently than the tested small-pore MFU-4 derivatives.

The previously presented separation experiment was performed after exposure to a 10 mbar 1:1 H_2/D_2 mixture at 40 K. For industrial separation of hydrogen gas, the operating conditions would be very different in three ways. Firstly, the hydrogen gas contains a large hydrogen excess with less than 0.02% deuterium. Secondly, the separation would be preferentially performed at higher exposure temperatures because cooling to 40 K requires liquid helium as a cooling agent whereas 80 K only requires the much cheaper liquid nitrogen. Thirdly, a higher gas pressure would allow the purification of a larger amount of gas. All three aspects were addressed experimentally in this work. However, for a better understanding of the impact of the three parameters on the selectivity, only one of these parameters is changed per experiment.

The problem of hydrogen excess in natural hydrogen gas is addressed by TDS experiments performed after exposure to gas atmospheres of different compositions. Additionally, these experiments show that the strong adsorption sites in MFU-4 *large* are very selective for deuterium. In the presence of a 1:1 mixture 95% of all occupied strong adsorption sites adsorbed deuterium. Reducing the deuterium content in the gas phase decreases the fraction of strong sites occupied by deuterium. However, even if the mixture contains 90% hydrogen, 75% of all occupied strong adsorption sites are populated by deuterium. Thus, the strong adsorption sites in MFU-4 *large* are highly selective for deuterium.

When MFU-4 *large* is exposed to 5 mbar of the isotope mixture, the small amount of gas is not enough to saturate the strong adsorption sites, i.e. they are hardly visible. An exposure pressure of 50 mbar results in condensation when cooling to 20 K. Therefore the high selectivity is mainly a result of “cryogenic distillation”.

An increase in exposure temperature from 40 K to 80 K reveals that the adsorbed amount of gas decreases but 87% of all occupied strong adsorption sites are still populated by deuterium. The spectra obtained after exposure to the mixture at RT also seem to imply selective adsorption at the strong sites at a first glance. However, the cooling to 20 K affects the adsorption state. One can therefore expect that additional deuterium was adsorbed upon cooling from RT to 20 K. In contrast to the experiment performed after gas exposure at RT, the TDS spectra obtained after exposure at 80 K yield a liquid gas signal indicating that the fast cooling from 80 K to 20 K led to a condensation of the excess gas rather than causing additional adsorption.

For MFU-4 *large* one can conclude that it does not exhibit the quantum sieving phenomenon due to its large aperture well above the kinetic diameter of hydrogen. However, MFU-4*large* possesses strong adsorption sites that are highly selective for deuterium. Therefore, these sites are mainly occupied by deuterium even for gas mixtures with low deuterium content and at higher adsorption temperatures (80 K).

5.10. Hydrogen isotope adsorption in MOF-5

MOF-5 has a comparable pore structure to MFU-4 *large*. Both exhibit alternating pores of similar size, i.e. 12 Å and 15 Å for MOF-5. Their ssa values are also similar.

The TDS spectra after exposure to pure gases at 40 K presented in this work nicely fit the course of the published hydrogen TDS spectrum obtained after gas exposure at RT (see chapter 3.1.6). Also the calculated uptake values (4.5 mg/g for hydrogen at 40 K and 10 mbar) are reasonable compared to the literature data.

Comparing the TDS spectra of MOF-5 and MFU-4 *large* after exposure to pure gases and to the mixture, the same trend can be seen. After exposure to the pure gases the two isotopes exhibit the same desorption spectrum, except that the deuterium uptake exceeds the hydrogen uptake by a factor of 1.4 due to the lower ZPE value and the smaller de Broglie wavelength of deuterium. The desorption spectra of MOF-5 exhibit two peaks after pure gas exposure. The first maximum is centered around 30 K. The second signal overlaps with the first one and ranges from roughly 40 K to 70 K. After exposure to the isotope mixture, the hydrogen desorption spectrum only exhibits one maximum centered around 30 K. However, the deuterium desorption spectrum exhibits three peaks with their maxima located at 30 K, 40 K and 45 K. As observed for MFU-4 *large*, in the presence of an isotope mixture deuterium occupies the strong adsorption sites and therefore hydrogen is adsorbed at the weaker adsorption sites. For MOF-5 the three desorption signals can be correlated to distinct adsorption sites by making use of the results of Yildirim et al. who determined the deuterium adsorption sites on the basis of neutron diffraction experiments (see Figure 5.13).[115] They found that the first occupied adsorption sites are the so-called cup-sites located in the center of the agminated ZnO_3 units. With higher loading the second adsorption sites on top of the single zinc oxide units are occupied. The third and fourth adsorption sites are simultaneously populated and are located above the oxygen ion and on top of the hexagonal linker. The three deuterium desorption signals in MOF-5 can be ascribed to the adsorption sites determined by QENS. Thus, the desorption signal at 45 K is

attributed to the cup sites, the desorption signal at 40 K is attributed to the top of the single zinc oxide units and the desorption signal at 30 K is attributed to the adsorption on the oxygen atoms and the linker. As the third and fourth adsorption sites on the oxygen atom and the linker are populated simultaneously, they can be considered to desorb simultaneously and therefore form one joint peak.

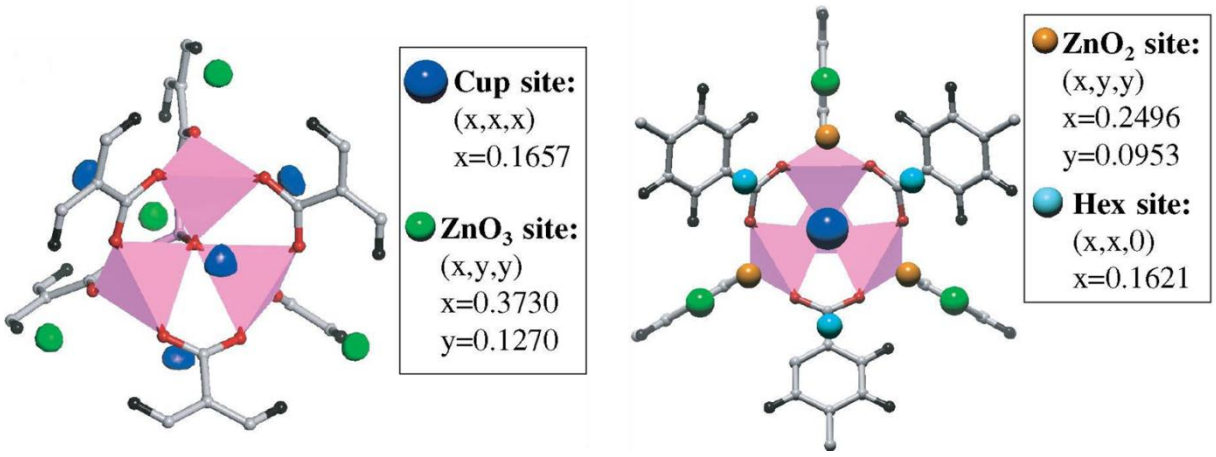

Figure 5.13: Adsorption sites in MOF-5 determine by QENS. [115]

Comparing the determined adsorption sites by QENS to the hydrogen and deuterium TDS spectra obtained after exposure to the mixture one can conclude that deuterium adsorbs mainly at the metal clusters whereas hydrogen adsorption occurs predominantly at the weakly binding (organic) parts of the MOF-5 framework, e.g. to the linker positions.

A partial desorption experiment yielded a selectivity of 6.8 of the strong adsorption sites in MOF-5.

Summing up, also in MOF-5 deuterium adsorbs predominantly at the strong adsorption sites. The strong adsorption sites in MOF-5 are less selective for deuterium compared to MFU-4 *large*.

5.11. A comparison of the applied TDS procedure to the standard procedure

In current investigations applying low temperature TDS for the investigation of porous materials, the samples were exposed to gas at RT and subsequently cooled down to 20 K under the gas atmosphere. Additionally, the number of peaks in the desorption spectra were related to the number of differently sized pores in the considered porous materials.[73,74,79,83,100] The applied TDS procedure in this work, i.e. gas exposure at low temperatures and the use of isotope mixtures, will now be compared to the up to now applied standard procedure.

Cryogenic loading was not possible in the devices described in the above given publications because they are only high vacuum devices. Therefore the base pressure in the sample chamber is higher and the sample takes up all gases in the sample chamber (mainly water) during long-term low temperature loading. The TDS device built up as part of this thesis only uses UHV gaskets for the connections of the sample chamber and therefore the base pressure in the sample chamber is in the low 10^{-9} mbar region. Exposing the sample to a gas atmosphere at RT requires the crossing of a large temperature window when cooling to 20 K. For small-pore samples where hydrogen isotope diffusion is slow, the uptake is then strongly dependent on the cooling rate which was shown for MFU-4(Zn, Cl) by applying two different cooling procedures. Therefore, the low temperature loading describes the adsorption state at the exposure temperature more accurately and the inverse kinetics of the quantum sieving phenomenon could be shown. The spectra of MFU-4 *large* obtained after exposure to the mixture at RT imply that the cooling leads to additional adsorption. Owing to the fast adsorption kinetics in the large-pore samples, one can assume a fast change in adsorption state upon cooling from RT to 20 K.

The use of isotope mixtures allows a direct measurement of the selectivity. Further, the inverse kinetics of the quantum sieving phenomenon could be shown for the small-pore samples. Additionally, it was revealed that the isotope mixture does not behave like an ideal solution. Exposing the large-pore samples to the mixture yielded that deuterium occupies the strongest adsorption sites which can be very selective for deuterium.

Another fundamental difference is the correlation between TDS spectrum and pore structure. The previous works related the number of desorption maxima mainly to the number of pores of different sizes in the investigated framework. The current work could more clearly relate the number of desorption maxima to the number of adsorption sites of different adsorption energy.

5.12. Technical implementation of light gas isotope separation in MOFs

5.12.1. A comparison of the separation effectiveness

The usability of nanoporous materials for industrial isotope separation does not only depend on the selectivity but additionally on the amount of obtained product (deuterium) per sample mass. Figure 5.14 compares the selectivity of the investigated MOF samples and Takeda 3A as a function of the adsorbed amount of deuterium.

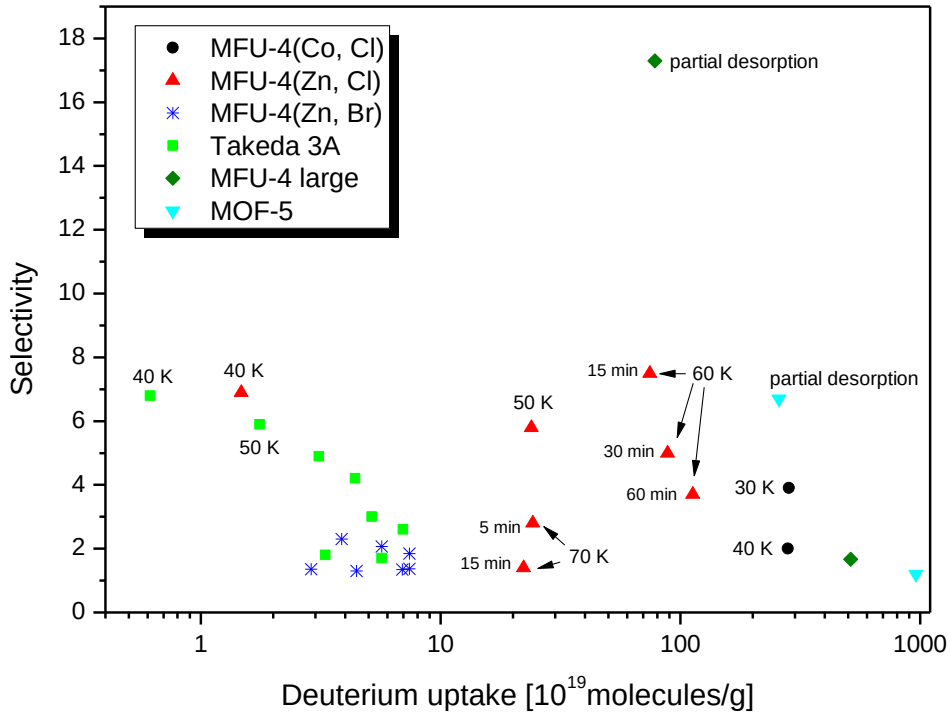

Figure 5.14: Selectivity as a function of the adsorbed amount of deuterium for all investigated MOF structures and Takeda 3A. All experimental results of the samples MFU-4(Co, Cl), MFU-4(Zn, Cl) and MOF-5 are presented. The results of MFU-4(Zn, Br) are those obtained with MFU-4(Zn, Br)_T2. The selectivity values of Takeda 3A are those obtained after gas exposure between 40 K and 110 K. For MFU-4 *large* only the selectivity values after gas exposure to a 10 mbar 1:1 isotope mixture at 40 K are plotted.

Owing to its combination of low gas uptake even at elevated pressure and low selectivity values, MFU-(Zn, Br) is not a suitable materials for isotope separation at any operating condition. The low uptake but high selectivity values at low temperatures make Takeda 3A suitable mainly below liquid nitrogen temperature. Nevertheless, MFU-4(Zn, Cl) exhibits the same selectivity values at 40 K and 50 K but a deuterium uptake that exceeds the values of Takeda 3A by roughly one order of magnitude at 50 K. Making use of the kinetic nature of the quantum sieving which still occurs at 60 K, one can reach high uptake

values and additionally high selectivity values in MFU-4(Zn, Cl). Thus, MFU-4(Zn, Cl) is superior to Takeda 3A. However, when the kinetic barrier vanishes at 70 K this MOF structure is not usable for isotope separation any more. MFU-4(Co, Cl) exhibits a low selectivity of maximum 4.0 at 30 K but the adsorbed amount of deuterium is large for a small-pore material. If the separation process in done in several steps, MFU-4(Co, Cl) could be used in a first separation step, followed by a second step which uses a MOF with a higher selectivity.

The results obtained with MFU-4(Zn, Br) suggested that the separation temperature cannot easily be increased by tuning the aperture/pore. Thus, isotope separation by kinetic quantum sieving is probably restricted to cryogenic operating temperatures.

The large-pore samples MOF-5 and in particular MFU-4 *large* exhibit excellent separation capability if only the strong adsorption sites are considered but they are inferior when all adsorption sites are taken into account because the strong adsorption sites in MFU-4 *large* only make ~13% of all adsorption sites. However, MFU-4 *large* shows the great potential of MOFs to separate isotope mixtures by means different from kinetic quantum sieving, i.e. by highly selective adsorption sites. It has to be pointed out that these sites are mainly populated by deuterium even in the presence of mixtures with high hydrogen content and at LN_2 temperature (~80 K). Maximizing the number of highly selective adsorption sites could yield an ideal material for hydrogen isotope separation.

5.12.2. Isotope separation with small-pore MOFs

The kinetic separation by exploiting the quantum sieving effect in small-pore MOFs can be realized by membrane based gas separation. Polymer and zeolite membranes are industrially used for conventional gas separation. The mainly used and cheaply produced polymeric membranes would not be usable for isotope separation as they do not possess well-ordered pore structures. Their void volume is only generated by unordered raveling of the hydrocarbon chains i.e. they are amorphous. In contrast, zeolite membranes exhibit uniform cages and therefore could also allow quantum sieving but they have not been tested up to now to the best of our knowledge. Naturally occurring zeolites possess a limited and non-tunable cage structure which might not have the ideal size to facilitate quantum sieving. Synthetically produced zeolites allow a moderate variance of the cage structure but the synthetic membranes are found to be prone to grain boundary cracking.[116] Furthermore the production of zeolite membranes is expensive due to the demanding conditions of the

synthesis, i.e. high temperature and pressure as well as calcination.[117] MOF membranes possess several advantages compared to zeolite or polymer based membranes. The pore structure is precisely tunable, their production does not require complex synthesis conditions and they can be activated in the sense of solvent and water removal under rather mild conditions (<350°C). Membranes made of MFU-4 frameworks have not been synthesized up to now but other MOF membranes were successfully fabricated.[117-120] The gas separation performance of a membrane can be clearly seen in a selectivity-versus-permeability-diagram, i.e. the separation performance of a membrane is governed by thermodynamics of adsorption and the diffusion of the different gas species through the membrane.[120] Also for isotope separation by quantum sieving, permeability and selectivity are rival quantities. A high selectivity demands a high kinetic barrier to diffusion, thereby decreasing the permeability.

The membranes can be produced by the layer-by-layer method and subsequently separated from the supporting substrate, i.e. a nearly single-crystalline and defect-free MOF membrane with desired orientation can be produced.[18,119]

One possible technical problem associated with the MOF membranes is the cycle stability. The membrane might degrade after several cycles of high temperature activation and cryogenic gas separation. Small defects, induced after several cycles, act as fast pathways without separation effect which would lead to a lifetime-dependent decrease in selectivity.

5.12.3. Isotope separation with large-pore MOFs

The exploitation of the preferred adsorption of the heavier isotope on the strong adsorption sites in large-pore frameworks can be realized in either swing adsorption procedures like vacuum swing adsorption (VSA) and temperature swing adsorption (TSA) or by chromatography.

Swing adsorption techniques

Vacuum swing adsorption is a special variant of pressure swing adsorption operated at pressures below atmospheric pressure. All swing methods separate gas mixtures in fixed beds that consist of porous adsorbents (see Figure 5.15). The adsorbent strongly adsorbs one of the mixture components. The component with weak interaction can easily penetrate the bed and therefore be griped at the end of the bed. The diffusion of the strongly adsorbed component is delayed until the bed is saturated. After saturation the strongly

adsorbed component also reaches the end of the bed (breakthrough) and can be gripped there either by pressure drop (pressure swing adsorption, vacuum swing adsorption) or by temperature increase (temperature swing adsorption).

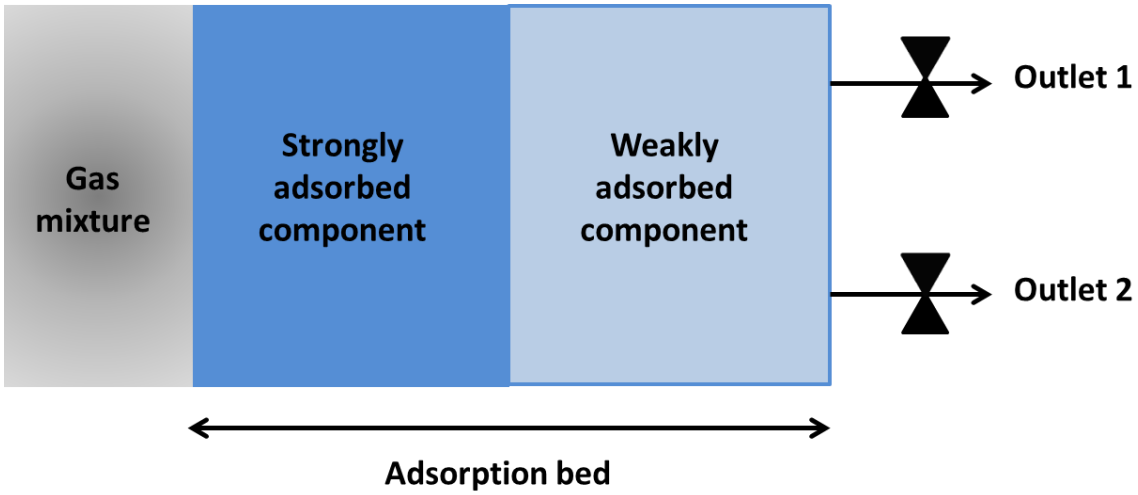

Figure 5.15: Illustration of the separation mechanism in swing adsorption techniques. The gas mixture is exposed to a fixed bed adsorbing one gas component more strongly. The weakly adsorbed component penetrates the bed more easily and therefore reaches the end of the bed first. Outlet 1 releases the weaker component until the strongly adsorbed component reaches the outlet due to a saturation of the fixed bed. The strongly adsorbed component is released on outlet 2. The degasing is achieved by either pressure decrease or temperature increase.

Pressure/Vacuum swing adsorption might be somewhat easier to handle from a technical point of view as it can be operated isothermally and therefore rather continuously. In temperature swing adsorption the temperature of the cooled sample has to be increased in order to degas the adsorbed component. The re-cooling of the sample might require some time (dead time of the equipment) due to low thermal conductivity of the powder. However, the thermal conductivity strongly depends on the packing density of the powder.

Gas chromatography

Gas chromatography based gas separation with columns filled or covered with nanoporous materials with high specific surface areas can be found in literature. Single-walled carbon nanotubes[121], a zeolitic imidazolate framework[122] and a MOF[123] have already been tested in chromatography concerning the separation of different conventional mixtures. Isotope separation would apply gas chromatography. In conventional gas chromatography the gas separation takes place in columns filled with a stationary adsorbing phase like a zeolite or a carbon material. According to the different strength of interaction

between the stationary phase and the incoming molecules of the gas mixture, the component interacting more strongly with the adsorbent reaches the end of the column with a delay, i.e. longer retention time. For isotope separation the isotope mixture should be separated as deuterium interacts more strongly with the stationary phase due to the binding to the strongest adsorption sites. As hydrogen remains in the gas phase, the light isotope will exhibit the shorter retention time. The columns for isotope separation might be coated with a MOF applying a procedure similar to the layer-by-layer method.[18] The proposed procedure of MOF deposition on thin capillaries by stepwise exposure to the organic or inorganic component was already performed successfully.[124] MOF-5 was deposited on fused silica capillaries by the controlled SBU-approach. Metallic capillaries would allow better cooling of the attached MOF layer. The only problem associated with the MOF deposition on the capillary is probably delamination caused by thermal stresses. The layer on the capillary will grow during synthesis in a way to minimize its stress caused by the mismatch between layer and support. However, the system is cooled for the separation and heated repeatedly in order to reactivate the MOF whereat both procedures cause thermal stresses. These stresses are proportional to the difference between actual system temperature and deposition temperature as well as to the difference in coefficient of thermal expansion for the layer and the capillary material. Experimental and theoretical results propose negative thermal coefficients of expansion for MOFs.[125-127] From this point of view, metallic capillaries are not suitable as they have a comparably large and positive coefficient of thermal expansion. Applying glasses with typically near-zero coefficient of thermal expansion as capillary materials would reduce the thermal stresses. If MOF layers should tend to detach during service, the columns could also be stuffed with powder MOFs. This will decrease the temperature/thermal conductivity due to insufficient contact of the powder particles with the cooled capillary wall and between the particles themselves. MOFs have found to have low thermal conductivity as expected for highly porous frameworks. For a single crystal of MOF-5 the thermal conductivity was found to be between 0.1 W/mK and 0.6 W/mK in the temperature range from 6 K to 300 K.[128] The thermal conductivity is expected to be higher for the single crystal compared to the powder MOF. For MIL-101(Fe) powder with a packing density of 0.51 g/ml the values of the thermal conductivity are 0.018 W/mK and 0.18 W/mK at 90 K and 340 K, respectively.[93] However the effect of low thermal conductivity in powders is also faced if other powders like zeolites or carbon materials are used.

6. Summary and outlook

This work studies the H_2/D_2 adsorption and separation in microporous materials by measuring the H_2/D_2 selectivity values, defined as the molar uptake ratios $n(D_2)/n(H_2)$, by applying isotope mixtures in low temperature thermal desorption spectroscopy. The experimental results are partially supported by theoretical contributions provided by the group of Prof. Heine (Jacobs University, Bremen, Germany). The experimentally investigated samples are

1) a carbon molecular sieve named Takeda 3A which is known to adsorb deuterium preferentially and to exhibit inverse H_2/D_2 kinetics, i.e. higher diffusivity of deuterium compared to hydrogen below 100 K.
2) a small-pore isoreticular framework series (MFU-4 series) with alternating bimodal pore structure where the small and the large pore are connected via a narrow aperture that is close to the kinetic diameter of hydrogen in size. The derivatives of this framework series differ slightly in pore size (diameters of the small pore ~3.5 Å-4.5 Å) and aperture size (2.3 Å-3 Å).
3) MFU-4 *large* and MOF-5 which possess an alternating bimodal pore structure but pore diameters of 12 Å to 18.5 Å, i.e. pore sizes well above the kinetic diameter of hydrogen.

In order to measure the selectivity, the samples are exposed to a 1:1 H_2/D_2 mixture at the chosen exposure temperature (30 K-150 K) for a selected exposure time (mostly 90 min). The loading pressures in most experiments are 10 mbar and 50 mbar. After gas exposure for the selected time, the samples are cooled to 20 K under the gas atmosphere and the remaining excess gas is pumped off. Subsequently, the loaded sample is subjected to a temperature program with a constant heating rate of 0.1 K/s. This leads to thermally activated desorption whereat the desorbing gas is continuously detected by a mass spectrometer.

In the following, the main results will be summarized.

Takeda 3A:

- The gas uptake increases with rising exposure temperature, revealing that the adsorption process is kinetically limited.
- The quantum sieving phenomenon separates the H_2/D_2 mixtures. The selectivity decreases with rising exposure temperature and remains constant above 100 K which

can be attributed to the higher diffusivity of deuterium below 100 K. The maximum selectivity of 6.8 is measured after exposure at 40 K.

- The selectivity is larger than the H_2/D_2 ratio measured under the same measurement conditions, indicating that the H_2/D_2 mixture does not behave like an ideal solution.

MFU-4 series:

- A decreasing selectivity with rising exposure time reveal that kinetic quantum sieving also occurs in small-pore MFU-4 samples and therefore, the small-pore MFU samples are also capable of separating H_2/D_2 mixtures. Knudsen diffusion is not observed.
- The samples show a gate opening due to phonon excitations, i.e. below the opening temperature gas molecules can barely penetrate. MFU-4(Zn, Cl) and MFU-4(Zn, Br) open at ~45 K and 80/90 K, respectively.
- Isotope separation by quantum sieving only works in a very limited size window of the aperture. The aperture of 3 Å in MFU-4(Co, Cl), i.e. an aperture slightly above the kinetic diameter of hydrogen, shows a noticeable selectivity value of 4.0 only at 30 K. The aperture of 2.5 Å in MFU-4(Zn, Cl) allows high selectivity up to 7.5 at 60 K for short exposure times, i.e. if the inverse kinetics are exploited for the separation. The aperture of 2.3 Å (below the kinetic diameter of hydrogen) in MFU-4(Zn, Br) leads to selectivity values of less than 3 which can be attributed to the high opening temperature where the difference in isotope diffusivity might already be rather small.

Large-pore samples:

- The large-pore samples do not show kinetic quantum sieving. But they suggest that there are other means of H_2/D_2 isotope separation than quantum sieving because deuterium binds preferentially to the strongest adsorption sites if mixtures are applied.
- In MOF-5 deuterium adsorbs at all available adsorption sites whereas hydrogen is adsorbed mainly at the organic ligands, i.e. at the weak adsorption sites. The selectivity of the strong adsorption sites is 6.8 at 40 K.
- Three adsorption sites are experimentally and theoretically found in MFU-4 *large*. The strong adsorption sites in MFU-4 large are highly selective for deuterium, exhibiting a selectivity of 17.3 at 40 K. Even in case of only 10 % deuterium in the isotope mixture, 75% of all occupied strong adsorption sites adsorbed deuterium.

The adsorption sites remain selective for deuterium even at elevated exposure temperatures of 80 K where 87% of the strong adsorption sites are occupied by deuterium.

- Kinetic quantum sieving and selective adsorption sites can be exploited for isotope separation. The small-pore MOFs could be prepared as membranes and therefore be applied in membrane based separation. The preferred adsorption of deuterium at the strong adsorption sites could be used in chromatography or swing adsorption techniques; in particular if the number of selective adsorption sites in the MOF structures can be increased.

Zusammenfassung

Grundlagen

In den 1990er Jahren wurden die ersten Vertreter einer neuartigen hoch porösen Klasse von Hybridsubstanzen hergestellt, die sogenannten metall-organischen Gerüstverbindungen (engl. **m**etal-**o**rganic **f**ramework, kurz MOF). Sogleich wurden sie aufgrund ihrer hohen spezifischen Oberfläche und gezielt veränderbaren Porenstruktur als potenzielle Materialien für Gasspeicherung und Gastrennung diskutiert. Zur Trennung konventioneller Gasgemische in seine Bestandteile gibt es zwei Möglichkeiten. Zum einen können Gasgemische auf Basis der unterschiedlichen Adsorptionswärmen in ihre Bestandteile getrennt werden, wie zum Beispiel in Druckwechseladsorptionsanlagen. Zum anderen kann das Größenausschlussprinzip genutzt werden, also Gasteilchen mit einem kinetischen Durchmesser größer als der Porendurchmesser können nicht eindiffundieren und werden vom Adsorptionsprozess im Netzwerk ausgeschlossen. Mit ganz besonders feinporigen MOFs können allerdings nicht nur konventionelle Gasgemische getrennt werden, sondern unter geeigneten Bedingungen auch Isotopenmischungen. Das hierfür genutzte Phänomen bezeichnet man als „Quantentsiebung“ (engl. quantum sieving). Das unterschiedliche Adsorptionsverhalten der Isotope beruht auf ihrem Massenunterschied, der zu verschiedenen Werten der Nullpunktsenergie führt. Bei der Adsorption in größeren Poren kann man die Nullpunktsenergie gegenüber der Wechselwirkungsenergie in guter Näherung vernachlässigen und somit verhalten sich die Isotopen gleich. Bei der Adsorption in Poren, die nur um den Betrag der de Broglie Wellenlänge größer sind als das Gasteilchen selbst, steigt die Nullpunktsenergie der adsorbierenden Teilchen jedoch an, sodass die Nullpunktsenergie nicht mehr vernachlässigt werden kann. Letztlich führt dieses Quantenphänomen zu bevorzugter Adsorption und schnellerer Diffusion des schwereren Isotops im Vergleich zum leichteren. Die Nutzbarkeit der Quantensiebung zur Trennung gasförmiger H_2/D_2-Mischungen ist unklar, da kaum experimentellen Daten zur Trennung von Isotopenmischungen vorliegen. Es existieren lediglich Adsorptionsisothermen, die bei 77 K für die reinen Gase gemessen wurden. Auf Basis dieser Daten wird das Trennvermögen dann grob über das molare Verhältnis der Deuteriumaufnahme zur Wasserstoffaufnahme abgeschätzt, d.h. $n(D_2)/n(H_2)$. Mittels quasi-elastischer Neutronenstreuung können auch die unterschiedlichen Diffusivitäten der Isotopen gemessen werden, was jedoch aufgrund des großen experimentellen Aufwandes nur selten erfolgt. Allerdings kann mit keiner der beiden

oben genannten Methoden das Trennvermögen eines porösen Materials gemessen werden, da keine Isotopenmischungen verwendet werden können.

Experimentelles Vorgehen

In der vorliegenden Arbeit wird die Selektivität, d.h. das molare Adsorptionsverhältnis $n(D_2)/n(H_2)$ in Anwesenheit einer 1:1 Isotopenmischung, mittels Thermischer Desorptionsspektroskopie (TDS) bestimmt. Der Aufbau der verwendeten TDS-Anlage war Teil dieser Promotion. Der Probenhalter aus Kupfer befindet sich in einer UHV-Kammer und wird die mittels eines LHe-Kryostats gekühlt. Eine Widerstandsheizung ermöglicht das Erreichen von Probentemperaturen zwischen ca. 15 K und 600 K. Zum Erreichen tiefer Probentemperaturen befindet sich die Probenkammer in einem Isoliervakuum mit zusätzlichem LN_2-Schild. Die Detektion der desorbierenden Gase erfolgt mittels eines Quadrupol-Massenspektrometers (Microvision Plus 100 D). Um die desorbierende Gasmenge quantifizieren zu können, wurde das Massenspektrometer-Signal mit Hilfe einer $Pd_{95}Ce_5$-Legierung auf Wasserstoff und Deuterium kalibriert.

Zur Messung der Selektivität werden wenige Milligramm einer nanoporösen Probe erst bei geeignet hoher Temperatur aktiviert und anschließend bei der gewählten Adsorptionstemperatur zwischen 30 K und 150 K für eine gewählte Expositionsdauer (meist 90 min) der 1:1 Isotopenmischung mit festgelegtem Druck (meist 10 mbar oder 50 mbar) ausgesetzt. Nach Ablauf der Expositionsdauer wird die Probe unter der Gasatmosphäre auf 20 K abgekühlt und das Überschussgas bis zum Erreichen eines Vakuums im Bereich $\sim 10^{-5}$ mbar abgepumpt. Schließlich wird die Probentemperatur mit einer Aufheizrate von 0,1 K/s erhöht und das desorbierende Gas mit Hilfe des Massenspektrometers registriert.

Die Selektivität in einem TDS-Experiment hängt von der Gaszusammensetzung, dem Gasdruck, der Probentemperatur und der Expositionsdauer ab.

Untersuchte Proben

Zuerst wird eine Kohlenstoffprobe namens Takeda 3A mit ca. 3 Å großen Poren untersucht. Zu diesem Material gibt es eine Vielzahl von Veröffentlichungen, die Ergebnisse von Adsorptionsmessungen und Diffusionsmessungen von H_2 und D_2 zeigen, die nur mit Quanteneffekten zu erklären sind.

Des Weiteren wird eine Reihe MOFs mit gleicher Topologie auf das Auftreten von Quantenadsorptionseffekten untersucht. Diese MOFs sind Vertreter der MFU-4-Reihe (**m**etal-organic **f**ramework University of **U**lm), die eine bimodale alternierende Porenstruktur

aufweisen. Aufgrund dieser speziellen Porenstruktur aus abwechselnd großen (Durchmesser ~12 Å) und kleinen Poren (Durchmesser ~3,5 Å-4,5 Å) muss jedes adsorbierte Teilchen Poren beider Größen passieren und zusätzlich eine kleine Öffnung (~2,3 Å-3 Å), die die beiden Poren verbindet. Die kleine Pore sowie die Porenöffnung mit einer Größe vergleichbar dem kinetischen Durchmesser von Wasserstoff sollen das Isotopengemisch trennen wohingegen die große Pore eine hinreichend große innere Oberfläche zur Speicherung des Deuteriums bereitstellen soll. Die experimentellen Ergebnisse zu den kleinporigen MFU-4-Derivaten werden teilweise durch Theoriebeiträge der Arbeitsgruppe von Prof. Heine von der Jacobs University in Bremen ergänzt. Die kleinporigen MFU-4-Derivate unterscheiden sich entweder durch das verwendete Metallzentrum (Co oder Zn) oder durch das Halogen (Cl oder Br) von denen jeweils vier identische Halogenatome die quadratische Porenöffnung bilden. Auf Basis dieser Unterschiede erfolgt die Nomenklatur der Proben, d.h. MFU-4(Zn, Cl), MFU-(Co, Cl) und MFU-4(Zn, Br).

Zusätzlich werden zwei großporige MOFs mit Porengrößen/Porenöffnung deutlich größer dem kinetischen Durchmesser von Wasserstoff gemessen, die keine Quantensiebung wohl aber unterschiedliche Isotopenadsorption aufgrund der verschiedenen Nullpunktsenergien erlauben. Die eine Probe ist MFU-4 *large*, ein großporiges MFU-Derivat mit Porendurchmessern von ~12 Å und 18,5 Å sowie einer Porenöffnung von ~9 Å. Die zweite Probe ist MOF-5, auch IRMOF-1 genannt, mit Porendurchmessern von 12 Å und 15 Å.

Ergebnisse und Diskussion

Takeda 3A nimmt oberhalb von 30 K Gas auf und zeigt einen Anstieg der Gasaufnahme mit steigender Adsorptionstemperatur, was auf eine ausgeprägte kinetische Hemmung der Adsorption hindeutet. Die maximale Wasserstoffaufnahme wird bei einer Expositionstemperatur von 100 K und ein maximale Deuteriumaufnahme bei 90 K gemessen. Oberhalb einer Expositionstemperatur von 90 K/100 K sinkt die Gasaufnahme wieder. Der höchste Selektivitätswert von 6,8 wird nach Exposition bei 40 K gemessen. Danach nimmt die Selektivität bis zu einer Expositionstemperatur von 100 K linear mit der Temperatur ab, was gut mit Literaturdaten übereinstimmt, die eine höhere Diffusivität von Deuterium gegenüber Wasserstoff unterhalb von 100 K angeben. Für Expositionstemperaturen zwischen 100 K und 140 K erhält man eine weitgehend konstante Selektivität von 1,6-1,9.

Zudem werden bei einer Probentemperatur von 40 K identische TDS-Messungen mit den Reingasen durchgeführt. Es zeigt sich, dass die Selektivität doppelt so groß ist wie das

molare D_2/H_2-Verhältnis was bedeutet, dass sich die Isotopenmischung nicht wie eine ideale Lösung verhält. Die mittels TDS gemessene Selektivität ist deutlich größer als die in der Literatur angegebenen D_2/H_2-Verhältnisse bei ähnlicher Temperatur und Druck. Grund hierfür ist vermutlich auch die langsame Diffusion. Die in der Literatur angegebenen D_2/H_2-Verhältnisse sind als Gleichgewichtsverhältnisse nach langer Expositionszeit zu verstehen, wohingegen die Probe im TDS-Experiment nur 90 min der Mischung ausgesetzt war. Daher sind die gemessenen Selektivitäten als Nichtgleichgewichtswerte zu verstehen, die aufgrund der kinetischen Präferenz von Deuterium immer größer sein müssen als der GG-Wert.

Die Ergebnisse des MFU-4-Derivats MFU-4(Zn, Cl), mit 2,52 Å großer Öffnung und 3,88 Å Durchmesser der kleinen Pore, zeigt bei 40 K und 50 K gleiche Selektivität wie Takeda 3A. Jedoch steigt beim Anstieg der Expositionstemperatur von 40 K auf 50 K die aufgenommene Gasmenge stark an, was auf eine Öffnung der Porenstruktur hindeutet. Diese These kann durch ein berechnetes Phononenspektrum gestützt werden. Da oberhalb von ca. 45 K die effektive Porengröße kontinuierlich ansteigt, nimmt die Diffusionsbarriere rasch ab und die Selektivität sinkt. Daher wird bei einer Expositionstemperatur von 60 K nur noch für kurze Haltezeiten eine hohe Selektivität gemessen. Bei 70 K ist keine nennenswerte Diffusionsbarriere mehr nachweisbar, sodass die Selektivität selbst für kurze Expositionsdauern gering ist ($S<3$). Eine Berechnung der Wahrscheinlichkeitsdichten führt zu dem Schluss, dass die D_2-Dichte im Bereich der Porenöffnung und an der inneren Oberfläche größer ist als die für Wasserstoff. Ersteres ist der typische Quantensiebungseffekt. Letzteres ist ein nicht-kinetischer ZPE-Effekt, da Deuterium immer aufgrund seiner niedrigeren ZPE bevorzugt adsorbiert wird. Letztlich führt dies in der Pore dazu, dass Deuterium eine dichte Adsorptionsschicht ähnlich einem Quantenliquid an der Porenoberfläche bildet, wohingegen Wasserstoff ins Zentrum der Pore gedrängt wird.

Die TDS-Ergebnisse des MFU-4(Co, Cl) mit leicht größerer Pore und Porenöffnung als MFU-4(Zn, Cl) zeigen bereits bei 30 K eine hohe Gasaufnahme, was auf eine relativ geringe Diffusionsbarriere hindeutet. Daher sind auch die Selektivitätswerte bei gleichen Messbedingungen geringer (4,0 bei 30 K und 2,0 bei 40 K) als bei den zuvor abgehandelten Proben.

Der dritte Vertreter der kleinporigen MFU-4-Derivate ist MFU-4(Zn, Br) mit einer Porenöffnung von nur 2,33 Å. Da diese Probe eine extreme Diffusionsbarriere bildet, muss sie unter erhöhtem Beladungsdruck gemessen werden, nämlich 50 mbar statt 10 mbar.

Zudem werden zwei unterschiedlich hergestellte MFU(Zn, Br)-Proben untersucht. MFU-4(Zn, Br)_T1 ist solvothermal hegestellt und weist eine bimodale Korngrößenverteilung des Pulvers auf. MFU-4(Zn, Br)_T2 hingegen zeigt eine gleichmäßige Korngröße. Aufgrund der hohen Diffusionsbarriere kann erst bei erhöhter Beladungstemperatur (80-90 K) Gas ins Innere der Struktur eindiffundieren. Da bei diesen Temperaturen die Diffusivitäten von Wasserstoff und Deuterium vermutlich recht ähnlich sind, zeigt MFU-4(Zn, Br) nur eine geringe Selektivität (<3).

Aus den erhaltenen Ergebnissen der kleinporigen MFU-4 Derivate kann gefolgert werden, dass Quantensiebung nur in einem sehr engen Größenbereich der Porenöffnung auftritt. Zudem tritt Quantensiebung nur bei hinreichend tiefen Temperaturen auf ($T<LN_2$ Temperatur) und daher kann eine hohe Selektivität bei erhöhter Temperatur nicht ohne weiteres durch eine Reduzierung der Porenöffnung erreicht werden.

TDS-Experimente mit den großporigen MOF-Strukturen zeigen, dass in Anwesenheit einer Mischung Deuterium zuerst adsorbiert wird und daher die stärksten Adsorptionsstellen besetzt. Im TDS-Experiment desorbiert daher Wasserstoff bereits bei tiefen Temperaturen, wohingegen bei hoher Temperatur fast ausschließlich Deuterium desorbiert. Dies ermöglicht ein Trennexperiment durch schrittweises Entgasen. Dabei zeigt sich, dass die starken Adsorptionsstellen sehr selektiv für Deuterium sind. Die Selektivität der starken Adsorptionsstellen beträgt 6,8 in MOF-5 und 17,3 in MFU-4 *large* nach Gasexposition bei 40 K. Die besonders hohe Selektivität der starken Adsorptionsstellen in MFU-4 *large* zeigt sich auch bei Adsorptionsexperimenten mit Isotopenmischungen, die eine geringere Deuteriumkonzentration in der Gasphase aufweisen. Betrachtet man jedoch nicht nur die starken Adsorptionsstellen, sondern alle Adsorptionsstellen der großporigen Proben, ist ihre Selektivität gering gegenüber den kleinporigen Proben (S<2).

Potential der MOFs zur Isotopentrennung

Die untersuchten Proben Takeda 3A, MFU-4(Zn, Cl) und MFU-4(Co, Cl) besitzen Potential zur industriellen Gastrennung. Takeda 3A zeigt hohe Selektivität weitgehend unter LN_2-Temperatur. MFU-4(Zn, Cl) zeigt die gleiche Selektivität bei tiefen Temperaturen (40 K und 50 K), jedoch eine deutliche größere Menge an adsorbiertem Deuterium und ist damit Takeda 3A überlegen. Hohe Selektivität kann mit MFU-4(Zn, Cl) auch bei 60 K noch erzielt werden, wenn die kinetische Komponente der Trennung genutzt wird. Die kleinporigen

Proben könnten in Form von Membranen hergestellt und in dieser Form zur Isotopentrennung genutzt werden.

Die großporigen MOF-Strukturen bergen auch großes Potential zur Isotopentrennung wenn es gelingt die Anzahl der selektiven Adsorptionsstellen zu erhöhen. Sie können dann zur Gastrennung in Gaschromatographen oder in Druckwechseladsorptionsanlagen genutzt werden.

Literature

(1) Horcajada, P.; Chalati, T.; Serre, C.; Gillet, B.; Sebrie, C.; Baati, T.; Eubank, J. F.; Heurtaux, D.; Clayette, P.; Kreuz, C.; Chang, J. S.; Hwang, Y. K.; Marsaud, V.; Bories, P. N.; Cynober, L.; Gil, S.; Ferey, G.; Couvreur, P.; Gref, R.: Porous metal-organic-framework nanoscale carriers as a potential platform for drug delivery and imaging. *Nat Mater* 2010, *9*, 172-178.

(2) Lu, Z. Z.; Zhang, R.; Li, Y. Z.; Guo, Z. J.; Zheng, H. G.: Solvatochromic Behavior of a Nanotubular Metal-Organic Framework for Sensing Small Molecules. *Journal of the American Chemical Society* 2011, *133*, 4172-4174.

(3) Allendorf, M. D.; Schwartzberg, A.; Stavila, V.; Talin, A. A.: A Roadmap to Implementing Metal-Organic Frameworks in Electronic Devices: Challenges and Critical Directions. *Chemistry-a European Journal* 2011, *17*, 11372-11388.

(4) Morris, R. E.; Wheatley, P. S.: Gas storage in nanoporous materials. *Angewandte Chemie-International Edition* 2008, *47*, 4966-4981.

(5) Panella, B.; Hirscher, M.; Roth, S.: Hydrogen adsorption in different carbon nanostructures. *Carbon* 2005, *43*, 2209-2214.

(6) Furukawa, H.; Ko, N.; Go, Y. B.; Aratani, N.; Choi, S. B.; Choi, E.; Yazaydin, A. O.; Snurr, R. Q.; O'Keeffe, M.; Kim, J.; Yaghi, O. M.: Ultrahigh Porosity in Metal-Organic Frameworks. *Science* 2010, *329*, 424-428.

(7) http://www.auto-motor-und-sport.de/eco/mercedes-f-125-auf-der-iaa-erstklassig-abgasfrei-in-die-zukunft-3996068.html. Auto Motor und Sport.

(8) Luebbers, M. T.; Wu, T. J.; Shen, L. J.; Masel, R. I.: Trends in the Adsorption of Volatile Organic Compounds in a Large-Pore Metal-Organic Framework, IRMOF-1. *Langmuir* 2010, *26*, 11319-11329.

(9) Tagliabue, M.; Farrusseng, D.; Valencia, S.; Aguado, S.; Ravon, U.; Rizzo, C.; Corma, A.; Mirodatos, C.: Natural gas treating by selective adsorption: Material science and chemical engineering interplay. *Chem Eng J* 2009, *155*, 553-566.

(10) Beenakker, J. J. M.; Borman, V. D.; Krylov, S. Y.: Molecular-Transport in Subnanometer Pores - Zero-Point Energy, Reduced Dimensionality and Quantum Sieving. *Chemical Physics Letters* 1995, *232*, 379-382.

(11) Greenwood, N. N.; Earnshaw, A.: *Chemistry of the Elements*; Elsevier Butterworth-Heinemann: Amsterdam, Heidelberg, a.o., 2005.

(12) Centrone, A.; Siberio-Perez, D. Y.; Millward, A. R.; Yaghi, O. M.; Matzger, A. J.; Zerbi, G.: Raman spectra of hydrogen and deuterium adsorbed on a metal-organic framework. *Chemical Physics Letters* 2005, *411*, 516-519.

(13) Zhou, W.; Wu, H.; Yildirim, T.: Enhanced H(2) Adsorption in Isostructural Metal-Organic Frameworks with Open Metal Sites: Strong Dependence of the Binding Strength on Metal Ions. *Journal of the American Chemical Society* 2008, *130*, 15268-+.

(14) Eddaoudi, M.; Kim, J.; Rosi, N.; Vodak, D.; Wachter, J.; O'Keeffe, M.; Yaghi, O. M.: Systematic design of pore size and functionality in isoreticular MOFs and their application in methane storage. *Science* 2002, *295*, 469-472.

(15) Kuppler, R. J.; Timmons, D. J.; Fang, Q. R.; Li, J. R.; Makal, T. A.; Young, M. D.; Yuan, D. Q.; Zhao, D.; Zhuang, W. J.; Zhou, H. C.: Potential applications of metal-organic frameworks. *Coordin Chem Rev* 2009, *253*, 3042-3066.

(16) Czaja, A. U.; Trukhan, N.; Muller, U.: Industrial applications of metal-organic frameworks. *Chemical Society Reviews* 2009, *38*, 1284-1293.

(17) Zacher, D.; Shekhah, O.; Woll, C.; Fischer, R. A.: Thin films of metal-organic frameworks. *Chemical Society Reviews* 2009, *38*, 1418-1429. Reproduced by permission of the Royal Society of Chemistry. http://dx.doi.org./10.1039/B805038B

(18) Shekhah, C.; Wang, H.; Kowarik, S.; Schreiber, F.; Paulus, M.; Tolan, M.; Sternemann, C.; Evers, F.; Zacher, D.; Fischer, R. A.; Woll, C.: Step-by-step route for the synthesis of metal-organic frameworks. *Journal of the American Chemical Society* 2007, *129*, 15118-+.

(19) Schwochow, F.; Puppe, L.: Zeolites - Their Synthesis, Structure, and Applications. *Angew Chem Int Edit* 1975, *14*, 620-628.

(20) Breck, D. W.: *Zeolite Molecular Sieves*; Wiley: New York, 1974.

(21) Nune, S. K.; Thallapally, P. K.; Dohnalkova, A.; Wang, C. M.; Liu, J.; Exarhos, G. J.: Synthesis and properties of nano zeolitic imidazolate frameworks. *Chemical Communications* 2010, *46*, 4878-4880.

(22) Wang, B.; Cote, A. P.; Furukawa, H.; Yaghi, O. M.: INOR 896-Zeolitic imidazolate frameworks with exceptional chemical and thermal stability. *Abstr Pap Am Chem S* 2008, *235*.

(23) Fairen-Jimenez, D.; Moggach, S. A.; Wharmby, M. T.; Wright, P. A.; Parsons, S.; Duren, T.: Opening the Gate: Framework Flexibility in ZIF-8 Explored by Experiments and Simulations. *Journal of the American Chemical Society* 2011, *133*, 8900-8902.

(24) Banerjee, R.; Phan, A.; Wang, B.; Knobler, C.; Furukawa, H.; O'Keeffe, M.; Yaghi, O. M.: High-throughput synthesis of zeolitic imidazolate frameworks and application to CO2 capture. *Science* 2008, *319*, 939-943.

(25) Dawson, R.; Cooper, A. I.; Adams, D. J.: Nanoporous organic polymer networks. *Prog Polym Sci* 2012, *37*, 530-563.

(26) Wan, S.; Guo, J.; Kim, J.; Ihee, H.; Jiang, D. L.: A Belt-Shaped, Blue Luminescent, and Semiconducting Covalent Organic Framework. *Angewandte Chemie-International Edition* 2008, *47*, 8826-8830.

(27) Hollemann, A. F.; Wiberg, E.; Wiberg, N.: *Lehrbuch der anorganischen Chemie*; 102 ed.; de Gruyter: Berlin, New York, 2007.

(28) Trimm, D. L.; Cooper, B. J.: Preparation of Selective Carbon Molecular Sieve Catalysts. *J Chem Soc Chem Comm* 1970, 477-&.

(29) Kyotani, T.: Control of pore structure in carbon. *Carbon* 2000, *38*, 269-286.

(30) Ryoo, R.; Joo, S. H.; Jun, S.: Synthesis of highly ordered carbon molecular sieves via template-mediated structural transformation. *Journal of Physical Chemistry B* 1999, *103*, 7743-7746.

(31) Reichenbach, C.; Kalies, G.; Lincke, J.; Lassig, D.; Krautscheid, H.; Moellmer, J.; Thommes, M.: Unusual adsorption behavior of a highly flexible copper-based MOF. *Microporous and Mesoporous Materials* 2011, *142*, 592-600.

(32) Zeise, H.: *Thermodynamik*; Hirzel Verlag: Leipzig, 1954.

(33) Kumar, A. V. A.; Bhatia, S. K.: Quantum effect induced reverse kinetic molecular sieving in microporous materials. *Phys Rev Lett* 2005, *95*.

(34) Kowalczyk, P.; Gauden, P. A.; Terzyk, A. P.: Cryogenic separation of hydrogen isotopes in single-walled carbon and boron-nitride nanotubes: Insight into the mechanism of equilibrium quantum sieving in quasi-one-dimensional pores. *Journal of Physical Chemistry B* 2008, *112*, 8275-8284.

(35) Kowalczyk, P.; Gauden, P. A.; Terzyk, A. P.; Bhatia, S. K.: Thermodynamics of hydrogen adsorption in slit-like carbon nanopores at 77 K. Classical versus path-integral Monte Carlo simulations. *Langmuir* 2007, *23*, 3666-3672.

(36) Kowalczyk, P.; Gauden, P. A.; Terzyk, A. P.; Furmaniak, S.: Impact of the carbon pore size and topology on the equilibrium quantum sieving of hydrogen isotopes at zero coverage and finite pressures. *J Phys-Condens Mat* 2009, *21*.

(37) Kowalczyk, P.; Gauden, P. A.; Terzyk, A. P.; Furmaniak, S.: Quantum fluctuations increase the self-diffusive motion of para-hydrogen in narrow carbon nanotubes. *Physical Chemistry Chemical Physics* 2011, *13*, 9824-9830.

(38) Kowalczyk, P.; Gauden, P. A.; Terzyk, A. P.; Furmaniak, S.; Kaneko, K.: Cryogenic Helium Adsorbed in Zeolite Rho: Inside Localization Controlled Self-Diffusion of Confined Quantum Particles. *Journal of Physical Chemistry C* 2011, *115*, 18105-18110.

(39) *Monte Carlo Simulation in Statistical Physics*; Binder, K.; Heermann, D. W., Eds.; Springer-Verlag: Berlin, 2002.

(40) Tanaka, H.; Kanoh, H.; Yudasaka, M.; Lijima, S.; Kaneko, K.: Quantum effects on hydrogen isotope adsorption on single-wall carbon nanohorns. *Journal of the American Chemical Society* 2005, *127*, 7511-7516.

(41) Xu, Q.; Liu, D. H.; Yang, Q. Y.; Zhong, C. L.: Molecular simulation study of the quantum effects of hydrogen adsorption in metal-organic frameworks: influences of pore size and temperature. *Mol Simulat* 2009, *35*, 748-754.

(42) Noguchi, D.; Tanaka, H.; Fujimori, T.; Kagita, H.; Hattori, Y.; Honda, H.; Urita, K.; Utsumi, S.; Wang, Z. M.; Ohba, T.; Kanoh, H.; Hata, K.; Kaneko, K.: Selective D-2 adsorption enhanced by the quantum sieving effect on entangled single-wall carbon nanotubes. *J Phys-Condens Mat* 2010, *22*.

(43) Kumar, A. V. A.; Jobic, H.; Bhatia, S. K.: Quantum effect induced kinetic molecular sieving of hydrogen and deuterium in microporous materials. *Adsorption* 2007, *13*, 501-508.

(44) Wang, Q. Y.; Johnson, J. K.: Hydrogen adsorption on graphite and in carbon slit pores from path integral simulations. *Mol Phys* 1998, *95*, 299-309.

(45) Hankel, M.; Zhang, H.; Nguyen, T. X.; Bhatia, S. K.; Gray, S. K.; Smith, S. C.: Kinetic modelling of molecular hydrogen transport in microporous carbon materials. *Physical Chemistry Chemical Physics* 2011, *13*, 7834-7844. Reproduced by permission of the Royal Society of Chemistry. http://dx.doi.org./10.1039/C0CP02235G

(46) Garberoglio, G.; DeKlavon, M. M.; Johnson, J. K.: Quantum sieving in single-walled carbon nanotubes: Effect of interaction potential and rotational-translational coupling. *Journal of Physical Chemistry B* 2006, *110*, 1733-1741.

(47) Hathorn, B. C.; Sumpter, B. G.; Noid, D. W.: Contribution of restricted rotors to quantum sieving of hydrogen isotopes. *Phys Rev A* 2001, *64*, art. no.-022903.

(48) Patchkovskii, S.; Heine, T.: Evaluation of the adsorption free energy of light guest molecules in nanoporous host structures. *Physical Chemistry Chemical Physics* 2007, *9*, 2697-2705.

(49) Patchkovskii, S.; Heine, T.: Quantized liquid density-functional theory for hydrogen adsorption in nanoporous materials. *Phys Rev E* 2009, *80*.

(50) Martinez-Mesa, A.; Yurchenko, S. N.; Patchkovskii, S.; Heine, T.; Seifert, G.: Influence of quantum effects on the physisorption of molecular hydrogen in model carbon foams. *Journal of Chemical Physics* 2011, *135*.

(51) Hattori, Y.; Tanaka, H.; Okino, F.; Touhara, H.; Nakahigashi, Y.; Utsumi, S.; Kanoh, H.; Kaneko, K.: Quantum sieving effect of modified activated carbon fibers on H(2) and D(2) adsorption at 20 K. *Journal of Physical Chemistry B* 2006, *110*, 9764-9767.

(52) Noguchi, D.; Tanaka, H.; Fujimori, T.; Kagita, H.; Hattori, Y.; Honda, H.; Urita, K.; Utsumi, S.; Wang, Z. M.; Ohba, T.; Kanoh, H.; Hata, K.; Kaneko, K.: Selective D(2) adsorption enhanced by the quantum sieving effect on entangled single-wall carbon nanotubes. *J Phys-Condens Mat* 2010, *22*.

(53) Noguchi, D.; Tanaka, H.; Kondo, A.; Kajiro, H.; Noguchi, H.; Ohba, T.; Kanoh, H.; Kaneko, K.: Quantum sieving effect of three-dimensional Cu-based organic framework for H-2 and D-2. *Journal of the American Chemical Society* 2008, *130*, 6367-6372.

(54) Nguyen, T. X.; Jobic, H.; Bhatia, S. K.: Microscopic Observation of Kinetic Molecular Sieving of Hydrogen Isotopes in a Nanoporous Material. *Phys Rev Lett* 2010, *105*.

(55) Zhao, X. B.; Villar-Rodil, S.; Fletcher, A. J.; Thomas, K. M.: Kinetic isotope effect for H-2 and D-2 quantum molecular sieving in adsorption/desorption on porous carbon materials. *Journal of Physical Chemistry B* 2006, *110*, 9947-9955.

(56) Chu, X. Z.; Zhou, Y. P.; Zhang, Y. Z.; Su, W.; Sun, Y.; Zhou, L.: Adsorption of hydrogen isotopes on micro- and mesoporous adsorbents with orderly structure. *Journal of Physical Chemistry B* 2006, *110*, 22596-22600.

(57) Brickwedde, F. G.; Scott, R. B.; Taylor, H. S.: The difference in vapor pressures of ortho and para deuterium. *Journal of Chemical Physics* 1935, *3*, 653-660.

(58) Sandler, Y. L.: The Adsorption and the Magnetic Ortho-Para Conversion of Hydrogen on Diamagnetic Solids .1. Some Experiments in Surface Paramagnetism. *J Phys Chem-Us* 1954, *58*, 54-57.

(59) Sandler, Y. L.: The Adsorption and Ortho-Para Conversion of Hydrogen on Diamagnetic Solids .2. The Relative Adsorbabilities of Orthohydrogen and Parahydrogen. *J Phys Chem-Us* 1954, *58*, 58-61.

(60) Sandler, Y. L.: The Ortho-Para Conversion of Hydrogen and Deuterium on Inhomogeneous Paramagnetic Surfaces. *Can J Chem* 1954, *32*, 249-260.

(61) Moore, W. R.; Ward, H. R.: The Separation of Orthohydrogen and Parahydrogen. *Journal of the American Chemical Society* 1958, *80*, 2909-2910.

(62) FitzGerald, S. A.; Hopkins, J.; Burkholder, B.; Friedman, M.; Rowsell, J. L. C.: Quantum dynamics of adsorbed normal- and para-H-2, HD, and D-2 in the microporous framework MOF-74 analyzed using infrared spectroscopy. *Physical Review B* 2010, *81*.

(63) Bordiga, S.; Regli, L.; Bonino, F.; Groppo, E.; Lamberti, C.; Xiao, B.; Wheatley, P. S.; Morris, R. E.; Zecchina, A.: Adsorption properties of HKUST-1 toward hydrogen and other small molecules monitored by IR. *Physical Chemistry Chemical Physics* 2007, *9*, 2676-2685.

(64) Timmerhaus, K. D.; Weitzel, D. H.; Flynn, T. M.: Low-temperature distillation of hydrogen isotopes. *Chem Eng Prog* 1958, *54*, 35-46.

(65) Glueckauf, E.; Kitt, G. P.: Separation of Hydrogen Isotopes by Gas Chromatography. *Angewandte Chemie-International Edition* 1957, *69*, 567-567.

(66) Rutherford, W. M.; Lindsay, C. N.: Separation of Hydrogen Isotopes by Thermal-Diffusion. *Fusion Technol* 1985, *8*, 2278-2284.

(67) Washburn, E. W.; Urey, H. C.: Concentration of the H-2 isotope of hydrogen by the fractional electrolysis of water. *Proceedings of the National Academy of Sciences of the United States of America* 1932, *18*, 496-498.

(68) GESTIS Stoffdatenbank www.gestis.itrust.de. IFA Institut für Arbeitsschutz der Deutschen Gesetzlichen Unfallversicherung.

(69) Falconer, J. L.; Schwarz, J. A.: Temperature-Programmed Desorption and Reaction - Applications to Supported Catalysts. *Catal Rev* 1983, *25*, 141-227.

(70) Cvetanov.Rj; Amenomiy.Y: Temperature Programmed Desorption Technique for Investigation of Practical Catalysts. *Cataly Rev* 1972, *6*, 21-&.

(71) Somorjai, G. A.: *Introduction to surface chemistry and catalysis* Wiley: New York, 1994.

(72) Tomkova, E.: TDS spectra analysis. *Surface Science* 1996, *351*, 309-318.

(73) Panella, B.; Hones, K.; Muller, U.; Trukhan, N.; Schubert, M.; Putter, H.; Hirscher, M.: Desorption studies of hydrogen in metal-organic frameworks. *Angewandte Chemie-International Edition* 2008, *47*, 2138-2142.

(74) Krkljus, I.; Hirscher, M.: Characterization of hydrogen/deuterium adsorption sites in nanoporous Cu-BTC by low-temperature thermal-desorption mass spectroscopy. *Microporous and Mesoporous Materials* 2011, *142*, 725-729.

(75) Haluska, M.; Hirscher, M.; Becher, M.; Dettlaff-Weglikowska, U.; Chen, X.; Roth, S.: Interaction of hydrogen isotopes with carbon nanostructures. *Mat Sci Eng B-Solid* 2004, *108*, 130-133.

(76) Carter, G.: The deduction of desorption parameters using an exponential tempering function. *Vacuum* 2000, *57*, 399-403.

(77) Ehrlich, G.: Kinetic and Experimental Basis of Flash Desorption. *J Appl Phys* 1961, *32*, 4-&.

(78) Redhead, P. A.: Thermal Desorption of Gases. *Vacuum* 1962, *12*, 203-211.

(79) Panella, B.; Hirscher, M.; Ludescher, B.: Low-temperature thermal-desorption mass spectroscopy applied to investigate the hydrogen adsorption on porous materials. *Microporous and Mesoporous Materials* 2007, *103*, 230-234.

(80) Hirscher, M.; Panella, B.; Schmitz, B.: Metal-organic frameworks for hydrogen storage. *Microporous and Mesoporous Materials* 2010, *129*, 335-339.

(81) Redhead, P. A.: Citation Classic - Thermal-Desorption of Gases. *Current Contents/Engineering Technology & Applied Sciences* 1980, 16-16.

(82) Rutherford, S. W.; Coons, J. E.: Adsorption equilibrium and transport kinetics for a range of probe gases in Takeda 3A carbon molecular sieve. *J Colloid Interf Sci* 2005, *284*, 432-439.

(83) Krkljus, I. B.: Correlation between the Microstructure of Porous Materials and the Adsorption Properties of H_2 and D_2. PhD Thesis, Universität Stuttgart, 2011.

(84) Sample Preparation by D. Denysenko und D. Volkmer, Augsburg University, Institute of Physics, Universitätsstr. 1, 86159 Augsburg.

(85) Biswas, S.; Grzywa, M.; Nayek, H. P.; Dehnen, S.; Senkovska, I.; Kaskel, S.; Volkmer, D.: A cubic coordination framework constructed from benzobistriazolate ligands and zinc ions having selective gas sorption properties. *Dalton Transactions* 2009, 6487-6495.

(86) Cambridge Crystallographic Data Center , www.ccdc.cam.ac.uk, CCDC-723714.

(87) SEM images were taken by U. Eigenthaler, Max Planck Institute of Intelligent Systems, Stuttgart.

(88) Denysenko, D.; Grzywa, M.; Tonigold, M.; Streppel, B.; Krkljus, I.; Hirscher, M.; Mugnaioli, E.; Kolb, U.; Hanss, J.; Volkmer, D.: Elucidating Gating Effects for Hydrogen Sorption in MFU-4-Type Triazolate-Based Metal-Organic Frameworks Featuring Different Pore Sizes. *Chemistry-a European Journal* 2011, *17*, 1837-1848.

(89) Duren, T.; Millange, F.; Ferey, G.; Walton, K. S.; Snurr, R. Q.: Calculating geometric surface areas as a characterization tool for metal-organic frameworks. *Journal of Physical Chemistry C* 2007, *111*, 15350-15356.

(90) Streppel, B.; Hirscher, M.: BET specific surface area and pore structure of MOFs determined by hydrogen adsorption at 20 K. *Physical Chemistry Chemical Physics* 2011, *13*, 3220-3222.

(91) Streppel, B.: Hydrogen Adsorption on Metal-Organic Frameworks. PhD Thesis, Universität Stuttgart, 2011.

(92) Cambridge Crystallographic Data Center , www.ccdc.cam.ac.uk, CCDC-847583.

(93) Schlichtenmayer, M.: Wasserstoffspeicherkapazität poröser Materialien in Kryoadsorptionstanks. PhD Thesis, Universität Stuttgart, 2012.

(94) Structure analysis by P. Schmieder, M. Grzywa und D. Volkmer, Augsburg University, Institute of Physics, Universitätsstr. 1, 86159 Augsburg.

(95) Sample Preparation by P. Schmieder und D. Volkmer, Augsburg University, Institute of Physics, Universitätsstr. 1, 86159 Augsburg.

(96) Personal communication with Phillip Schmieder, Institute of Physics, Augsburg University.

(97) Cambridge Crystallographic Data Center , www.ccdc.cam.ac.uk, CCDC-776578.

(98) Rowsell, J. L. C.; Spencer, E. C.; Eckert, J.; Howard, J. A. K.; Yaghi, O. M.: Gas adsorption sites in a large-pore metal-organic framework. *Science* 2005, *309*, 1350-1354.

(99) Li, H.; Eddaoudi, M.; O'Keeffe, M.; Yaghi, O. M.: Design and synthesis of an exceptionally stable and highly porous metal-organic framework. *NATURE* 1999, *402*, 276-279.

(100) Panella, B.: Hydrogen Storage by Physisorption on Porous Materials. PhD Thesis, Universität Stuttgart, 2006.

(101) Construction plan by Bernd Ludescher, Max Planck Institute for Intelligent Systems, Stuttgart.

(102) Ege, M.; Kronmuller, H.: Mechanical relaxation processes of hydrogen in dilute palladium rare earth alloys. *Journal of Alloys and Compounds* 1997, *261*, 231-241.

(103) Teufel, J.; Oh, H.; Hirscher, M.; Wahiduzzaman, M.; Zhechkov, L.; Kuc, A.; Heine, T.; Denysenko, D.; Volkmer, D.: MFU-4 – a metal-organic framework for highly effective H2/D2 separation (in press). *Advanced Materials* 2012.

(104) Li, J. R.; Kuppler, R. J.; Zhou, H. C.: Selective gas adsorption and separation in metal-organic frameworks. *Chemical Society Reviews* 2009, *38*, 1477-1504.

(105) *Diffusion in Nanoporous Materials*; Kärger, J.; Ruthven, D. M.; Theodorou, D. N., Eds.; Wiley-VCH: Weinheim, 2012; Vol. 1.

(106) Bhatia, S. K.: Modeling Pure Gas Permeation in Nanoporous Materials and Membranes. *Langmuir* 2010, *26*, 8373-8385.

(107) Personal communication (unpublished) with Prof. T. Heine, School of Engineering and Science, Jacobs University, Bremen.

(108) Breck, D. W.; Eversole, W. G.; Milton, R. M.; Reed, T. B.; Thomas, T. L.: Crystalline Zeolites .1. The Properties of a New Synthetic Zeolite, Type-A. *Journal of the American Chemical Society* 1956, *78*, 5963-5971.

(109) Kim, H.; Samsonenko, D. G.; Yoon, M.; Yoon, J. W.; Hwang, Y. K.; Chang, J. S.; Kim, K.: Temperature-triggered gate opening for gas adsorption in microporous manganese formate. *Chemical Communications* 2008, 4697-4699. Reproduced by permission of the Royal Society of Chemistry. http://dx.doi.org./10.1039/B811087E

(110) Onishi, S.; Ohmori, T.; Ohkubo, T.; Noguchi, H.; Di, L.; Hanzawa, Y.; Kanoh, H.; Kaneko, K.: Hydrogen-bond change-associated gas adsorption in inorganic-organic hybrid microporous crystals. *Appl Surf Sci* 2002, *196*, 81-88.

(111) Maji, T. K.; Mostafa, G.; Matsuda, R.; Kitagawa, S.: Guest-induced asymmetry in a metal-organic porous solid with reversible single-crystal-to-single-crystal structural transformation. *Journal of the American Chemical Society* 2005, *127*, 17152-17153.

(112) Uemura, K.; Matsuda, R.; Kitagawa, S.: Flexible microporous coordination polymers. *Journal of solid state chemistry* 2005, *178*, 2420-2429.

(113) *Characterization of porous solids and powders: surface area, pore size and density*; Lowell, S.; Shields, J. E.; Thomas, M. A.; Thommes, M., Eds.; Kluwer Academic Press, 2004.

(114) Personal communication with I. Savchenko (preliminary results, to be published), group of Prof. T. Heine, School of Engineering and Science, Jacobs University, Bremen.

(115) Yildirim, T.; Hartman, M. R.: Direct observation of hydrogen adsorption sites and nanocage formation in metal-organic frameworks. *Phys Rev Lett* 2005, *95*.

(116) Lin, C. C. H.; Dambrowitz, K. A.; Kuznicki, S. M.: Evolving applications of zeolite molecular sieves. *Can J Chem Eng* 2012, *90*, 207-216.

(117) Shah, M.; McCarthy, M. C.; Sachdeva, S.; Lee, A. K.; Jeong, H. K.: Current Status of Metal-Organic Framework Membranes for Gas Separations: Promises and Challenges. *Industrial & Engineering Chemistry Research* 2012, *51*, 2179-2199.

(118) Betard, A.; Bux, H.; Henke, S.; Zacher, D.; Caro, J.; Fischer, R. A.: Fabrication of a CO2-selective membrane by stepwise liquid-phase deposition of an alkylether functionalized pillared-layered metal-organic framework [Cu2L2P](n) on a macroporous support. *Microporous and Mesoporous Materials* 2012, *150*, 76-82.

(119) Shekhah, O.; Liu, J.; Fischer, R. A.; Woll, C.: MOF thin films: existing and future applications. *Chemical Society Reviews* 2011, *40*, 1081-1106.

(120) Bernardo, P.; Drioli, E.; Golemme, G.: Membrane Gas Separation: A Review/State of the Art. *Industrial & Engineering Chemistry Research* 2009, *48*, 4638-4663.

(121) Gu, Z. Y.; Yan, X. P.: Metal-Organic Framework MIL-101 for High-Resolution Gas-Chromatographic Separation of Xylene Isomers and Ethylbenzene. *Angewandte Chemie-International Edition* 2010, *49*, 1477-1480.

(122) Luebbers, M. T.; Wu, T. J.; Shen, L. J.; Masel, R. I.: Effects of Molecular Sieving and Electrostatic Enhancement in the Adsorption of Organic Compounds on the Zeolitic Imidazolate Framework ZIF-8. *Langmuir* 2010, *26*, 15625-15633.

(123) Chen, B. L.; Liang, C. D.; Yang, J.; Contreras, D. S.; Clancy, Y. L.; Lobkovsky, E. B.; Yaghi, O. M.; Dai, S.: A microporous metal-organic framework for gas-chromatographic separation of alkanes. *Angewandte Chemie-International Edition* 2006, *45*, 1390-1393.

(124) Munch, A. S.; Seidel, J.; Obst, A.; Weber, E.; Mertens, F. O. R. L.: High-Separation Performance of Chromatographic Capillaries Coated with MOF-5 by the Controlled SBU Approach. *Chemistry-a European Journal* 2011, *17*, 10958-10964.

(125) Lock, N.; Wu, Y.; Christensen, M.; Cameron, L. J.; Peterson, V. K.; Bridgeman, A. J.; Kepert, C. J.; Iversen, B. B.: Elucidating Negative Thermal Expansion in MOF-5. *Journal of Physical Chemistry C* 2010, *114*, 16181-16186.

(126) Zhou, W.; Wu, H.; Yildirim, T.; Simpson, J. R.; Walker, A. R. H.: Origin of the exceptional negative thermal expansion in metal-organic framework-5 Zn(4)O(1,4-benzenedicarboxylate)(3). *Physical Review B* 2008, *78*.

(127) Han, S. S.; Goddard, W. A.: Metal-organic frameworks provide large negative thermal expansion Behavior. *Journal of Physical Chemistry C* 2007, *111*, 15185-15191.

(128) Huang, B. L.; Ni, Z.; Millward, A.; McGaughey, A. J. H.; Uher, C.; Kaviany, M.; Yaghi, O.: Thermal conductivity of a metal-organic framework (MOF-5): Part II. Measurement. *International Journal of Heat and Mass Transfer* 2007, *50*, 405-411.

(129) Doonan, C.J.; Tranchemontagne, D.J.; Glover, T.G.; Hunt, J.R.; Yaghi, O.M.: Exceptional ammonia uptake by a covalent organic framework. *Nature Chemistry* 2010, *2*, 235-238

(130) Cote, A.P.; Benin, A.I., Ockwig, N.W.; O'Keeffe, M.; Matzger, A.J.; Yaghi, O.M.: Porous, crystalline, covalent organic frameworks. *Science* 2005, *310*, 1166-1170

Eidesstattliche Erklärung

Hiermit erkläre ich, dass ich die Dissertation eigenständig verfasst habe und nur die genannten Hilfsmittel und Quellen verwendet habe.

_____

Ort, Datum, Unterschrift

Danksagung

Zuerst möchte ich mich bei Herrn Professor Emil Roduner und Frau Professor Gisela Schütz für die Übernahme des Haupt- und Mitberichts bedanken. Insbesondere danke ich Prof. Roduner für die intensiven und sehr hilfreichen Diskussionen.

Des Weiteren bedanke ich mich bei Doktor Michael Hirscher für die Chance, die Doktorarbeit in seiner Arbeitsgruppe im Rahmen des DFG-Schwerpunktprogramms SPP 1362 anzufertigen. In diesem Zusammenhang möchte ich mich auch sehr herzlich bei Professor Thomas Heine und seinen Mitarbeitern bedanken (A. Kuc, L. Zhechkov, M. Wahiduzzaman, I. Savchenko), ohne deren Theoriebeiträge die Interpretation der Ergebnisse deutlich schwieriger gewesen wäre. Auch der Gruppe von Prof. Volkmer und insbesondere D. Denysenko gilt mein Dank für die Bereitstellung qualitativ hochwertiger Proben und gewinnbringender Diskussionen.

Ein besonderer Dank gilt Bernd Ludescher für seine Unterstützung bei der Planung und dem Bau der TDS-Anlage, sowie seiner Hilfe bei technischen Problemen jeglicher Art.

Danken möchte ich auch meinen Arbeitskollegen für die Einarbeitung und, insbesondere Hyunchul Oh, für die zahlreichen fachlichen Diskussionen.

Zuletzt aber doch von ganzem Herzen danke ich meiner Familie, meinen Freunden und meinem Freund Thomas für die mentale Unterstützung, wenn immer ich sie gebraucht habe.